VOLUME 35 JUNE 1957 NUMBER 6

Canadian Journal of Physics

Editor: H. E. DUCKWORTH

Associate Editors:

L. G. ELLIOTT, *Atomic Energy of Canada, Ltd., Chalk River*
J. S. FOSTER, *McGill University*
G. HERZBERG, *National Research Council of Canada*
L. LEPRINCE-RINGUET, *Ecole Polytechnique, Paris*
B. W. SARGENT, *Queen's University*
G. M. VOLKOFF, *University of British Columbia*
W. H. WATSON, *University of Toronto*
G. A. WOONTON, *McGill University*

Published by THE NATIONAL RESEARCH COUNCIL
OTTAWA CANADA

CANADIAN JOURNAL OF PHYSICS

(*Formerly Section A, Canadian Journal of Research*)

Under the authority of the Chairman of the Committee of the Privy Council on Scientific and Industrial Research, the National Research Council issues THE CANADIAN JOURNAL OF PHYSICS and five other journals devoted to the publication, in English or French, of the results of original scientific research. Matters of general policy concerning these journals are the responsibility of a joint Editorial Board consisting of: members representing the National Research Council of Canada; the Editors of the Journals; and members representing the Royal Society of Canada and four other scientific societies.

EDITORIAL BOARD

Representatives of the National Research Council

R. B. Miller, *University of Alberta*
H. G. Thode, *McMaster University*
D. L. Thomson, *McGill University*
W. H. Watson (Chairman), *University of Toronto*

Editors of the Journals

D. L. Bailey, *University of Toronto*
T. W. M. Cameron, *Macdonald College*
H. E. Duckworth, *McMaster University*
K. A. C. Elliott, *Montreal Neurological Institute*
Léo Marion, *National Research Council*
R. G. E. Murray, *University of Western Ontario*

Representatives of Societies

D. L. Bailey, *University of Toronto*
Royal Society of Canada
T. W. M. Cameron, *Macdonald College*
Royal Society of Canada
H. E. Duckworth, *McMaster University*
Royal Society of Canada
Canadian Association of Physicists
K. A. C. Elliott, *Montreal Neurological Institute*
Canadian Physiological Society
R. G. E. Murray, *University of Western Ontario*
Canadian Society of Microbiologists
H. G. Thode, *McMaster University*
Chemical Institute of Canada
T. Thorvaldson, *University of Saskatchewan*
Royal Society of Canada

Ex officio

Léo Marion (Editor-in-Chief), *National Research Council*
F. T. Rosser, Vice-President (Administration), *National Research Council*

Manuscripts for publications should be submitted to Dr. Léo Marion, Editor-in-Chief, Canadian Journal of Physics, National Research Council, Ottawa 2, Canada.

(For instructions on preparation of copy, see **Notes to Contributors** (inside back cover).)

Proof, correspondence concerning proof, and orders for reprints should be sent to the Manager, Editorial Office (Research Journals), Division of Administration, National Research Council, Ottawa 2, Canada.

Subscriptions, renewals, requests for single or back numbers, and all remittances should be sent to Division of Administration, National Research Council, Ottawa 2, Canada. Remittances should be made payable to the Receiver General of Canada, credit National Research Council.

The journals published, frequency of publication, and prices are:

Canadian Journal of Biochemistry and Physiology	Monthly	$3.00 a year
Canadian Journal of Botany	Bimonthly	$4.00 a year
Canadian Journal of Chemistry	Monthly	$5.00 a year
Canadian Journal of Microbiology	Bimonthly	$3.00 a year
Canadian Journal of Physics	Monthly	$4.00 a year
Canadian Journal of Zoology	Bimonthly	$3.00 a year

The price of single numbers of all journals is 75 cents.

Canadian Journal of Physics

Issued by THE NATIONAL RESEARCH COUNCIL OF CANADA

VOLUME 35 JUNE 1957 NUMBER 6

NEUTRON SPECTRUM OF AN ACTINIUM–BERYLLIUM SOURCE[1]

W. R. DIXON, ALICE BIELESCH, AND K. W. GEIGER

ABSTRACT

The neutron spectrum of an Ac^{227}-α-Be source has been determined from proton recoil tracks in nuclear emulsions, and found to be in general agreement with the spectra of Po-α-Be and Ra-α-Be sources. Direct observation is limited to neutron energies above about 0.5 Mev. The question of neutrons below this energy is also considered.

INTRODUCTION

The $Be^9(\alpha, n)C^{12}$ reaction (Q = 5.7 Mev.) is commonly used in radioactive neutron sources, with Ra^{226} in equilibrium with its decay products, or Po^{210}, being used as α-emitters. Recently however, other α-emitters, in particular Ac^{227}, have become available and relative neutron yields have been published (Runnalls and Boucher 1956; Hanna and Runnalls 1956). Since an Ac^{227}-α-Be source ($T_{\frac{1}{2}}$ = 22 years) has the practical advantage of having a considerably lower gamma-ray-to-neutron ratio than a Ra-α-Be source, without the disadvantage of the short half-life of a Po-α-Be source (140 days), the neutron spectrum of such a source is of considerable interest. A determination using proton recoil tracks in nuclear emulsions has been carried out and is reported here.

METHODS AND RESULTS

Ilford C2 plates of 200 microns thickness were exposed to two Ac^{227}-α-Be sources. Data on the sources and exposures are summarized in Table I. Standard development, scanning, and measuring procedures were used. The proton tracks were required to start and stop in the emulsion, and only those in a forward cone of half-angle 15° were accepted. The shrinkage factor for the emulsion was determined daily and individual calculations were made on each track to determine its true length. The proton energies were obtained from the range–energy relation of Rotblat (1951) and from these the neutron energies were calculated by dividing by $\cos^2\theta$, where θ is the angle between the incident neutron and the proton. The background was measured on a similar unexposed plate and was found to be practically negligible. No evidence of alpha-particle contamination was found.

[1]Manuscript received February 7, 1957.
Contribution from Division of Applied Physics, National Research Council, Ottawa.
Issued as N.R.C. No. 4327.

TABLE I

DATA ON SOURCES AND EXPOSURE

	Source number		
	AN-10-2	AC-9-4	Background
Total neutron flux (n./sec.)	3.0×10^5	3.5×10^6	
Ac^{227} (mc.)	12	190	
Beryllium (mg.)	500	190	
Source diameter (mm.)	13.9	9	
Source length (mm.)	7.1	9	
Wall thickness (mm. monel)	1	1	
Distance to emulsion (cm.)	30	48	
Irradiation time (hours)	88	46.25	
Lead absorber (in.)	0	0.125	
Area scanned ($mm.^2$)	36.6	95.3	45.4
Number of useful tracks	175	836	8

Exposure times and lead absorber thickness were chosen so as to keep gamma-ray fogging at a tolerable level and the proton track density high enough to facilitate scanning. The lead absorber was sufficiently thin not to distort the neutron spectrum. This is in contrast to the situation with a Ra-α-Be source, where the gamma-ray-to-neutron ratio is so high that the amount of lead required distorts the neutron spectrum. In the present case it was possible to distinguish from the gamma-ray fog only those tracks with energies greater than about 0.5 Mev. The initial portions of tracks due to protons of energies greater than about 11 Mev. were also obscured because of the low specific ionization. The practical result of this was to bunch all higher energy tracks at about 10–11 Mev.

The number of neutrons in each energy interval was multiplied by a correction for the escape of tracks from the emulsion (Rosen 1953), and divided by the total cross section for neutron–proton scattering (Hughes and Harvey 1955) in order to obtain the neutron spectrum. No statistically significant difference was found in the spectrum of the two sources. The combined result is shown in Fig. 1 with the errors shown being statistical

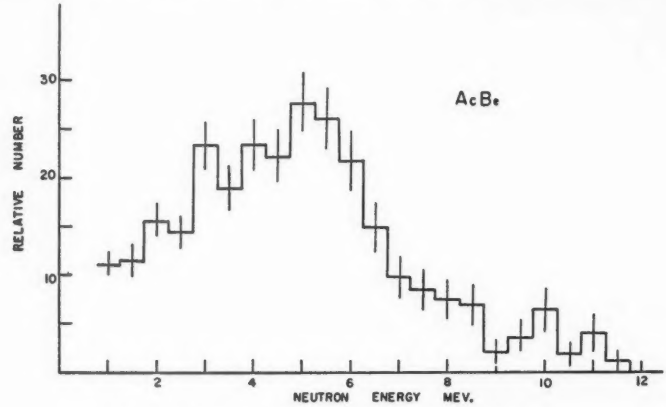

FIG. 1. Neutron spectrum of an Ac^{227}-α-Be source.

only. No correction has been made for neutron attenuation in the emulsion. As a check on the measurements and calculations, the distribution of tracks with respect to the angle θ has also been determined. Satisfactory agreement with the expected $\sin\theta\cos\theta$ variation was found.

DISCUSSION

For a fixed α-energy, and a fixed angle of observation with respect to the incident α-particle, the energy distribution of neutrons emitted in the $Be^9(\alpha, n)$ reaction should show sharp peaks corresponding to the energy levels of the C^{12} nucleus. However, in a neutron source, the slowing down of the α-particles before reacting and the distribution of neutrons over all angles tend to smear out the peaks and hence to reduce recognizable differences between the neutron spectra for different α-emitters. In fact, the neutron spectrum found here for an Ac^{227}-α-Be source (average α-energy 6.4 Mev.) is in essential agreement with the spectrum for a Po-α-Be source (α-energy 5.3 Mev.) as reported by Whitmore and Baker (1950) and by Elliot *et al.* (1954), aside from a displacement of about 0.5 Mev. towards higher energies in the latter spectrum. Several other results on Po-α-Be sources have been reported in the literature (for references, see Stewart 1955), the most recent of which is that of Medveczky (1956) based on 12,000 tracks. Measurements of the neutron spectra of Ra-α-Be sources have been reported by Hill (1947), Teucher (1949), and Schmidt-Rohr (1953), and of a Pu-α-Be source by Stewart (1955). While there is over-all agreement among these various spectra, the details differ, and it seems fruitless to make detailed comparisons, especially if different Po-α-Be sources can have different spectra, as reported by Cochran and Henry (1953).

In much of the early work with Ra-α-Be sources evidence was put forward for the existence of a neutron group at about 100 kev., with estimates of its relative intensity ranging as high as 90%. (See, in particular, Auger 1933; Bjerge 1938; Stuhlinger 1939; Houtermans and Teucher 1948.) These neutrons were thought to arise from a $Be^9(\alpha, n)3\alpha$ reaction that has an effective threshold of about 4.8 Mev. (Bjerge 1938). For Ac^{227}-α-Be sources, the maximum α-energy is 7.4 Mev., compared with 7.7 Mev. for Ra-α-Be sources, so that a lower energy group might also be expected. However, since no tracks of energies less than 0.5 Mev. could be observed in the present experiment, no direct confirmation of such a group could be obtained. A comparison of the known total flux of neutrons of all energies with the flux calculated from the observed proton track density shows that the fraction of neutrons of energies greater than 0.5 Mev. is about 85%, but since the error in this figure amounts to about 25%, it is possible to set only an upper limit to the relative intensity of the lower energy neutrons.

ACKNOWLEDGMENTS

The authors wish to thank Mr. J. Anstee and Mr. H. Crosby of the Commercial Products Division, Atomic Energy of Canada Limited, for arranging the loan of the sources. We are grateful to Dr. E. Pickup and Mr. H. A. MacDonald for supplying a microscope and developing the plates.

REFERENCES

AUGER, P. 1933. J. phys. radium, **4**, 719.
BJERGE, T. 1938. Proc. Roy. Soc. A, **164**, 243.
COCHRAN, R. G. and HENRY, K. M. 1953. Oak Ridge National Laboratory Report, ORNL-1479.
ELLIOT, J. O., MCGARRY, W. I., and FAUST, W. R. 1954. Phys. Rev. **93**, 1348.
HANNA, G. C. and RUNNALLS, O. J. C. 1956. Can. J. Phys. **34**, 959.
HILL, D. L. 1947. U.S. Atomic Energy Commission Report AECD-1945.
HOUTERMANS, F. G. and TEUCHER, M. 1948. Z. Physik, **124**, 700.
HUGHES, D. J. and HARVEY, J. A. 1955. Neutron cross sections, Brookhaven National Laboratory Report BNL-325.
MEDVECZKY, L. 1956. Acta Phys. Acad. Sci. Hung. **6**, 261.
ROSEN, L. 1953. Nucleonics, **11**, No. 8, 38.
ROTBLAT, J. 1951. Nature, **167**, 550.
RUNNALLS, O. J. C. and BOUCHER, R. R. 1956. Can. J. Phys. **34**, 949.
SCHMIDT-ROHR, U. 1953. Z. Naturforsch. **8a**, 470.
STEWART, L. 1955. Phys. Rev. **98**, 740.
STUHLINGER, E. 1939. Z. Physik, **114**, 185.
TEUCHER, M. 1949. Z. Physik, **126**, 410.
WHITMORE, B. G. and BAKER, W. B. 1950. Phys. Rev. **78**, 799.

VARIATIONS IN THE INTRINSIC STRENGTH OF THE 1956 QUADRANTID METEOR SHOWER[1]

C. O. Hines and E. L. Vogan

ABSTRACT

The occurrence rate of meteoric signals, detected on a V.H.F. forward-scatter path, is analyzed for the time of the 1956 Quadrantid shower. The detection rate of the shower meteors is converted to an incidence rate, by use of the appropriate forward-scatter theory. The variation in the intrinsic strength of the shower is thereby determined, on an hour-to-hour basis, and it is compared with variations which have been obtained in other years by other methods. The comparison reveals a distinct secular shifting of the orbit of the Quadrantid meteor stream. It also illustrates the marked advantage of the new technique in assessing variations in the strengths of short-lived showers.

INTRODUCTION

The experimental technique employed in the present study has been outlined by Forsyth and Vogan (1955). Meteor trails were detected by the forward-scattering of V.H.F. radio waves over an extended path. Specifically, the frequency employed was 49.98 Mc./s., the transmitter was located at Greenwood, N.S. (lat. 45.0° N., long. 64.9° W.), and the receiver was at the Radio Physics Laboratory (lat. 45.4° N., long. 75.9° W.) just west of Ottawa, Ont.; the path length was approximately 860 km., and it lay almost directly east–west at a latitude of 45° N. Five-element yagi antennas oriented along the great circle path were employed, with beam widths (between half-power points) of approximately 50° in azimuth. The antenna heights were such as to direct the principal lobes from each end towards the 95 km. level above the mid-point. The radiated power was 100 watts.

Continuous recordings made at the receiving site exhibited the usual array of spiky signals attributed to scattering from individual meteor trails. Care was taken to ensure that the maximum amplitude of each spike was recorded correctly, by introducing peak-reading circuitry (Forsyth and Rolfe 1955) to overcome the effects of an inherent lag in the response of the Esterline-Angus recorder used. The number of spikes exceeding a 0.5 μv. counting level was determined, for each hour throughout the period in question. These provide the observational data analyzed here.

The theoretical treatment of meteoric forward-scattering was initiated by Eshleman (1952) and further developed by Eshleman and Manning (1954). It was reformulated by Hines (1955) for application to meteor showers, and compared with preliminary shower data by Forsyth, Hines, and Vogan (1955). The data used in that comparison were obtained on a forward-scatter path from Cedar Rapids, Iowa, to Ottawa. The Cedar Rapids antenna produced a narrow beam directed well away from the great circle path, and thereby introduced serious uncertainties in the theoretical interpretation. Accordingly,

[1]Manuscript received January 7, 1957.
Contribution from the Radio Physics Laboratory of the Defence Research Board, Ottawa, Canada. The work was performed under projects PCC No. D48-95-11-01 and PCC No. D48-28-35-05.

a detailed quantitative analysis of the records was not felt to be warranted at the time, and the comparison was purely qualitative. The simpler antenna systems employed in the present work lead to a more certain theoretical interpretation, which in turn justifies the full analysis which follows.

ANALYSIS OF FORWARD-SCATTER RECORDS

The forward-scatter records showed an apparently normal background of meteor signals throughout the last week of 1955 and during the first two weeks of 1956, except for a varying excess of signals throughout January 2, 3, and 4. The excess is, of course, attributable to the Quadrantid meteor shower, which is known to reach maximum intensity during that period.

To analyze the excess, it is necessary to remove the background. This has been done statistically, with the use of data recorded on 3 days somewhat before the shower and 3 days somewhat later, namely, December 27, 28, and 29, 1955, and January 8, 9, and 10, 1956. The number of signals which exceeded the counting level in each hour of each of these days contributes to the array of dots in Fig. 1. In this figure, 'date' information is ignored, but 'hour'

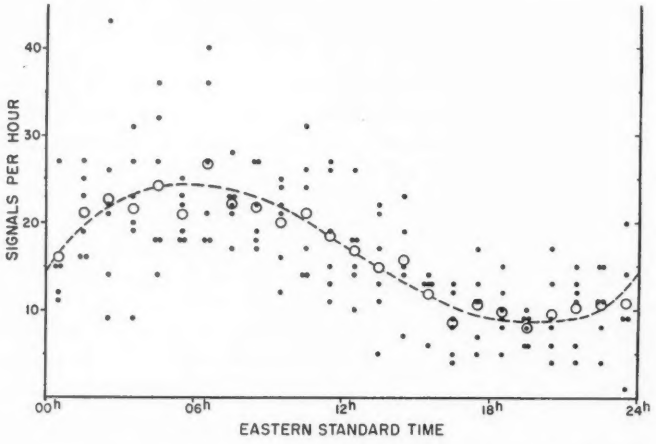

FIG. 1. Diurnal variation in the occurrence rate of forward-scattered signals, attributed to the sporadic background of meteors.

information is retained as abscissa (E.S.T. = G.M.T. − 5 hours). The results are averaged for each hour in turn, and the mean values are indicated by open circles; the spread of individual values about each mean is no greater than might be expected on statistical grounds. Three individual results are missing from the display, as a result of equipment failure.

The broken-line curve which has been drawn through the array yields an arbitrarily smoothed diurnal variation in the background count. The number of signals represented by the curve, measured to the nearest integral value at the half-hour points, is taken to be the background count at the corresponding hours during the shower period.

The data obtained during the shower period itself are displayed in Fig. 2. The background count derived from Fig. 1 is plotted *downwards* from the horizontal axis to provide a varying base line, represented by a series of solid circles. The total count obtained in each hour (with one exception, due to equipment failure) is plotted *upwards* from this varying base line, and is represented by the vertical distance between corresponding solid and open circles. Accordingly, the set of open circles indicates the variation in the

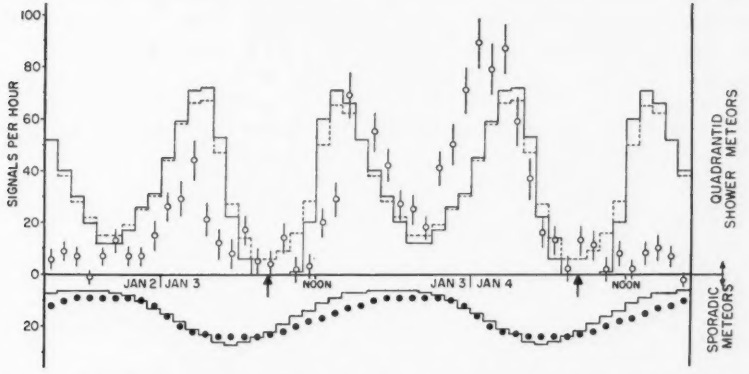

FIG. 2. Occurrence rate of forward-scattered signals at the time of the 1956 Quadrantid shower (vertical separation between circles), and theoretical variations (histograms). The indicated noon and midnight points refer to Eastern Standard Time.

number of signals attributed to the Quadrantid shower, when measured from the horizontal axis. The vertical bars through these indicate the standard deviations, to the nearest integral value, expected on purely statistical grounds from the total number of counts obtained in the relevant hour.

The passage of time (E.S.T.) is indicated on the horizontal axis. Also marked, by solid arrowheads on the axis, are the times at which the Quadrantid radiant reaches upper transit as observed from the mid-point of the path. Purely geometrical factors indicate, of course, that the fraction of incident shower meteors which appear in a given observer's sky should maximize at upper transit. The fact that a minimum actually occurs, on January 3 at least, is attributable to the complexities of the forward-scatter geometry.

Superimposed on the experimental data in Fig. 2 are histograms representing theoretical predictions. Plotted downwards from the horizontal axis is the predicted variation in the background count, based on an assumed isotropic distribution of radiants in a heliocentric coordinate system, and on the assumption that the ionization produced in a meteor trail is independent of the speed of the parent meteor. Both of these assumptions are open to serious question, and the histogram is presented for interest's sake alone. The scale is arbitrary, and the theoretical variation has been normalized to provide a reasonable fit.

Two histograms have been plotted above the horizontal axis, as theoretical predictions for the Quadrantid shower itself. The one drawn as a solid line is

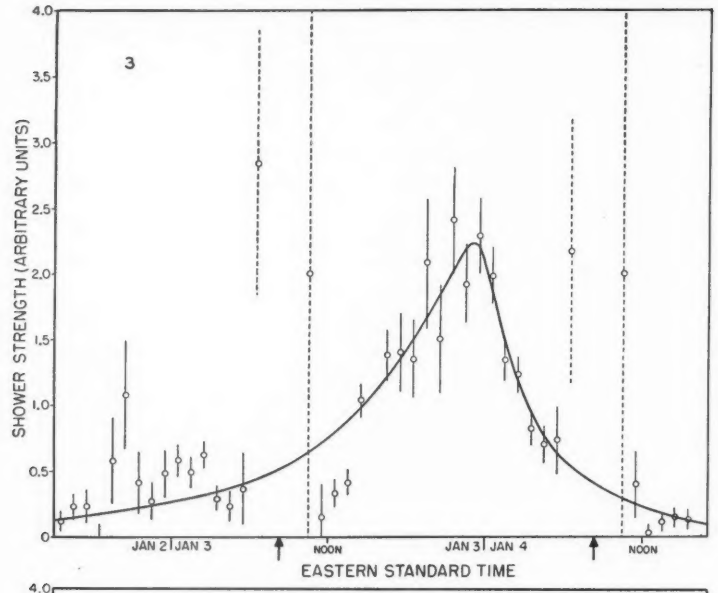

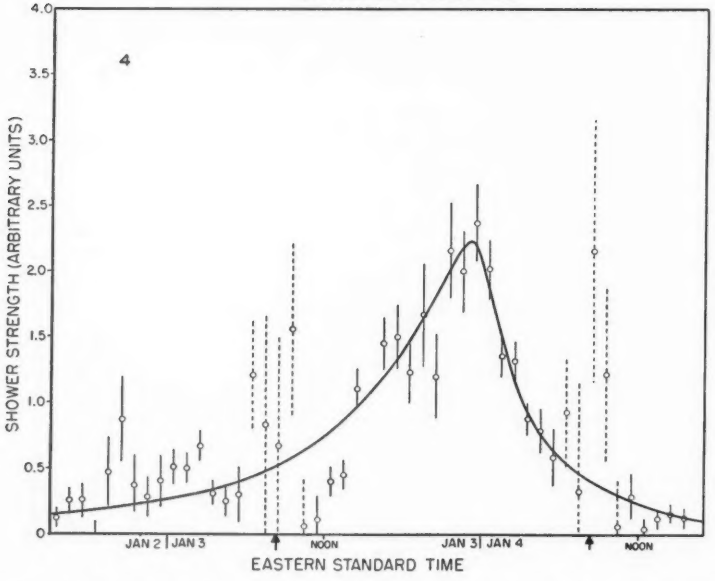

FIG. 3. Variation of the intrinsic strength of the 1956 Quadrantid shower, as determined for a point radiant.

FIG. 4. Variation of the intrinsic strength of the 1956 Quadrantid shower, as determined for a diffuse radiant.

applicable to a point radiant located at dec. +50°, R.A. 231°, with an error of one or two degrees in either direction being negligible in comparison with other possible sources of error in the theory. The second histogram, drawn in a broken line, is applicable to a very diffuse radiant centered on the point just specified. It was actually computed as the average of five results, obtained by combining the initial point radiant with four others differing in declination or right ascension by ±10°. The derivation followed essentially the same course as that outlined in the earlier comparison (Forsyth, Hines, and Vogan 1955), but it employed the 'observability' contour chart displayed in Fig. 7 of the theoretical paper (Hines 1955), since that chart is appropriate to the antenna systems now in use. The vertical scale of the histograms is taken directly from the observability function itself, which is arbitrarily normalized to a maximum possible value of 100 for an optimum radiant position.

Both of the shower histograms are drawn on the assumption that the strength of the shower, or the absolute incidence rate of shower meteors, remains constant. This assumption must be faulty, and from the diagram it evidently is. The theory predicts too many signals at the start, too few in the middle, and too many again at the end. Clearly, the strength of the shower increased during January 2 and the early part of January 3, reached a peak, and decreased on January 4.

To assess the varying strength of the shower quantitatively, it is necessary only to divide the predicted value into the observed value. This has been done for both sets of predictions, and the results are displayed in Figs. 3 and 4 (for the point and diffuse radiants, respectively). Near the time of upper transit, the detected Quadrantid trails lie near the southern edge of the main antenna lobes, on this particular forward-scatter path. The possible error in the prediction is particularly great at such times, because of uncertainties in the exact lobe structure, and the corresponding entries on the diagrams are just dotted in. For 3 hours about upper transit, in Fig. 3, points at infinity are completely ignored. They result from a predicted zero which, if divided into even one extra sporadic count, would yield an infinity; they are not to be taken seriously.

The solid curves which have been drawn through the arrays in Figs. 3 and 4 are identical. (The fact that identical curves do fit the two plots so well indicates that the possible diffuseness of the radiant is not of critical importance to the analysis.) They provide an arbitrarily smoothed description of the variation in the strength of the 1956 Quadrantid shower. Alternatively, they provide the variation in the density of the Quadrantid stream itself, along the section swept out by the earth.

In order to illustrate properly the degree of fit provided by the deduced variation, without exaggerating the discrepancies at upper transit, a further comparison has been made in Fig. 5. The shower data have been plotted exactly as in Fig. 2, while the theoretical histograms have been modified by including the smooth variation in the intrinsic strength of the shower as just deduced. With few exceptions, the fit is excellent.

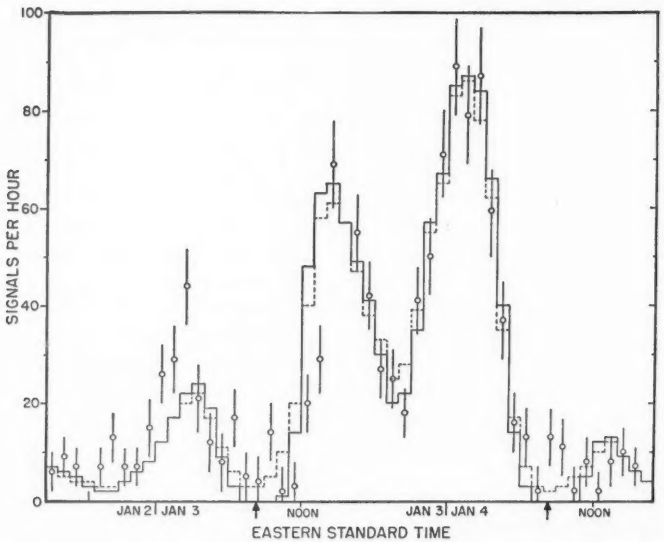

FIG. 5. Comparison between observed shower rates (open circles, with vertical 'probable error' bars) and theoretical variation (histograms), the latter including the smoothed variation of the intrinsic shower strength obtained in Figs. 3 and 4.

COMPARISON WITH EARLIER STUDIES

The Quadrantids have been recognized and observed visually for more than a century. The most detailed analysis of the visual results, to obtain the variation of the shower strength, appears to have been carried out by Prentice (1940). His data were derived from observations of the shower over a 20 year period, from 1921 to 1940. The duration of any single period of observation never exceeded a few hours, and periods of 1 or 2 hours were common. A number of observers participated, and they made their counts, as darkness and weather conditions would permit. The results were obtained, then, as isolated values for various times through the life of the shower, with individual years being represented by a few values at best. No attempt was made to correct for any visual observability effects.

To correlate the data obtained in the various years, the values were plotted as a function of the earth's position in its orbit (measured by the longitude of the sun, epoch 1950), rather than as a function of date and hour. The plotted points showed a wide scatter, and no clearly defined curve could be drawn through them. Prentice did, however, draw an envelope curve enclosing the great majority of the individual results. His curve, including alternative forms at the shower peak, is reproduced in Fig. 6 as a broken-line curve.

The Quadrantids have been studied by radar (back-scatter) methods more recently. Hawkins and Almond (1952) have published preliminary data of this type, and their later work has been quoted by Lovell (1954). Their

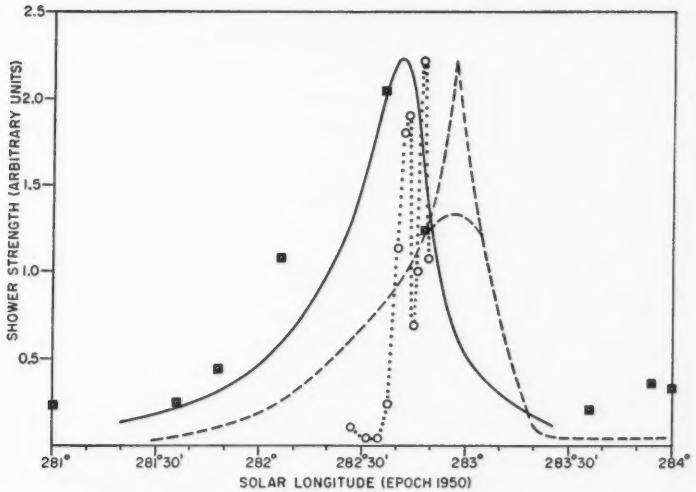

FIG. 6. Comparison between variations of the intrinsic strength of the Quadrantid shower, as deduced by a number of techniques: (*a*) 1956 shower by forward-scatter (solid curve), (*b*) 1921–1940 showers by eye (broken curve), (*c*) 1951–1953 showers by pencil-beam radar (solid squares), (*d*) 1951 shower by omnidirectional radar (open circles joined by dots).

measurements were made with a highly directive radar system, which provided information near times of upper transit only. Unfortunately, then, their results are of an intermittent nature similar to those of the visual workers. Their data for 1951, 1952, and 1953 are shown by solid squares in Fig. 6.

The radar technique is more appropriately applied to the present problem with the use of omnidirectional antennas. Millman and McKinley (1953) have analyzed results obtained in this way for the 1951 Quadrantid shower. Their observed counts were subjected to an empirical correction to yield, in effect, the variation in the intrinsic shower strength during several hours of January 3, 1951. Their corrected results have been replotted in Fig. 6, against solar longitude (epoch 1950), where they are represented by open circles joined by dotted lines. (A theoretical analysis of the back-scatter situation, analogous to the observability analysis for forward-scatter, confirms the empirical correction which was applied.)

The curve obtained in Figs. 3 and 4 has been replotted in Fig. 6 for comparison with the other results. It is shown as a solid-line curve. The visual data and the two sets of radar data have been scaled vertically to match the forward-scatter results.

One striking feature is immediately apparent. The present analysis yields a variation which agrees extremely well with the envelope of visual data, but the two curves are shifted appreciably in time. The maxima occur at 282° 41′ and 282° 57′ respectively (in solar longitude, epoch 1950), a separation which corresponds to something more than 6 hours in the time of the maximum. Neither technique is liable to introduce an error of this magnitude, and the

discrepancy must be considered a real one. A more recent determination by Prentice (1953), including earlier and later data, yielded a weighted mean of 282° 53′ for the epoch of maximum activity. The radar results of Hawkins and Almond, however, tend to confirm the present findings.

Two possible explanations of the discrepancy come quickly to mind. In the first place, it is quite certain that the radio observations are concerned with much smaller meteors, on the whole, than are the visual observations. It is then possible that the distribution of meteor masses is variable throughout the Quadrantid stream, with the larger ones predominating during the later stages of the earth's passage through it. This suggestion receives no theoretical support, however, and it appears to be incompatible with other experimental evidence (Hawkins and Almond 1952, Fig. 5*c*).

The alternative suggestion is, simply, that the orbit of the Quadrantid stream has been shifting with time, presumably as a result of perturbations imposed by Jupiter. Shifts due to this cause are not unexpected (cf. Porter 1952), and the sense of the shift is that predicted by theory. It should be mentioned, however, that Prentice (1953) finds no evidence of such a shift, even though his comparison includes results dating back to 1863. But he does find random shifts in the epoch of the shower maximum, amounting to $\pm 10'$ in solar longitude, and he suggests that these might lead to a systematic variation if corrections for zenithal magnitude were applied.

The results of Millman and McKinley show a relatively sharp distribution of the 1951 Quadrantids, apparently with fine structure. Millman and McKinley found the center of mass of their distribution to lie at 1729 hours (E.S.T.), January 3, which corresponds to 282° 44.3′ solar longitude (epoch 1950). The effective maximum cannot lie far from this time in spite of the fine-structure minimum which occurs there. Coupled with the forward-scatter maximum (for 1956), and with the visual maximum (if assigned to 1930, the central year of the visual observations), this result might suggest that the shifting of the Quadrantid stream has been a uniform motion. The possible errors in time of maximum are appreciable, however, and future comparisons will be of interest.*

CONCLUSION

Besides the specific results relating to the Quadrantid shower, certain general comments arise from this work. It should be pointed out that the fit obtained in Figs. 3 and 4 provides some degree of confirmation of the theory. Because the path is so nearly east–west, the theoretical variation is nearly symmetrical about the times of upper and lower transit. Any serious

*NOTE ADDED IN PROOF: Hawkins and Southworth have now completed a detailed analysis of the times of maximum Quadrantid activity observed over more than a century. They found a steady advance in the time of the maximum, at a slightly slower rate than that implied here, with random fluctuations apparently superimposed. The time of maximum obtained here lies almost exactly on their straight-line approximation of the advance. Their work, which also includes a revised presentation of Prentice's data, is published in preliminary form as "The regression of the node of the Quadrantid meteor stream", Interim Report 17, Feb. 1957, under Contract AF 19(122)–458, Subcontract 57, by the Meteor Department of Harvard College Observatory, Harvard University; it is now in press, Contributions of the Meteoritical Society of America, "Meteoritics", 1957.

error in the theory, and any serious discrepancy between the individual observations and the smooth curve in these figures due to such a cause, should also appear symmetrically and should repeat on successive days. Those discrepancies which do exist do not lend themselves to ready interpretation on this basis, with the previously-mentioned exception at times of upper transit.

It is now apparent that the forward-scatter technique provides a new and reasonably accurate tool for determining the variation in the intrinsic strengths of meteor showers. Its particular advantage lies in its ability to provide relevant data for almost the whole of the time that a shower is incident above the horizon, a fact which is of great importance in the case of short-lived showers. Since the whole variation can be traced out each year, it is possible to compare the strengths of short-lived showers from year to year. This was not possible with the visual method, of course, since it required several years' data to produce a single variation curve.

The only limitation to the value of this technique occurs if the radiant passes close to the vertical plane containing the transmitter and receiver, for then the number of detected signals is expected to fall to zero. Even this limitation can be overcome by the use of two scatter paths, differently oriented, such as those which have now been installed in western Canada by the Radio Physics Laboratory.

The advantages of the forward-scatter technique can be obtained with back-scatter, provided omnidirectional antennas are employed. The discrepancies between the variation found in the present work and that found by Millman and McKinley are certainly striking, but it must be remembered that the results refer to different years. Future measurements, in a cooperative back- and forward-scattering program, may be expected to resolve the discrepancies and provide detailed information on variations in shower strengths.

Observations are continuing on three forward-scatter paths, which will provide triple-checks, and data for a number of short-lived showers will be analyzed in due course.

ACKNOWLEDGMENTS

The authors are indebted to Mr. J. Brown for maintenance of the recording system, and to personnel of R.C.A.F. Station, Greenwood, N.S., for maintenance of the transmitter.

REFERENCES

ESHLEMAN, V. R. 1952. Electronics Research Laboratory, Stanford University, Palo Alto, California, Tech. Rept. No. 49.
ESHLEMAN, V. R. and MANNING, L. A. 1954. Proc. Inst. Radio Engrs. **42**, 530.
FORSYTH, P. A., HINES, C. O., and VOGAN, E. L. 1955. Can. J. Phys. **33**, 600.
FORSYTH, P. A. and ROLFE, W. 1955. Radio Physics Laboratory, Defence Research Board, Ottawa, Ontario, Project Report 12-1-8.
FORSYTH, P. A. and VOGAN, E. L. 1955. Can. J. Phys. **33**, 176.
HAWKINS, G. S. and ALMOND, M. 1952. Monthly Notices Roy. Astron. Soc. **112**, 219.
HINES, C. O. 1955. Can. J. Phys. **33**, 493.
LOVELL, A. C. B. 1954. Meteor astronomy (The Clarendon Press, Oxford).
MILLMAN, P. M. and MCKINLEY, D. W. R. 1953. J. Roy. Astron. Soc. Can. **47**, 237.
PORTER, J. G. 1952. Comets and meteor streams (Chapman & Hall, Ltd., London).
PRENTICE, J. P. M. 1940. Brit. Astron. Assoc. J. **51**, 19
——— 1953. Brit. Astron. Assoc. J. **63**, 175.

STRUCTURE OF THE FUNDAMENTAL INFRARED BAND OF HYDROGEN IN PRESSURE INDUCED ABSORPTION[1]

H. P. GUSH,[2] A. NANASSY, AND H. L. WELSH

ABSTRACT

The doublet structures observed by Coulon, Galatry, Robin, and Vodar (1955) in the Q_P and $S(1)$ components of the pressure-induced fundamental infrared band of hydrogen have been reinvestigated under various conditions of temperature and pressure. It is concluded that the structures can be interpreted in terms of kinetic energy interactions which have already been shown to give rise to the main components, Q_P and Q_R, of the Q branch.

INTRODUCTION

The fundamental infrared absorption band of hydrogen, induced by intermolecular forces, has been studied extensively in the pure gas and in mixtures with foreign gases at pressures up to 5000 atm. (Crawford, Welsh, MacDonald, and Locke 1950; Chisholm, MacDonald, Crawford, and Welsh 1952; Chisholm and Welsh 1954; Hare and Welsh 1957). The band consists of a broad Q component, corresponding to a purely vibrational transition of the hydrogen molecule, and weaker $S(0)$ and $S(1)$ components, for which the vibrational transition is accompanied by the rotational transitions $J = 0 \rightarrow J = 2$ and $J = 1 \rightarrow J = 3$, respectively. The Q branch is split into two components, Q_P and Q_R, the separation of which increases with the density of the perturbing gas from a finite value, obtained by extrapolation, at zero density. The splitting has been interpreted as arising from the participation of the relative kinetic energies of the collision partners and of the surrounding molecules in the absorption process.

A recent investigation with somewhat higher dispersion by Coulon, Galatry, Robin, and Vodar (1955) has shown what appears to be a doublet structure in the Q_P and $S(1)$ components. In these experiments the hydrogen gas had a density of about 90 Amagat units and a temperature of 140° C. They interpreted the structure in the Q_P branch as the superposition of two absorption components, $Q(3)$ and $Q(4)$, on the normal Q_P absorption. The additional absorptions are considered to be due to the induced dipole in an isolated molecule (i.e., not part of a collision pair), situated in the electric field of the induced moments of the neighboring collision pairs.

This explanation must be considered unsatisfactory from several points of view; however, the published experimental data are insufficient to decide between various alternative hypotheses. In the present investigation the effect has been studied under different conditions of temperature and pressure in pure hydrogen and in mixtures with foreign gases in an attempt to arrive at a more convincing interpretation.

[1]Manuscript received February 19, 1957.
Contribution from the McLennan Laboratory, University of Toronto, Toronto, Canada.
[2]Holder of a National Research Council of Canada Scholarship, 1954–1956.

EXPERIMENTAL

The absorption cell for high pressures, shown in Fig. 1, is of the transmission type and provides a light path of 30 cm. The main body of the cell, *A*, is a steel cylinder, 4 in. in diameter, with a central bore $\frac{1}{2}$ in. in diameter. Windows of fused quartz, 1 in. in diameter and $\frac{1}{2}$ in. thick, are cemented to the hardened steel lens rings, *E*, which are forced against shoulders in the cell body by

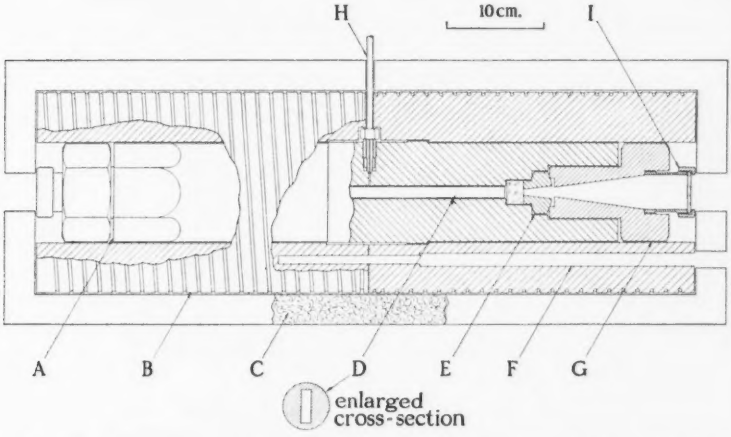

FIG. 1. The high pressure, high temperature absorption cell. *A*—cell body; *B*—aluminum heating jacket; *C*—insulation; *D*—light guide; *E*—lens ring and window; *F*—platinum resistance thermometer; *G*—retaining nut; *H*—inlet tube; *I*—auxiliary window.

heavy nuts, *G*, to make a pressure seal. A polished steel light guide, *D*, with a rectangular cross section, 1 mm. by 5 mm., is fitted into the central bore of the cell; this reduces the volume of the high pressure gas and still permits a cone of radiation of large aperture to pass through the cell by multiple reflections.

The cell is heated by a thick-walled aluminum cylinder, *B*, on the outside of which is wound an electrical heating element with a power rating of 1 kw. Auxiliary windows, *I*, mounted on the cell nuts, *G*, prevent air circulation from cooling the pressure windows. A platinum resistance thermometer deeply embedded in the recess, *F*, in the aluminum cylinder acts as the sensing element for a temperature control system of conventional design. The temperature can be maintained constant to within $\pm 0.5°$ C. at any required value between room temperature and 200° C.

The gases, of commercial grade, were passed through liquid-air traps to remove oil and water-vapor impurities. They were compressed with a hand-operated gas compressor, and the pressures were measured with Bourdon gauges calibrated with a pressure balance. The densities of the gases were calculated from the isothermal data of Michels and Goudeket (1941); Michels, Wijker, and Wijker (1949); and Michels, Wouters, and de Boer (1934, 1936).

The absorption spectra were obtained with a modified Perkin Elmer 12B spectrometer equipped with a LiF prism and a cooled PbS detector; the spectral slit width was 6 cm.$^{-1}$ in the region of the hydrogen fundamental.

RESULTS AND DISCUSSION

The essential experimental data are presented graphically in Figs. 2, 3, and 4, as absorption profiles of the hydrogen fundamental under various experimental conditions. In Fig. 2 the Q branch for pure hydrogen at 150° C.

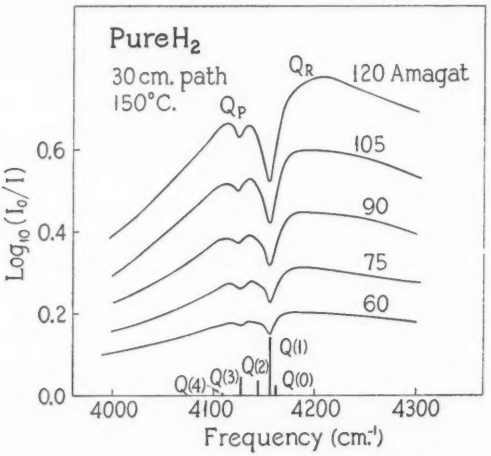

FIG. 2. The fundamental absorption of compressed hydrogen at 150° C. in the frequency region of the Q_P and Q_R branches showing the splitting of the Q_P branch. The Q branch as observed in the Raman effect is shown below the contours.

is plotted for a series of densities in the range 60 to 120 Amagat units. The main splitting of the Q branch into Q_P and Q_R components increases with increasing density as has been observed previously. The finer splitting of the Q_P branch, observed by Coulon *et al.* (1955), is also evident. At a density of 90 Amagat units the frequencies of the maxima in the Q_P branch are 4135 and 4112 cm.$^{-1}$, in fair agreement with the values 4130 and 4110 cm.$^{-1}$ given by Coulon *et al.* at roughly the same temperature and density. A close examination indicates that the maxima show some change in frequency and relative intensity as the density changes. *However, the minimum between the two maxima remains at fixed frequency, 4125 cm.$^{-1}$, for all densities.* The vertical lines drawn on the frequency scale in Fig. 2 show the frequencies of the components, $Q(J)$, of the Q branch as they are observed in the Raman effect (Cumming 1952); the heights of the lines represent the relative intensities calculated for a temperature of 150° C. The components $Q(J)$ are of course separated from one another by the rotation-vibrational interaction. The identification of the two maxima in the Q_P branch with $Q(3)$ and $Q(4)$, as suggested by Coulon *et al.*, is clearly unsatisfactory from the standpoint both

of the frequencies and of the relative intensities. On the other hand, the minimum corresponds to the Raman frequency, $Q(3)$, at 4125.88 cm.$^{-1}$, just as the main minimum of the Q branch corresponds to the strongest Raman component, $Q(1)$, at 4155.48 cm.$^{-1}$ (Cumming 1952).

In Fig. 3 the profiles of the Q branch are shown for a constant density of hydrogen and three different temperatures, 25°, 75°, and 150° C. The total

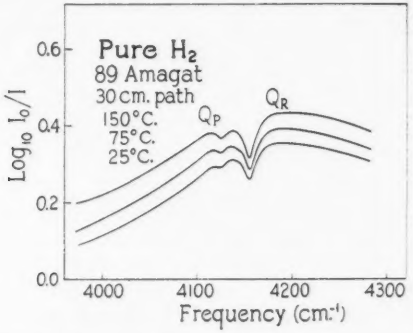

FIG. 3. The fundamental absorption of compressed hydrogen in the frequency region of the Q_P and Q_R branches, at three different temperatures.

absorption increases slightly with increasing temperature, as observed by Chisholm and Welsh (1954). The absorption maxima in the Q_P branch show some changes as the temperature is varied; however, the minimum remains at a fixed frequency, 4125 cm.$^{-1}$, that is, the frequency of $Q(3)$. The minimum is less pronounced at the lower temperatures; also in this respect it shows a correspondence with the $Q(3)$ Raman line, which, since it originates in the first excited rotational state of orthohydrogen, decreases in intensity as the temperature is lowered.

The effect of argon as a foreign gas is shown in Fig. 4, where the absorption profiles for the whole region of the fundamental at 150° C. are presented. For a density ratio of 1:1 in Amagat units the splitting of the Q_P branch is evident, as is also the splitting of the $S(1)$ line, previously observed by Coulon *et al.* The minimum in the $S(1)$ line occurs at 4711 cm.$^{-1}$, and thus corresponds closely to the Raman frequency, 4713.08 cm.$^{-1}$ (Cumming 1952). When the mixture ratio, H_2: A, is 1:96, the over-all intensity of the band at a pressure of 2000 atm. is approximately the same as for the 1:1 ratio at 150 atm. However, the splitting in both the Q_P and $S(1)$ components disappears entirely at the higher pressure. The greatly increased separation of the Q_P and Q_R components at the higher pressure of the foreign gas can also be noted in Fig. 4. Entirely similar results were obtained with helium and nitrogen as foreign gases.

It is clear that the interpretation proposed by Coulon *et al.* for the splitting of the Q_P component is not valid. Apart from the fact that the electric field due to the induced dipoles in neighboring collision pairs is probably not great

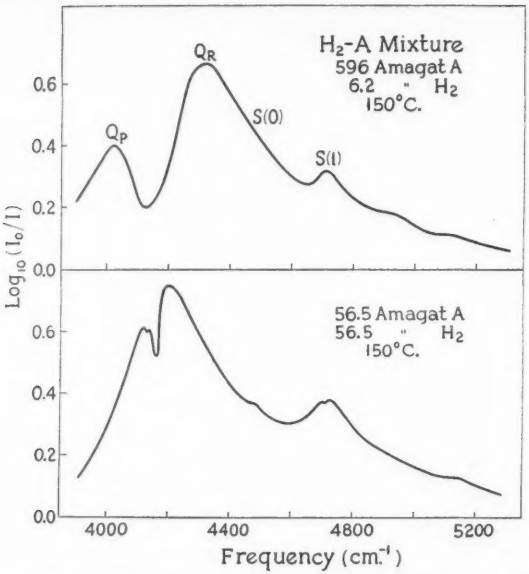

FIG. 4. The fundamental absorption of hydrogen in an argon–hydrogen mixture for two different mixture ratios.

enough to produce an induced absorption in an isolated molecule, similar to that observed by Crawford and Dagg (1953) in a static electric field, other objections based on the experimental evidence can be raised. The frequencies of the two maxima in the Q_P branch do not correspond with the Raman values for $Q(3)$ and $Q(4)$, although the frequencies in absorption induced either by collisions or by a static field show scarcely any deviation from the Raman values. The intensity ratio of the two maxima is also not correct for $Q(3)$ and $Q(4)$. However, the fact that the maxima disappear with high pressures of foreign gases is not necessarily incompatible with the hypothesis since the number of "isolated" hydrogen molecules is greatly reduced.

To arrive at a more satisfactory explanation it is necessary to recall the interpretation of the main splitting of the Q branch into Q_P and Q_R components (Chisholm and Welsh 1954). The greater part of the intensity of the Q branch derives from the dipole moment induced in the collision pairs by overlap forces, the longer range quadrupole forces contributing perhaps only 10% of the intensity (van Kranendonk and Bird 1952). The induced dipole is directed along the line joining the two colliding molecules. As the two molecules move past one another in close collision, the induced dipole rotates and the collision pair assumes a certain angular momentum which depends on the impact parameter. The splitting of the Q branch in the region of lower densities can then be explained by assuming that this angular momentum can change during the absorption process, so that the vibrational transition of the hydrogen

molecule is accompanied by an increase or decrease in the relative kinetic energy of the collision pair. The observed Q branch is consequently not a sharply defined line at the vibrational frequency, but is a broad feature with two maxima similar in shape to a Bjerrum double band in the infrared spectrum of a diatomic molecule. It is not a strict Bjerrum double band, however, since the closest distance of approach, which defines the effective B value of the rotating pair at the time of absorption, is not the same for all collisions; furthermore, the short duration of the collision gives the fundamental frequency of absorption a wide frequency spread. Thus, the two components, Q_P and Q_R, would not be expected to show a "rotational" fine structure even with high spectrographic resolution.

The significant point to consider for the present purpose is that *each one* of the components of the Q branch, $Q(0)$, $Q(1)$, $Q(2)$ . . . , has a profile similar to a Bjerrum double band, and that the composite profile of the Q branch is the sum of these overlapping individual profiles properly weighted to take into account the populations of the various rotational states, $J = 0, 1, 2, \ldots$, of the hydrogen molecule. For normal hydrogen at room temperature the level $J = 1$ is by far the most highly populated, so that the Bjerrum profile of the intense $Q(1)$ component dominates the absorption contour and forms the major part of the intensity of the Q_P and Q_R branches. This accounts for the fact that the minimum between the Q_P and Q_R components occurs at 4155 cm.$^{-1}$, the frequency of the $Q(1)$ transition, rather than at 4160 cm.$^{-1}$, the frequency of the band origin. It is now clear that the splitting of the Q_P branch can be accounted for by the kinetic energy splitting of the $Q(3)$ component, the minimum of which lies directly under the maximum of the main Q_P for the lower range of pressures. The minima corresponding to $Q(0)$ and $Q(2)$, the only other components which have appreciable intensity, can be assumed to disappear because of the nature of the overlapping.

The explanation can be put on a more quantitative basis by the construction of a synthetic profile for the Q branch as has been done for hydrogen at a density of 120 Amagat units and 150° C. in Fig. 5, and 25° C. in Fig. 6. A profile for $Q(1)$ was assumed; this was taken to be similar to the total Q branch profile but with a slightly sharper and deeper minimum. This profile was scaled down to the appropriate relative intensities for $Q(0)$, $Q(2)$, and $Q(3)$, as given by the populations of the rotational levels at the temperature in question. Each curve was then shifted in frequency to correspond to the transition involved, and the four curves were added. The agreement between the synthetic and observed profiles for the two temperatures is excellent. It is apparent that the change in the structure of the Q_P component as the temperature is lowered is caused in the main by the decrease in the population of the $J = 3$ level.

The disappearance of the splitting when the pressure of the foreign gas is increased is consistent with the explanation given. At high gas densities the main maxima Q_P and Q_R become more diffuse and spread further apart as the kinetic energies of neighboring molecules at van der Waals distance also

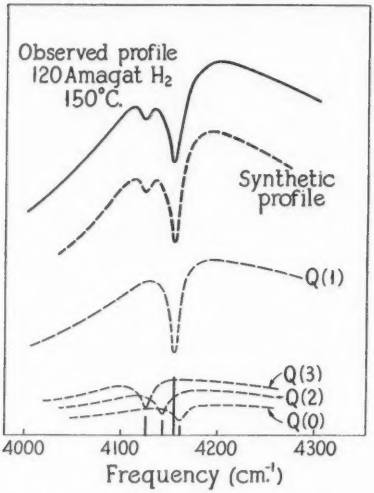

FIG. 5. The construction of a synthetic profile for the hydrogen Q branch at 150° C. The profiles $Q(0)$, $Q(1)$, $Q(2)$, $Q(3)$, are summed to give the synthetic profile.

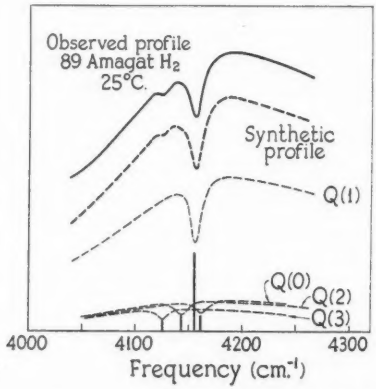

FIG. 6. The construction of a synthetic profile for the hydrogen Q branch at 25° C.

participate in the absorption process (Chisholm and Welsh 1954). This wider splitting also occurs in each of the components $Q(0)$, $Q(1)$, $Q(2)$ . . . , but the overlapping is so extensive that the splitting of the weaker components, including $Q(3)$, is no longer observable in the composite pattern.

The splitting of the $S(1)$ line was interpreted by Coulon *et al.* (1955) as a kinetic energy interaction similar to that which produces the two main components of the Q branch. This explanation is undoubtedly correct but can be slightly elaborated. The S lines arise mainly from the dipole moment

induced by quadrupole interactions (van Kranendonk and Bird 1952). Since the quadrupole forces have a longer range than the overlap forces, the effective B value of the collision pair is smaller for the quadrupole effect. The splitting of the S lines should therefore be less than that of the Q branch, if the interaction of the kinetic energy is assumed to take place mainly through the rotation of the collision pair. The observed splitting is 25 cm.$^{-1}$ as compared with 80 cm.$^{-1}$ for the Q branch under the same experimental conditions. On the other hand, the splitting of the $S(1)$ line may well be due to the small overlap contribution to the intensity of the line, the profile of the overlap component being essentially the same as for the Q branch; however, since this component is superimposed on a much stronger quadrupole component, presumably unsplit, the apparent splitting is less than for the Q branch. Since the S lines persist as comparatively sharp lines to very high densities (Hare and Welsh 1957), it is probable that the kinetic energy interactions are very small for the quadrupole effect; the second explanation given for the splitting of the $S(1)$ line is therefore to be preferred.

ACKNOWLEDGMENTS

The authors are greatly indebted to Professor J. C. Strijland for advice and assistance in the course of this investigation. They also gratefully acknowledge the financial assistance of the National Research Council.

REFERENCES

CHISHOLM, D. A., MACDONALD, J. C. F., CRAWFORD, M. F., and WELSH, H. L. 1952. Phys. Rev. **88**, 957.
CHISHOLM, D. A. and WELSH, H. L. 1954. Can. J. Phys. **32**, 291.
COULON, R., GALATRY, L., ROBIN, J., and VODAR, B. 1955. J. phys. radium, **16**, 728.
CRAWFORD, M. F. and DAGG, I. R. 1953. Phys. Rev. **91**, 1569.
CRAWFORD, M. F., WELSH, H. L., MACDONALD, J. C. F., and LOCKE, J. L. 1950. Phys. Rev. **80**, 469.
CUMMING, C. 1952. Ph.D. Thesis, University of Toronto, Toronto, Ont.
HARE, W. F. J. and WELSH, H. L. 1957. To be published.
VAN KRANENDONK, J. and BIRD, R. 1952. Physica, **17**, 953, 968.
MICHELS, A. and GOUDEKET, M. 1941. Physica, **8**, 347.
MICHELS, A., WIJKER, H., and WIJKER, H. K. 1949. Physica, **15**, 627.
MICHELS, A., WOUTERS, H., and DE BOER, J. 1934. Physica, **1**, 587.
——— 1936. Physica, **3**, 585.

THE EFFECT OF PRESSURE ON THE ELECTRICAL RESISTANCE OF RUBIDIUM[1]

J. S. DUGDALE AND J. A. HULBERT[2]

ABSTRACT

By using helium in both the solid and the fluid state as a pressure-transmitting medium, it has been possible to measure the resistance of rubidium over the temperature range from 2° K. to room temperature at pressures up to 2500 atmospheres. In particular the effect of pressure on the transition at ~200° K., on the low temperature ideal resistivity, and on the residual resistivity was examined.

INTRODUCTION

Until recently there have been scarcely any measurements on the effect of volume change on the electrical resistance of materials at very low temperatures. Fischer (1930) made measurements on some metals down to liquid hydrogen temperatures at pressures up to about 150 atm. Bridgman (1932) made measurements down to liquid oxygen temperatures up to 7000 atm. pressure using a gaseous transmitting medium. Sizoo and Kamerlingh Onnes (1925) studied superconductivity under small pressures and since then there has been considerable work on the change with pressure of the superconducting transition temperature. Hatton (1955), using solid hydrogen as the pressure-transmitting medium, has measured changes of residual resistance under pressures up to 5000 atm. in the helium temperature range. For further references, the reader is referred to a recent review by Lawson (1956) of the effects of hydrostatic pressure on the resistivity of metals.

Because of the great theoretical interest in the alkali metals we wished to make measurements on the properties of this group of metals over a wide temperature range under pressure. Pressure measurements of the resistance of these metals have hitherto been confined to the neighborhood of room temperature and above. The present apparatus is designed for measuring electrical resistance down to low temperatures (~2° K.) under moderately high pressures (up to 3000 atm.). With such a temperature range available, it now becomes possible to determine (assuming Matthiessen's rule) the effect of pressure both on the residual resistivity and on the "ideal" thermal component of resistance of the same specimen.

At low temperatures and under sufficient pressure all substances become solid so that a major problem of studying pressure effects at low temperatures is to find a suitable pressure transmitting medium. We have chosen helium since at a given pressure it retains its ideal fluid properties to a lower temperature than any other substance. Furthermore even in the solid state it is a useful pressure medium. In the pressure range with which we are concerned

[1]Manuscript received February 14, 1957.
Contribution from the Division of Pure Physics, National Research Council, Ottawa, Canada.
Issued as N.R.C. No. 4335.
[2]National Research Laboratories Postdoctorate Fellow; now at Radar Research Establishment, Malvern, England.

the equation of state of the solid is known (Dugdale and Simon 1953); it shows that at constant density, the pressure in the solid is only weakly temperature dependent. This means (*a*) that, if the temperature and density are known, the pressure in the solid can be deduced and (*b*) that, after applying the pressure at such a temperature that the helium is fluid, the system can be cooled at constant volume to the working temperature without serious loss of pressure. To show this, we give in Table I the pressures applied in the fluid state at the solidification point and the corresponding pressure in the solid after it has been cooled at constant volume to 2° K. About one-quarter of the pressure is lost in each case.

TABLE I

Filling pressure, atm.	Solidification temperature, ° K.	Pressure in solid at 2° K.
3000	28.3	2300
2500	25.2	1900
2000	21.9	1500
1500	18.2	1100
1000	14.1	730
500	9.1	350

THE APPARATUS

The pressure bomb, *A* (see Fig. 1), made of beryllium copper hangs from its high pressure input tube, *B*, inside an evacuated vessel, which itself is immersed in either liquid helium or liquid nitrogen contained in a glass dewar. A copper braid (not shown) is soldered at one end to a point on the tube about 30 cm. from the bomb and at the other end to the wall of the vacuum space. This serves to divert some of the heat flux down *B* to the helium or nitrogen bath. Helium exchange gas may be introduced into the vacuum space, *C*, to provide thermal contact with the refrigerant liquid and so cool the bomb; the temperature of the bomb may be raised by means of a constantan heater wound on the outside.

The specimen temperature is determined by either a platinum or a carbon resistance thermometer (*D* and *E*) mounted on the top of the bomb cap and shielded from external radiation by a copper screen.

The pressure-seal between the bomb and cap is made with a hardened steel lens ring, *F*. A seal which is reliable down to helium temperatures, and to pressures of helium up to 4000 atm., is achieved by using a ring of tool steel (e.g., Vasco "Speedcut"), hardened to 45–50 Rockwell "C". The contacting surfaces of the ring are ground to be accurately conical with an included angle of 60° and bear against the slightly chamfered square edges of the bomb body and cap. The high pressure input tube, a length of Aminco chrome–molybdenum steel (o.d. 1/4 in., i.d. 1/16 in.), is screwed and soft-soldered into the cap of the bomb. Occasional failures of this seal were ended by the application of a soldered, perforated soft copper disk to the inside of the seal.*

*This method was originally due to Mr. C. Chase of the Jefferson Laboratory of Harvard University. We are indebted to Dr. W. Paul of that laboratory for drawing our attention to it.

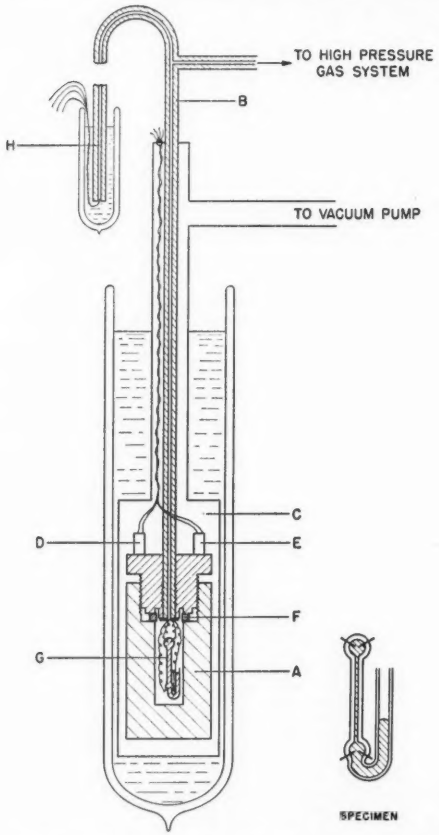

FIG. 1. Diagram of the apparatus for studying resistance under pressure over a wide temperature range (see text). Inset: rubidium specimen holder in soft glass with platinum electrodes.

The all-copper current and potential leads to the specimen, *G*, are introduced down the high pressure tube, entering through a frozen silicone oil seal contained in a side arm, *H*. Such a seal of oil kept frozen in liquid nitrogen has proved very satisfactory.

The high pressures are generated by an oil press and the pressure is transmitted to the helium gas through what is in effect a mercury-filled U-tube. The mercury separates the oil from the gas and thus prevents contamination of the helium. The dead volume in the high pressure part of the apparatus is kept to a minimum (about 4 cc.) in order to reduce the time required to reach the highest pressure and to minimize explosion dangers from the compressed gas.

The pressures were measured with a conventional Bourdon gauge to an accuracy of about 1%.

THE SPECIMENS

The rubidium specimens were of the form shown in the figure (inset to Fig. 1). The container was of soft glass with platinum electrodes and was filled with rubidium under high vacuum. For most specimens the capillary had an inner diameter of 1 mm. and an approximate length of 5 cm. between the electrodes; for one sample, however, a capillary of 0.1 mm. diameter was used. The use of glass capillaries in pressure experiments is not entirely satisfactory even with materials as plastic as rubidium. Nevertheless because rubidium is such a highly reactive substance this has so far proved the only successful way of mounting a specimen of this element in the apparatus.

We assume that, since the deformation of the glass by the pressure (which acts both internally and externally on the specimen holder) is negligible, we are measuring resistivity directly as a function of pressure. In other words we assume that the dimensions of the specimen, which are determined only by the glass container, do not change appreciably with pressure.

ELECTRICAL MEASUREMENTS

The resistance of the platinum thermometer was measured by means of a potentiometer and the specimen resistance by a galvanometer amplifier (MacDonald 1947).

THE EXPERIMENTAL RESULTS

Measurements were made of electrical resistance over the entire range from helium temperatures to room temperature, in general at three different pressures (approximately 100, 1500, and 2500 atm.). Before the pressure effects are considered, the low pressure behavior of the resistance of rubidium as a function of temperature will be briefly discussed. Fig. 2 shows four examples of this behavior taken from the present measurements.*

Sample 1 is a rubidium specimen contained in a capillary of 0.1 mm. bore. The residual resistivity ratio $R_{0°K.}/R_{273°K.}$ was estimated from helium temperature measurements to be 1.3×10^{-2}.

Sample 2 was from the same batch of rubidium measured this time in a capillary of 1 mm. bore; its residual resistance ratio was 1×10^{-2}.

Sample 3 was prepared from rubidium chloride to be especially pure but in fact it was heavily oxidized. Its residual resistance ratio estimated from measurements down to nitrogen temperature only was $R_{0°K.}/R_{260°K.} = 3.8\times10^{-2}$. (We use R_{260} for reasons explained below.) It was contained in a 1 mm. bore tube.

Sample 4 was a further specimen in a wide bore tube (1 mm.) with a residual resistance ratio of just less than 1×10^{-2}.

(The material for all these samples except that of number 3 was obtained from Messrs. A. D. Mackay, New York.)

It is at once evident that the resistive behavior, particularly above about 200° K., varies from specimen to specimen.

*These measurements were made, for convenience, at helium cylinder pressure (about 100 atm.). This pressure changes the resistance by rather less than 1% of its value.

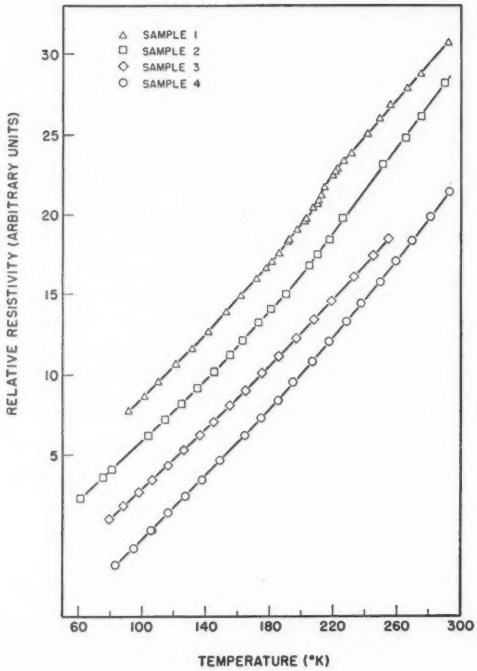

FIG. 2. The relative resistance of four rubidium samples as a function of temperature at low pressures (approximately 100 atm.). The resistances have been normalized to agree at 150° K. and then separated by intervals of 2 units to avoid overlapping.

MacDonald (1952) found an anomaly in the resistance of rubidium at about 180° K. and the present samples (except number 3) show this anomaly in various forms. In samples 1 and 2, the effect is quite evident, but in sample 4 the anomalous behavior takes the form of a gradual deviation from linearity with temperature which begins to be evident at about 150° K. Samples 1 and 2 showed marked thermal hysteresis in the neighborhood of the anomaly (cf. MacDonald 1952), the resistance measured with falling temperature being above that measured with rising temperature. To simplify the diagram only the falling temperature curves are shown here.

Sample number 3, which was heavily oxidized, shows little sign of the anomaly. (Its behavior is not shown above 260° K. since at this temperature premelting begins in this oxidized specimen and the resistance increases rapidly.) Other experiments in this laboratory (Hedgcock 1956) confirm that in highly oxidized rubidium the anomaly seems to be suppressed.

In addition to the work already referred to, Kelly and Pearson (1955) have investigated the anomaly in detail but at present its origin is still obscure.

PRESSURE EFFECTS

The isothermal change in resistance with pressure was measured in the neighborhood of room temperature on samples 1 and 2. As might be expected with such a fine capillary the change in resistance of sample 1 for a given pressure was appreciably lower than that in sample 2. Even with sample 2 the resistivity change at 2500 atm. was about 10% smaller than that deduced from Bridgman's measurements (Bridgman 1946) at higher pressures. (Bridgman's measurements refer to relative *resistance* changes of a given sample and have to be transformed into *resistivity* changes using the compressibility.) This difference is presumably due to the fact that we are using specimens melted into capillaries. The present experiments serve nevertheless to demonstrate that the general method is convenient and to give at least a qualitative picture of the pressure dependence of resistance down to very low temperatures.

In describing these results, it is convenient to divide the temperature range as follows:

(1) measurements between 50° K. and room temperature,

(2) measurements between 4° K. and 50° K.,

(3) measurement of the residual resistance.

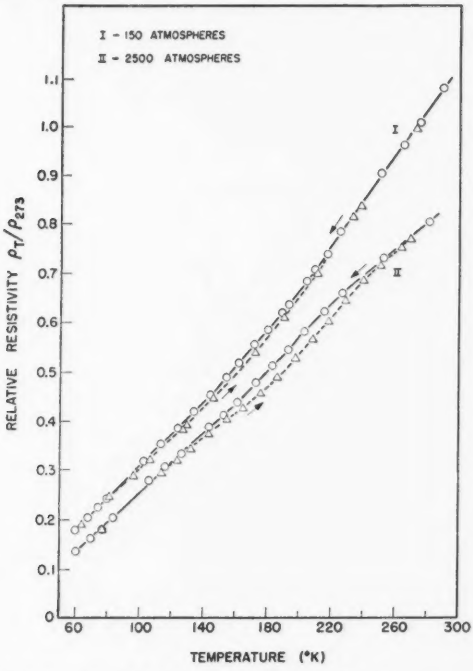

FIG. 3. The resistivity of a rubidium sample (sample 2) at two pressures in the higher temperature range.

(1) Fig. 3 shows the resistance of rubidium (sample 2) at two pressures (100 and 2500 atm.) in the temperature range around the anomaly, illustrating also the thermal hysteresis effects. It appears that because of temperature hysteresis and because the anomaly has no very well defined temperature it is impossible to judge from Fig. 3 whether the temperature of the anomaly is changed by pressure. However, the measurements on sample 1, for which the anomaly is more clearly defined, indicate that if there *is* a change it is certainly small.

The effect of pressure on sample 3 was also measured. It showed a considerably larger pressure coefficient than sample 2.

(2) In the lower temperature range, illustrated in Fig. 4, one sees that the high pressure and low pressure curves cross at about 6° K. This is because although the effect of pressure on the thermal component of resistance is always to lower it, the residual resistance (see below) is raised by pressure.

At about 25° K. helium under 2500 atm. pressure solidifies. Here we have approximately constant volume conditions since the pressure-filling tube is

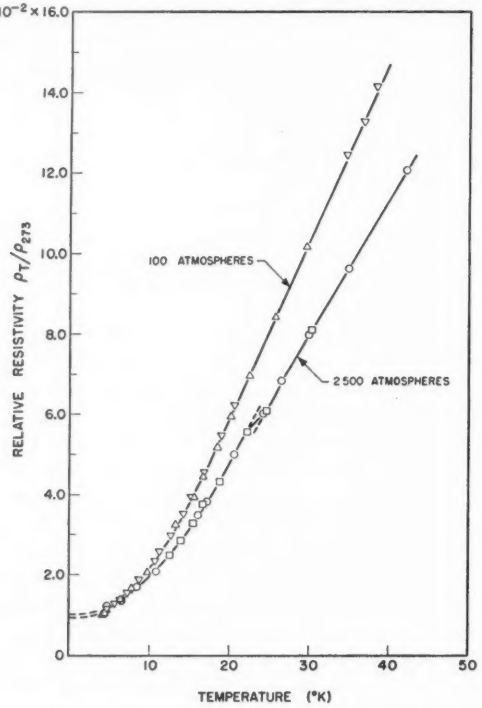

FIG. 4. The relative resistivity of a rubidium sample at low temperatures.

arranged to be slightly colder than the bomb and so freezes first. Thus at 25° K. solidification of the helium begins and it is complete when the temperature has fallen to 22° K. The pressure is now very nearly 2000 atm. (see Dugdale and Simon 1953) and it falls slowly from this value to about 1900 atm. at the lowest temperatures.

Because of the marked pressure changes between 25° and 22° K. the resistance–temperature curve will be correspondingly modified in this temperature region. This is shown in Fig. 4.

After the measurements from nitrogen temperatures down to helium temperatures at three different pressures, the system was returned to its starting conditions at the nitrogen boiling point. The resistance was found to return to its initial value. The results of the low pressure measurements have been compared with values of the resistivity of rubidium obtained by White and Woods (private communication) and were found to agree satisfactorily.

(3) The effect of pressure on the residual resistivity was measured by applying the highest pressure (2500 atm.) at such a temperature (greater than 25° K.) that the helium is fluid and then cooling the system to 2° K. and measuring the resistance. The temperature was next returned to just above 25° K. and the pressure was lowered to 2000 atm. After this the system was again cooled to 2° K. and then the process repeated, the temperature being raised each time to a value sufficient to melt the solid helium before the pressure was lowered. The experimental points are shown in Fig. 5.

From these measurements we deduce a pressure coefficient of residual resistivity of about $+4\%$ per thousand atmospheres for sample 2.

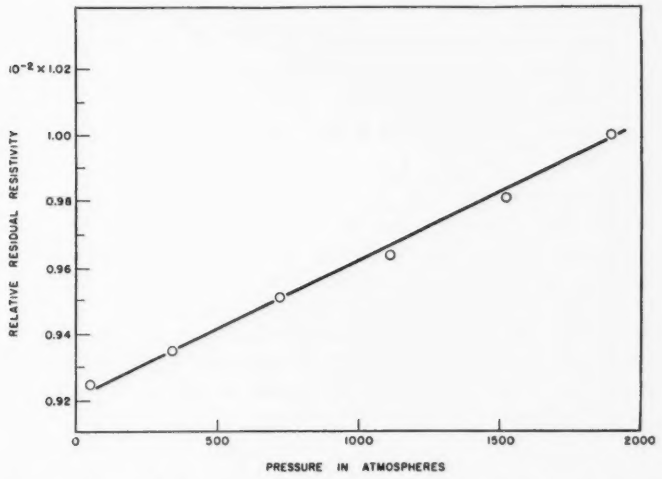

FIG. 5. The residual resistivity of a rubidium sample as a function of pressure.

DISCUSSION

(*a*) *The Thermal Component of Resistance*

A valuable summary of attempts to predict theoretically the effect of volume change on electrical resistivity and of comparisons with existing experimental data has recently been given by Lawson (1956). The main theoretical work on the volume dependence of resistivity at low temperatures is by Mott (1934) and by Grüneisen (1941). In these treatments, the Bloch–Grüneisen expression for the temperature dependence of resistivity was used as a basis for deriving the temperature dependence of the pressure coefficient.

For our present purpose this is not the best approach because the Bloch–Grüneisen theory does not describe at all satisfactorily the temperature dependence of the resistivity at constant volume of rubidium.

Consequently we have made a different comparison with theory. Instead of comparing the pressure coefficients directly, we have here computed the θ-values at several temperatures for two different pressures. The method used was that of comparing the logarithmic derivatives of resistivity with respect to temperature derived from experiment with those deduced from the Bloch–Grüneisen law (Kelly and MacDonald 1953). The results are given in Table II.

TABLE II

Temperature, ° K.	θ (100 atm.)	θ (2500 atm.)
10	45	45
20	58	58
30	63	65
45	50	65
50	46	65
60	50	65

We see thus that, as would be expected, the θ-value at a given temperature is usually increased when the volume is reduced, corresponding to a "stiffening" of the lattice under pressure, but that below about 30° K., although the ideal resistivities are markedly reduced by pressure, the θ-values appear to be unchanged.

(*b*) *The Residual Resistance*

Lenssen and Michels (1935) have discussed from a theoretical point of view the effect of pressure on the residual resistance. On the basis of the assumption that the electrons are truly free and that the scattering cross-section of the scattering centers is independent of volume, they deduce that $d \ln \rho_0 / d \ln V = -\frac{1}{3}$. If, on the other hand, the scattering centers are deformed by pressure in the same way as the dimensions of the specimen, then one deduces that $d \ln \rho_0 / d \ln V = +\frac{1}{3}$. From our measurements on sample II we deduce that for this specimen $d \ln \rho_0 / d \ln V = -1.1$.

ACKNOWLEDGMENTS

We are grateful to Dr. D. K. C. MacDonald for suggesting this investigation and for his interest and encouragement at all times. We also wish to thank

Mr. G. O. C. Paynter for his unfailing technical help, and Dr. D. Gugan for reading the manuscript.

REFERENCES

BRIDGMAN, P. W. 1932. Proc. Am. Acad. Arts Sci. **67**, 305.
——— 1946. The physics of high pressures (G. Bell & Sons, Ltd., London).
DUGDALE, J. S. and SIMON, F. E. 1953. Proc. Roy. Soc. A, **218**, 291.
FISCHER, U. 1930. Z. physik. Chem. B, **8**, 207.
GRÜNEISEN, E. 1941. Ann. Physik, **40**, 543.
HATTON, J. 1955. Phys. Rev. **100**, 681.
HEDGCOCK, F. T. 1956. Can. J. Phys. **34**, 1164.
KELLY, F. M. and PEARSON, W. B. 1955. Can. J. Phys. **33**, 17.
KELLY, F. M. and MACDONALD, D. K. C. 1953. Can. J. Phys. **31**, 147.
LAWSON, A. W. 1956. Progress in metal physics, Vol. 6 (The Pergamon Press, Ltd., London), p. 1.
LENSSEN, M. H. and MICHELS, A. 1935. Physica, **2**, 1091.
MACDONALD, D. K. C. 1947. J. Sci. Instr. **24**, 232.
——— 1952. Phil. Mag. **43**, 479.
MOTT, N. F. 1934. Proc. Phys. Soc. **46**, 680.
SIZOO, G. J. and ONNES, H. K. 1925. Leiden Comms. No. 180*b*.

HIGH RESOLUTION RAMAN SPECTROSCOPY OF GASES

IX. SPECTRA OF H_2, HD, AND D_2 [1]

B. P. STOICHEFF

ABSTRACT

The pure rotational lines and the Q branch lines of the 1–0 vibrational bands of H_2, HD, and D_2 have been photographed with a 21 ft. grating spectrograph. From these spectra, a complete set of constants for the $v = 0$ and 1 levels of all three molecules have been determined. When these constants are combined with Herzberg's results of the forbidden infrared spectra of H_2 and HD they lead to improved values of the electronic ground state constants of H_2 and HD. The leading terms in the Dunham power series expansion of the potential are calculated for H_2 and HD and are found to be mutually consistent. The isotopic relations are obeyed within experimental accuracy, and the small constants D_e, B_e, and H_e are in agreement with values given by theoretical formulae.

A. INTRODUCTION

The first reliable values of the ground state constants for the hydrogen molecule were obtained by Hori in 1927, from an analysis of the Lyman and Werner bands of the electronic spectrum. Shortly thereafter additional information was provided by the Raman spectrum of hydrogen (Rasetti 1929). Since that time extensive spectroscopic data have been collected for H_2 as well as for HD and D_2 and have been used in several determinations of the vibrational and rotational constants (see for example Urey and Teal 1935; Woolley, Scott, and Brickwedde 1948). The Raman spectra have provided data for the $v = 0$ and 1 levels (Rasetti 1929; Bhagavantam 1932; Teal and MacWood 1935) and the electronic spectra have supplied data for the higher vibrational levels (Hyman 1930; Jeppesen 1933, 1934, 1936).

The most recent values of the ground state constants for H_2 are due to Herzberg (1950*a*) and are based primarily on his investigation of the quadrupole absorption spectrum. Herzberg has also given preliminary values for the constants of HD (1950*b*) based on his measurements of the weak infrared spectrum. Both spectra occur in the photographic infrared region where the large wavenumber dispersion and reliable wavelength standards assure measurements of high accuracy. Herzberg observed a total of eight lines in the 2–0 and 3–0 bands of H_2 and 13 lines in the 3–0 and 4–0 bands of HD. Unfortunately, the number of lines was not sufficient to derive all of the rotational and vibrational constants independently, and it was necessary to use the less accurate measurements of the electronic and Raman spectra. Collectively, these data have made possible a fairly accurate determination of the larger and more important constants, for example ω_e and B_e; however, the limited accuracy in wavelength measurements has prevented the direct evaluation of the smaller, yet significant, constants such as D_e and H_e. Up to

[1]Manuscript received January 31, 1957.
Contribution from the Division of Pure Physics, National Research Council, Ottawa, Canada.
Issued as N.R.C. No. 4298.

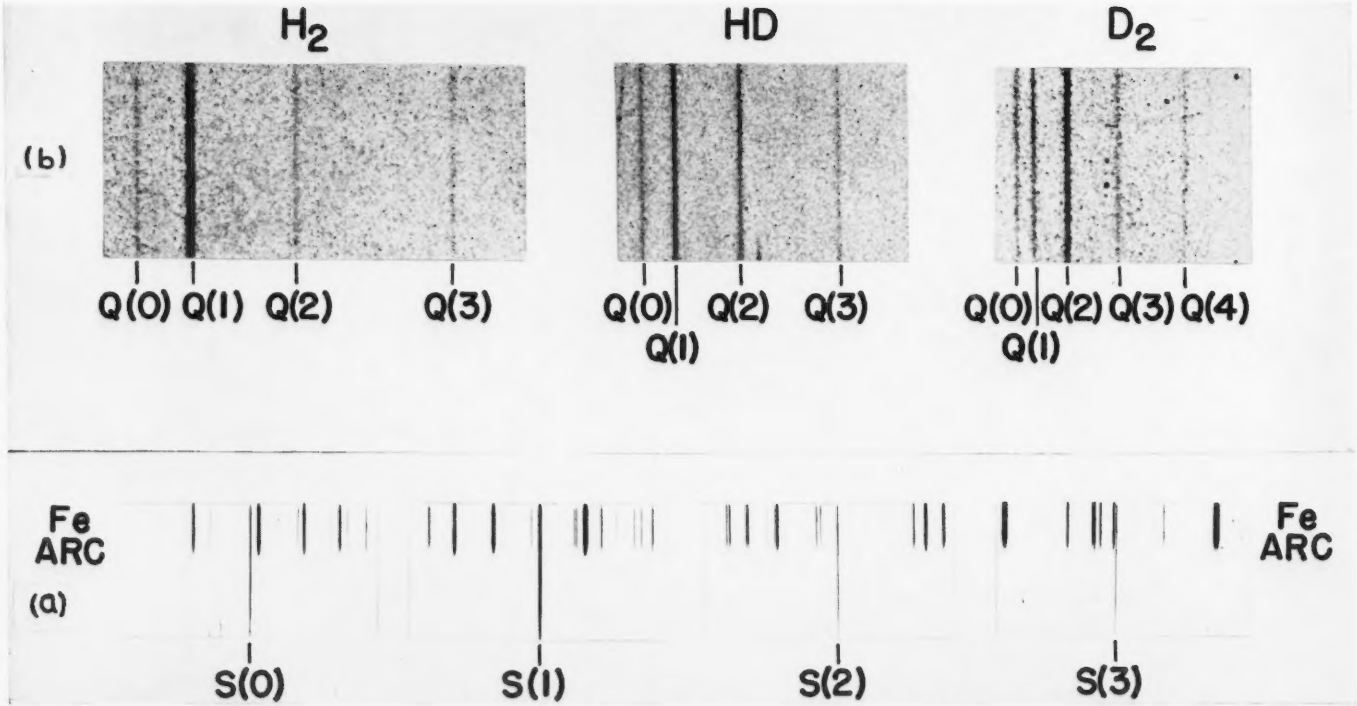

FIG. 1. Raman spectra of H_2, HD, and D_2 photographed in the second order of a 21-ft. grating spectrograph: (*a*) the pure rotational lines (Stokes) of H_2 excited by the Hg 4358.3 line; (*b*) the *Q* branch lines of the 1–0 vibrational bands of H_2, HD, and D_2 excited by the Hg 4046.6 line.

the present time, therefore, it has been necessary to calculate several of these smaller constants from theoretical formulae.

Since the Raman spectra of gases can now be photographed at high resolution, it seemed particularly desirable to repeat the earlier work on H_2, HD, and D_2, in an attempt to obtain more accurate constants for the hydrogen molecules. In the present research, measurements have been made of the pure rotational spectra and of the Q branches of the 1–0 vibrational bands. These results have led to the direct determination of a set of constants for the $v = 0$ and $v = 1$ levels of all three molecules, and, together with Herzberg's data, have yielded revised values for the equilibrium constants of the H_2 and HD molecules in their ground electronic states.

Aside from providing more precise values of the larger constants $\omega_e, B_e, \ldots$, the present experiment has allowed the determination of a more complete set of constants, including values of the relatively small but important constants D_e and H_e. This now makes it possible to check the theoretical formulae for these constants. Also, for the first time it is possible to take into account the corrections to the ground state values of ω_e and B_e proposed by Dunham and Van Vleck and thus to check the isotopic rules and to calculate the true equilibrium internuclear distance of the hydrogen molecule.

B. OBSERVED SPECTRA

In Fig. 1 are shown the pure rotational lines of H_2 and the resolved Q branches of the 1–0 vibrational bands of H_2, HD, and D_2. The spectra were photographed in the second order of the N.R.C. 21-ft. grating spectrograph at a dispersion of 1.2 Å/mm. with the apparatus described in paper I (Stoicheff 1954). Gas pressures of one to two atmospheres were used. The exposure times were 10–36 hours with Kodak 103a–0 photographic plates, and with a slit width of 0.02 mm.

In the pure rotational spectra, four Stokes and two anti-Stokes lines were observed for H_2 while five Stokes and two anti-Stokes lines were observed for each of HD and D_2, all excited by the Hg 4358 line.

In the 1–0 vibrational bands, only the Q branches excited by the Hg 4047 line were observed; unfortunately not one of the S or O rotation–vibration lines appeared on the plates. (The 1–0 band excited by the Hg 4358 line falls in a region of low plate sensitivity, and exposures of 36 hours with Kodak 103a–0, D, F, and J plates failed to show a single line of this band.)

Two plates of each spectrum were obtained. The pure rotational lines of all three molecules were photographed with sufficient intensity to assure the possibility of accurate measurement. It is estimated that each line could be measured to ± 0.02 cm^{-1} or better. Some of the Q branch lines of the vibrational bands, however, were rather weak and difficult to measure; an accuracy of about ± 0.05 cm^{-1} is estimated for these lines. Second- and third-order iron arc lines were used as wavelength standards. The wavelengths of the hydrogen lines were determined in the usual way from a linear dispersion equation and a correction curve. The vacuum corrections of Edlén (1953) were applied, and the wavenumber displacements were obtained using the wavenumbers

24705.350 cm^{-1} and 22938.134 cm^{-1} for the Hg 4046.5630 and Hg 4358.3277 lines respectively (Burns, Adams, and Longwell 1950).

In order to obtain the absolute wavenumber displacements of the Raman lines, any relative shift between the Raman and the iron comparison spectra was corrected in the following way: The average value of the displacements of the Stokes and anti-Stokes $S(0)$ and $S(1)$ rotational lines, $\Delta\nu_{av}$, was determined for each plate. For any one plate, the average value of $\Delta\nu_{av}-\Delta\nu_{Stokes}$ for the $S(0)$ and $S(1)$ lines was then applied as a correction to the remaining Stokes rotational lines and to the lines of the Q branches. Almost identical corrections were found in an alternative way by comparing the wavelengths measured for the three Hg lines λ3125.6681, λ3131.5485, λ3131.8391 (which appear in the third order) and those tabulated by Burns, Adams, and Longwell (1950). These mercury lines appear because of stray light and are photographed simultaneously with the Raman spectrum. The average values of the corrected wavenumber displacements of the Raman lines measured on two plates are listed in Table I. These values were used in the subsequent analysis.

TABLE I

OBSERVED WAVENUMBER DISPLACEMENTS (UNITS cm^{-1}) IN THE RAMAN SPECTRA OF H_2, HD, AND D_2

		H_2			HD		D_2	
Designation		$\lvert\Delta\nu\rvert$	$O-C_1$	$O-C_2$	$\lvert\Delta\nu\rvert$	$O-C_1$	$\lvert\Delta\nu\rvert$	$O-C_1$
Pure rotational spectrum	$S_0(0)$	354.381	−0.010	+0.002	267.086	+0.008	179.056	−0.001
	$S_0(1)$	587.055	+0.013	+0.015	443.081	−0.006	297.521	+0.003
	$S_0(2)$	814.406	−0.006	−0.003	616.089	+0.001	414.655	−0.006
	$S_0(3)$	1034.651	+0.001	+0.005	784.993	+0.002	529.907	+0.003
	$S_0(4)$				948.818	0.000	642.807	−0.002
1–0 vibrational band	$Q_1(0)$	4161.134	−0.003	+0.020	3632.055	+0.002	2993.548	−0.013
	$Q_1(1)$	4155.201	+0.003	+0.002	3628.197	−0.005	2991.446	+0.008
	$Q_1(2)$	4143.387	+0.002	−0.013	3620.511	+0.002	2987.230	+0.022
	$Q_1(3)$	4125.832	0.000	+0.008	3608.992	−0.002	2980.877	−0.022
	$Q_1(4)$						2972.557	+0.006

$O-C_1$ are differences between observed wavenumber displacements and those calculated with the values of constants given in Table II.

$O-C_2$ are differences between observed wavenumber displacements and those calculated with the equilibrium constants given in Section C(*b*).

C. ANALYSIS

(*a*) *General*

The vibrational and rotational energy levels of a diatomic molecule in a $^1\Sigma$ state are given by the equation

$$T(v, J) = G(v)+F_v(J)$$

where

(1) $$G(v) = \omega_e(v+\tfrac{1}{2})-\omega_e x_e(v+\tfrac{1}{2})^2+\omega_e y_e(v+\tfrac{1}{2})^3+\ldots,$$

(2) $$F_v(J) = B_v J(J+1)-D_v J^2(J+1)^2+H_v J^3(J+1)^3+\ldots,$$

and

(3) $B_v = B_e - \alpha_e(v+\frac{1}{2}) + \gamma_e(v+\frac{1}{2})^2 + \ldots,$

(4) $D_v = D_e + \beta_e(v+\frac{1}{2}) + \delta_e(v+\frac{1}{2})^2,$

$H_v \approx H_e \approx H_0 \approx H_1 \ldots$ (for v small).

(5) In eq. (1), $\omega_e = (1/2\pi c)(k/\mu)^{\frac{1}{2}}$ cm^{-1} and in eq. (3), $B_e = h/8\pi^2 c\mu r_e^2$ cm^{-1}, all in the usual notation. For a molecule with nuclear masses M_1 and M_2, $\mu = M_1M_2/(M_1+M_2)$. For the hydrogen molecule, small corrections must be applied to the above molecular constants in order that they have their usual meanings (for example, ω_e and B_e given by eq. (5)), and these corrections are discussed in Section D, below.

The selection rules for Raman scattering are $\Delta J = 0, \pm 2$ and $+ \leftrightarrow +$, $- \leftrightarrow -$, $+ \leftarrow|\rightarrow -$. In the pure rotational spectrum, only transitions with $\Delta J = 2$ give rise to displaced lines, designated as S lines. Their displacements from the exciting line are given by

(6) $$S_0(J) = F_0(J+2) - F_0(J) = (4B_0 - 6D_0 + 27/4\, H_e)(J+3/2) - (8D_0 - 34H_e)(J+3/2)^3 + 12H_e(J+3/2)^5.$$

Thus the pure rotational Raman lines are given in terms of the three constants B_0, D_0, and H_e, and these constants can be determined directly if accurate measurements of at least three rotational lines are available.

The Q lines ($\Delta J = 0$) of a rotation–vibration band can be expressed in an analogous way by

$$Q_v(J) = \nu_{v-0} + (B_v - B_0)J(J+1) - (D_v - D_0)J^2(J+1)^2.$$

When the values of B_0, D_0, and H_e obtained from the rotational spectrum are substituted in these equations (and in similar equations for the rotation–vibration lines with $\Delta J = \pm 2$), the lines of any one band are given in terms of three constants, ν_{v-0}, B_v, and D_v. The values of these constants can then be determined from the solution of the simultaneous equations. Finally, if the constants of a sufficient number of bands have been evaluated, the equilibrium constants can be determined from equations (1), (3), and (4).

(b) Analysis of the H_2 Spectrum

Only four lines of the pure rotational spectrum of H_2 were observed and measured. From these four lines the values of the rotational constants B_0, D_0, and H_e were determined graphically and by the method of least squares. It is, of course, essential to have measurements of high accuracy when evaluating three constants from only four measurements and, as mentioned in Section B, the present measurements are considered to be correct to within ± 0.02 cm^{-1}. The relative consistency of the present results is shown in the graph of Fig. 2 which is based on Eq. (6). In this graph are plotted the values of $S_0(J)/4(J+3/2)$ against $(J+3/2)^2$. The graph is drawn to a large scale by adding the term $0.085(J+3/2)^2$ to $S_0(J)/4(J+3/2)$, which takes out most of the slope. All four points lie very close to a smooth curve. The pronounced curvature in the graph shows that the quartic term is significant and hence

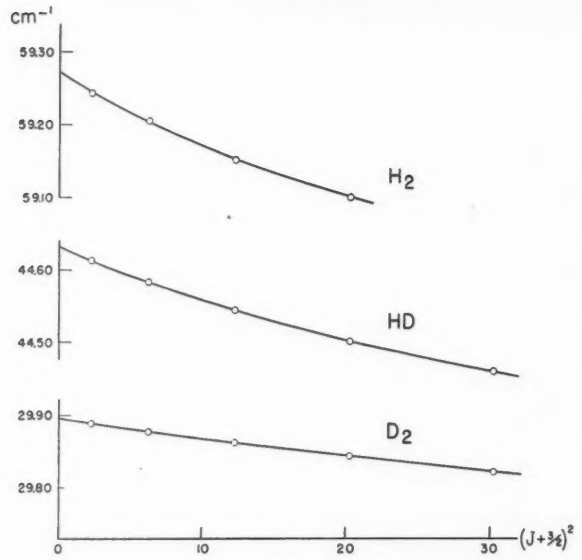

FIG. 2. Graphs of $[S_0(J)/4(J+3/2)]-a(J+3/2)^2$ vs. $(J+3/2)^2$. For H_2, $a = 0.085$; for HD, $a = 0.044$; and for D_2, $a = 0.020$ cm^{-1}.

shows that H_e can be evaluated from the present measurements. From Eq. (6) it is also seen that the constants can be obtained from this graph directly; the intercept on the ordinate axis is $B_0-3/2\ D_0+27/16\ H_e$, while the slope of the graph near $J = 0$ added to 0.085 gives $2D_0$.

The values of B_0, D_0, and H_e obtained by least squares are listed in Table II. These values reproduce the observed displacements of the four lines to

TABLE II

ROTATIONAL AND VIBRATIONAL CONSTANTS OF H_2, HD, AND D_2 FOR LOW VIBRATIONAL LEVELS

Constant (cm^{-1})	H_2				HD		D_2	
	$v = 0$	$v = 1$	$v = 2$	$v = 3$	$v = 0$	$v = 1$	$v = 0$	$v = 1$
B_v	59.339$_2$	56.364$_0$ (56.377$_5$)	53.475$_4$	50.628$_2$	44.667$_8$	42.741$_4$	29.910$_5$	28.848$_2$
D_v	0.0459$_9$	0.0432$_8$ (0.0443$_3$)	0.0427$_7$	0.0412$_5$	0.0259$_2$	0.0255$_8$	0.0113$_4$	0.0107$_2$
H_v	5.2×10^{-5}				2.2×10^{-5}		0.36×10^{-5}	
ν_{v-0}		4161.13$_7$ (4161.12$_9$)	8087.11$_2$	11782.35$_2$		3632.05$_2$		2993.56$_1$
I_0 (10^{-40} g. cm.^{2})	0.47168				0.62660		0.93576	
r_0 (Å)	0.75105				0.74973		0.74820	

within ±0.015 cm^{-1} as shown in Table I under the column designated $O-C_1$. Also listed in Table II are the values of the effective moment of inertia, I_0, and the effective internuclear distance, r_0, for the $v = 0$ level. These values

were calculated from B_0 using the constants of Cohen, DuMond, Layton, and Rollett (1955) and the atomic mass tables of Sègre (1953). In the calculation of r_0, the small contribution of the electrons to the moment of inertia was neglected (see below); also, r_0 is assumed to equal $[(1/r_0^2)_{av}]^{-\frac{1}{2}}$.

In the 1–0 vibration band, four Q branch lines were observed and measured. Again the relative consistency of the measurements was checked and all four lines were used to calculate ν_{1-0}, B_1, and D_1. The values are shown in Table II. In this calculation the values of B_0, D_0, and H_e derived from the rotational spectrum were used, as outlined in the general discussion of the analysis.

The present values of B_0, D_0, and H_e were also used to determine the vibrational and rotational constants of the $v = 2$ and 3 levels from Herzberg's measurements of the 2–0 and 3–0 infrared bands. Consistency checks (analogous to the graphs of Fig. 2 for the rotational lines) were applied and all lines but $S_2(0)$ were used in the analysis. The $S_2(0)$ line was considerably removed from the smooth curve representing the other lines of the 2–0 band. Values of the constants for the $v = 2$ and 3 levels are listed in Table II. These values reproduce the observed line positions to better than ± 0.01 cm^{-1} except for $S_2(0)$, which is observed to lie 0.06_5 cm^{-1} lower than its calculated position.

Finally, the equilibrium constants were calculated from the constants of Table II by least squares. Prior to these calculations, the values of each of the constants, $\Delta G_{v+\frac{1}{2}}$, B_v, and D_v for $v = 0, 1, 2$, and 3 were plotted on large-scale graphs to determine their relative consistency. All the values appeared to be acceptable except D_1, which deviated from the smooth curve drawn through D_0, D_2, and D_3 by 2% of its value. Therefore, D_e, β_e, and δ_e were derived from D_0, D_2, and D_3 only. A value for D_1 was then calculated from these constants. Since even a small change in the value of D_1 affects the value of B_1 to some extent, the calculated D_1 was substituted in the equations for the Q branch lines and new values of B_1 and ν_{1-0} were obtained. These are shown in brackets in Table II. They differ from the constants determined initially from the 1–0 band alone by approximately the estimated errors for the constants of the $v = 1$ level.

The equilibrium constants obtained from the present Raman data of the rotational spectrum and the 1–0 band, and from Herzberg's infrared data of the 2–0 and 3–0 bands, are:

$$G(v) = 4400.39_0(v+\tfrac{1}{2}) - 120.814_8(v+\tfrac{1}{2})^2 + 0.7241_9(v+\tfrac{1}{2})^3 \text{ cm}^{-1},$$

$$B_v = 60.840_7 - 3.0177_4(v+\tfrac{1}{2}) + 0.0285_5(v+\tfrac{1}{2})^2 \text{ cm}^{-1},$$

$$D_v = 0.04684_1 - 0.00170_6(v+\tfrac{1}{2}) + 0.000030_8(v+\tfrac{1}{2})^2 \text{ cm}^{-1},$$

$$H_v = 5.2_1 \times 10^{-5} \text{ cm}^{-1}.$$

The positions of all the lines used in the analysis were calculated from these constants and the deviations from the observed positions were found to be less than ± 0.020 cm^{-1} (O$-$C$_2$ in Table I).

The above value of the rotational constant, $B_e = 60.841$ cm^{-1}, is considered

to have an accuracy better than ± 0.010 cm^{-1} and yields for the equilibrium moment of inertia the value $I_e = (0.46004 \pm 0.00008) \times 10^{-40}$ g. cm.^{2} In calculating the internuclear distance from this value of I_e it is assumed that the moment of inertia can be expressed in the form $I_e = \mu r_e^2 + i$, where μr_e^2 is the contribution from the two point nuclei and i is the contribution from the two valence electrons. Now it is known that the electron cloud in H_2 does not rotate rigidly with the nuclei, but "slips" during the rotation of the molecule (Wick 1933). Thus the electron contribution to the moment of inertia, derived from measurements of the radio-frequency spectrum of H_2 in magnetic fields (Barnes, Bray, and Ramsey 1954), is found to be only 0.27×10^{-44} g. cm.^{2} (Espe 1956), a value which is much smaller than the present experimental error and is neglected here. (The assumption of an electron cloud rotating rigidly with the nuclei leads to a contribution about 30 times this value.) Therefore the moment of inertia determined in the present experiment is simply the product of the reduced mass of the two protons and the square of the distance between them. This yields a value of $r_e = 0.74173 \pm 0.00006$ Å for the equilibrium internuclear distance in H_2. The values of B_e, I_e, and r_e, together with the corrected values (see Section D), are listed in Table III.

TABLE III

EXPERIMENTAL AND CORRECTED VALUES OF THE ROTATIONAL CONSTANT (B_e), MOMENT OF INERTIA (I_e), AND INTERNUCLEAR DISTANCE (r_e) FOR H_2, HD, AND D_2

	H_2	HD	D_2
Experimental value			
B_e (cm^{-1})	60.841	45.638	30.442
I_e (10^{-40} g. cm.^{2})	0.46004	0.61329	0.91943
r_e (Å)	0.74173	0.74173	0.74165
Corrected value			
B_e^* (cm^{-1})	60.910	45.678	30.459†
I_e^* (10^{-40} g. cm.^{2})	0.45951	0.61274	0.91890
r_e^* (Å)	0.74130	0.74140	0.74143

†B_e^* for D_2 is an approximate value; $\gamma_a = -0.00014$ was obtained from provisional equilibrium constants calculated from the values of H_2 and HD using the simple isotopic rules, and $\gamma_b + \gamma_c + \gamma_d = -0.00044$ according to Van Vleck (1936).

(*c*) *Analysis of the* HD *Spectrum*

Five lines were observed and measured in the pure rotational spectrum of HD. An estimate of the relative consistency of the measurements can be obtained from the graph in Fig. 2, where values of $[S_0(J)/4(J+3/2)] - 0.044 \times (J+3/2)^2$ are plotted against $(J+3/2)^2$. Again all five points lie on a smooth curve and can be used in the least-squares calculation of the rotational constants. The curvature of this graph is again quite evident and indicates that H_e is significant. The derived values of B_0, D_0, H_e as well as I_0 and r_0 are given in Table II. Also included in this table are the constants of the $v = 1$ level, calculated from the four Q branch lines of the 1–0 band. As a check, the constants were used to calculate back the positions of all the Raman lines and the deviations from the observed values are within ± 0.010 cm^{-1} ($O - C_1$ in Table I).

As mentioned earlier, the most recent values of the equilibrium constants of HD are given in a preliminary note by Herzberg. Since these values do not reproduce the present Raman measurements satisfactorily, a new set of equilibrium constants was calculated from the combined Raman and infrared data:

$$G(v) = 3811.92_4(v+\tfrac{1}{2}) - 90.711_3(v+\tfrac{1}{2})^2 + 0.4775_9(v+\tfrac{1}{2})^3 \text{ cm}^{-1},$$
$$B_v = 45.637_8 - 1.9500_4(v+\tfrac{1}{2}) + 0.0140_2(v+\tfrac{1}{2})^2 \text{ cm}^{-1},$$
$$D_v = 0.02634_1 - 0.00085_7(v+\tfrac{1}{2}) + 0.000033(v+\tfrac{1}{2})^2 \text{ cm}^{-1},$$
$$H_e = 2.2_4 \times 10^{-5} \text{ cm}^{-1}.$$

The values for $G(v)$ and D_v differ slightly from those of Herzberg but it should be noted that the values for B_v are essentially the same. While the present constants are considered to be an improvement over earlier values, they are tentative only, since current measurements in this laboratory, of the 1–0 and 2–0 infrared bands, may alter these values. However, the present value of B_e is considered to have an accuracy better than ± 0.010 cm^{-1}, as in the case of H_2, and this value was used to calculate the values of I_e and r_e given in Table III.

(*d*) *Analysis of the* D_2 *Spectrum*

An estimate of the relative consistency of the five line measurements in the pure rotational spectrum of D_2 is obtained from the graph in Fig. 2, where the values of $[S_0(J)/4(J+3/2)] - 0.020(J+3/2)^2$ are plotted against $(J+3/2)^2$. The curvature in this graph is considerably smaller than for H_2 and HD but is still noticeable. The constants were again evaluated graphically and by least squares and the values are listed in Table II. These values reproduce the observed displacements of the five lines to within ± 0.010 cm^{-1} (cf. $O-C_1$ in Table I).

The constants for the $v = 1$ level were determined from the five lines of the Q branch and these are included in Table II. At present, measurements of comparable accuracy are not available for any of the overtone bands, so that the evaluation of the ground state constants of D_2 must await future investigations of the quadrupole infrared spectrum or the ultraviolet electronic spectrum. However, reasonable approximations to the equilibrium values of the constants B_e and D_e can be made by a linear extrapolation of the constants determined for the $v = 0$ and $v = 1$ levels. For example, $B_0 - B_1 = 1.0623$ cm$^{-1} \approx \alpha_e$ and $D_0 - D_1 = 0.00059$ cm$^{-1} \approx \beta_e$ and therefore $B_e = 30.442$ cm^{-1} with an estimated error of ± 0.010 cm^{-1}, and $D_e = 0.01164$ cm^{-1}. Values of I_e and r_e calculated from this value of B_e are shown in Table III. Approximate values for all of the equilibrium constants of D_2 can, of course, be obtained from the corresponding constants of H_2 and HD together with the isotopic relationships, but such values would be of limited use and are not included in the present paper.

D. DISCUSSION

Some comment on the estimated accuracy of the new constants is warranted particularly since the calculations are based on the measurement of only four

or five lines for each band. In the pure rotational spectra, the small deviations (± 0.015 cm^{-1}) of the observed and calculated wavenumber displacements ($O-C_1$ in Table I) are an indication of satisfactory accuracy. A further test of the accuracy was obtained by calculating the constants from the line spacings, $S_0(1)-S_0(0)$, $S_0(2)-S_0(1)$, and so on, which are, of course, expressed in terms of B_0, D_0, and H_e. The values of the line spacings have a much larger relative error than the line measurements and yet the constants obtained are almost identical with those listed in Table II. For example, the three line spacings in the spectrum of H_2 give the constants $B_0 = 59.343$ and $D_0 = 0.04604$ cm^{-1} (with H_e assumed to be $5.2_1\times10^{-5}$ cm^{-1}). The four line spacings in HD give $B_0 = 44.668$, $D_0 = 0.02591$, and $H_e = 2.2_3\times10^{-5}$ cm^{-1}, and the four line spacings in D_2 give $B_0 = 29.912$, $D_0 = 0.01137$, and $H_e = 4.04\times10^{-6}$ cm^{-1}. For all three molecules, it is estimated that the values of B_0 are reliable to 0.005 cm^{-1}, the values of D_0 to 0.0003 cm^{-1}, and the values of H_e to 0.5×10^{-5} cm^{-1}. The constants for the 1–0 bands cannot claim as high an accuracy as those for the rotational spectra since the present spectra of the 1–0 bands are weak and difficult to measure. Some improvement in these constants may be expected from measurements of the S and O lines of the 1–0 Raman bands.

Since the literature on the evaluation of the molecular constants of hydrogen is voluminous, no attempt will be made here to compare critically the new values of the constants with the earlier values. Nevertheless, it is desirable to note their substantial agreement, especially since the present values were all determined from experimental measurements, whereas preceding evaluations have been based in part on theoretical formulae. In particular, it should be mentioned that although small differences exist between the new constants of H_2 and those given by Herzberg (1950*a*), the values of B_v agree to within 0.05%. This close agreement of the rotational constants indicates that the conclusions of Ramsey (1952) and Barnes, Bray, and Ramsey (1954) derived from measurements of the nuclear radio-frequency spectra of H_2 and D_2 in magnetic fields, and based in part on Herzberg's constants of H_2 (1950*a*), remain essentially unchanged. However, the present constants may slightly alter some of the magnetic interaction constants determined by Ramsey and his co-workers.

While the new constants are believed to represent an improvement over preceding values for the $v = 0$ and 1 levels of D_2, up to $v = 3$ of H_2, and up to $v = 4$ of HD, they are limited to these low-lying vibrational levels. Further investigations of the electronic spectra with high resolution are desirable for the improvement of these constants and for their extension to higher vibrational levels. Nevertheless, the present constants can be used to determine the shape of the potential curve for low vibrational levels. Dunham (1932) has given the energy levels of a vibrating and rotating molecule, assuming for the potential function a power series in $(r-r_e)/r_e = \xi$, namely

$$U = hca_0\,\xi^2(1+a_1\xi+a_2\xi^2+\ldots).$$

The present values of ω_e, $\omega_e x_e$, $\omega_e y_e$, B_e, α_e, and γ_e permit the calculation of the first five coefficients in this series, giving the following values:

For H_2,

$$a_0 = 79566,\ a_1 = -1.598,\ a_2 = 1.868,\ a_3 = -2.072,\ a_4 = 2.261.$$

For HD,

$$a_0 = 79598,\ a_1 = -1.595,\ a_2 = 1.854,\ a_3 = -2.047,\ a_4 = 2.250.$$

The good agreement in the respective values for H_2 and HD attests to the accuracy and consistency of the new constants. It should be mentioned that a_0 is dependent on the absolute accuracy of wavelength measurements, while the other coefficients are more strongly dependent on the relative accuracy. It can readily be shown that the Morse potential function is not a good approximation for the hydrogen molecule by comparing the corresponding coefficients with the values of a_n obtained here. Even when the curves are fitted at the bottom, that is βr_e (of the Morse function) is equated to $-a_1$ (of Dunham's series), one finds the values $a_2 = 1.489$, $a_3 = -1.020$, $a_4 = 0.561$, etc., which differ markedly from the coefficients of Dunham's series. Other support for the conclusion that the Morse potential is not correct is found in the non-zero Dunham correction to ω_e, discussed below, and in the large discrepancy between the experimental value of α_e and that calculated from a theoretical expression based on the Morse potential (Pekeris 1934).

Theoretical formulae have been derived for the constants D_e, β_e, and H_e by Dunham (1932) in terms of the constants B_e, ω_e, $\omega_e x_e$, and α_e. When the new constants of H_2 are substituted in these formulae, the following values are obtained: $D_e = 0.04652$ cm^{-1}, $\beta_e = -0.00168$ cm^{-1}, and $H_e = 5.02\times10^{-5}$ cm^{-1}. For HD the calculated values are: $D_e = 0.02617$ cm^{-1}, $\beta_e = -0.000780$ cm^{-1}, $H_e = 2.12\times10^{-5}$ cm^{-1}. These are in very good agreement with the new experimental values, the differences being well within the experimental error.

Apart from experimental error, the new constants ω_e, B_e, . . . , can be considered to be reliable values for the equilibrium state only to the extent to which equations (5) are valid. It has been shown by Dunham (1932) and Van Vleck (1936) that for very light molecules such as H_2, HD, and D_2, deviations from these equations arise owing to (*a*) the interaction of rotation and vibration, (*b*) the interaction of electronic and nuclear motions, (*c*) *L*-uncoupling, and (*d*) the interaction of electronic states of the same Λ value. Thus small corrections must be applied to the coefficients of equations (1), (2), (3), and (4) in order to obtain the "true" constants for the equilibrium state. For example, the experimental value of B_e can only be considered as an effective value; the "true" B_e (say B_e^*) is obtained from the equation $B_e = B_e^*(1+\gamma_a+\gamma_b+\gamma_c+\gamma_d)$ where γ_a, γ_b, γ_c, γ_d are the corrections for the effects (*a*), (*b*), (*c*), (*d*) respectively. Similarly $\omega_e = \omega_e^*(1+\delta_a+\delta_b+\delta_c+\delta_d)$. It is these "true" or corrected constants which obey the isotopic rules and which give the "true" equilibrium internuclear distances.

The contribution of (*a*) to the various constants in the energy equations has been given in some detail by Dunham. The corrections to the values given above are of the order of B_e^2/ω_e^2 and lead to the following values for

some of the constants of H_2: $\omega_e{}^a = 4401.063$, $B_e{}^a = 60.856$, and $D_e{}^a = 0.04679$ cm^{-1}; for HD, the corrected values are $\omega_e{}^a = 3812.279$, $B_e{}^a = 45.646$, and $D_e{}^a = 0.02632$ cm^{-1}. Dunham also pointed out that if the experimental value of D_e is equal to the theoretical value $4B_e{}^3/\omega_e{}^2$, then the molecule is a simple rotator and the coupling effects and perturbations due to (*b*), (*c*), and (*d*) are small. As mentioned earlier, the observed and calculated values of D_e are the same to within 1%. On the basis of this good agreement, one can conclude with some assurance that the ground state of H_2 is not strongly perturbed. Although this result indicates that the contributions of (*b*), (*c*), and (*d*) are not predominant, approximate values given by Van Vleck show that they are of about the same order of magnitude as that due to (*a*). Up to the present time, the contributions of (*b*), (*c*), and (*d*) have been calculated theoretically only for the constants B_e and ω_e, by Van Vleck (1936), and his values were taken over for the purposes of this discussion. When Dunham's and Van Vleck's corrections for B_e and ω_e were applied, the following values were obtained: for H_2, $B_e{}^* = 60.910$ cm^{-1}, $\omega_e{}^* = 4404.18$ cm^{-1}; for HD, $B_e{}^* = 45.678$ cm^{-1}, $\omega_e{}^* = 3814.25$ cm^{-1}. The values of $B_e{}^*$ were then used to calculate the values of $I_e{}^*$ and $r_e{}^*$ shown in Table III.

According to the isotopic rules, the ratios $\omega_e{}^*(HD)/\omega_e{}^*(H_2)$ and $[B_e{}^*(HD)/B_e{}^*(H_2)]^{\frac{1}{2}}$ should equal $[\mu(H_2)/\mu(HD)]^{\frac{1}{2}}$, where μ is the reduced mass of the molecule, and the corresponding ratios for the uncorrected constants should deviate slightly from this number. The respective ratios are found to be 0.86606 and 0.86599 for the corrected constants, and 0.86627 and 0.86610 for the uncorrected constants. It is seen that the ratios of the uncorrected constants as well as those of the corrected constants are in agreement with the theoretical value of 0.86610 (calculated using nuclear masses†). In part, this result can be shown in another way. According to theory, the "true" equilibrium internuclear distances of H_2, HD, and D_2 should be identical. the present values are 0.74130 ± 0.00006 Å in H_2, 0.74140 ± 0.00008 Å in HD, and 0.74143 ± 0.00012 Å in D_2, and are identical to within experimental accuracy. However, as shown in Table III, even the uncorrected values of the internuclear distances are in mutual agreement. It is thus evident that, within the present limits of accuracy, neither this criterion nor that of the isotopic relations is sensitive to the small corrections (*a*, *b*, *c*, *d*). For this purpose it is desirable to obtain still more accurate constants for the electronic ground states of all three molecules, particularly of D_2, and if possible of the isotopic molecules containing tritium.

ACKNOWLEDGMENTS

The Raman spectra of H_2, HD, and D_2 discussed in this paper were photographed under lower resolution by Dr. C. Cumming and myself in 1950 at the University of Toronto. However, the accuracy of measurement, approximately ± 0.2 cm^{-1}, was not sufficient to overcome the difficulties of earlier

†While the neglect of the electron masses is not strictly correct, even in the extreme case of neutral atoms, the value only changes to 0.86614.

analyses. I am indebted to Dr. Cumming for his collaboration in the earlier experiments and to Drs. G. Herzberg, S. R. Polo, and J. D. Swalen for helpful discussions. I am also grateful to Dr. G. Herzberg for the sample of HD and to Miss L. L. Howe for assistance with the calculations.

REFERENCES

BARNES, R. G., BRAY, P. J., and RAMSEY, N. F. 1954. Phys. Rev. **94**, 893.
BHAGAVANTAM, S. 1932. Indian J. Phys. **7**, 107.
BURNS, K., ADAMS, K. B., and LONGWELL, J. 1950. J. Opt. Soc. Amer. **40**, 339.
COHEN, E. R., DUMOND, J. W. M., LAYTON, T. W., and ROLLETT, J. S. 1955. Revs. Mod. Phys. **27**, 363.
DUNHAM, J. L. 1932. Phys. Rev. **41**, 721.
EDLÉN, B. 1953. J. Opt. Soc. Amer. **43**, 339.
ESPE, I. 1956. Phys. Rev. **103**, 1254.
HERZBERG, G. 1950*a*. Can. J. Research, A, **28**, 144.
——— 1950*b*. Nature, **166**, 563.
HORI, T. 1927. Z. Physik, **44**, 834.
HYMAN, H. H. 1930. Phys. Rev. **36**, 187.
JEPPESEN, C. R. 1933. Phys. Rev. **44**, 165.
——— 1934. Phys. Rev. **45**, 480.
——— 1936. Phys. Rev. **49**, 797.
PEKERIS, C. L. 1934. Phys. Rev. **45**, 98.
RAMSEY, N. F. 1952. Phys. Rev. **85**, 937.
RASETTI, F. 1929. Phys. Rev. **34**, 367.
SÈGRE, E. 1953. Experimental nuclear physics, Vol. I (John Wiley & Sons, Inc., New York).
STOICHEFF, B. P. 1954. Can. J. Phys. **32**, 330.
TEAL, G. K. and MACWOOD, G. E. 1935. J. Chem. Phys. **3**, 760.
UREY, H. C. and TEAL, G. K. 1935. Revs. Mod. Phys. **7**, 34.
VAN VLECK, J. H. 1936. J. Chem. Phys. **4**, 327.
WICK, G. C. 1933. Z. Physik, **85**, 25; Nuovo cimento, **10**, 118.
WOOLLEY, H. W., SCOTT, R. B., and BRICKWEDDE, F. G. 1948. J. Research NBS, **41**, 379.

VELOCITY-JUMP AMPLIFICATION AT 10,000 MC./S.[1]

B. V. Dore

ABSTRACT

A vacuum tube using the velocity-jump principle was built to amplify microwave frequencies in the vicinity of 10,000 Mc./s. The design of the tube was based on a similar structure that had been built to operate at a lower frequency. A general theory previously developed for space-charge wave amplifiers was applied to the operation of the tube, in conjunction with approximations made to the theory of coupling to electron beams by means of helices. The experimentally measured gain was in moderate agreement with that predicted by this theoretical development. Conclusions are drawn regarding the operation of coupling helices, and the effect of small gaps in the amplifying section of the tube.

INTRODUCTION

In the development of efficient amplifiers for microwave frequencies, vacuum tubes of conventional design have been displaced largely by velocity-modulated tubes. In the past decade various methods of obtaining interaction between radio-frequency fields and electron beams have been examined, which have resulted in the development of several types of space-charge wave amplifiers, of which the travelling-wave tube is probably the best known.

In 1951 Field, Tien, and Watkins produced a microwave amplifier with a net power gain of 22 decibels at 3000 Mc./s. This amplification was obtained through the growth of space-charge waves in an electron beam, the beam being decelerated by a sudden change in potential. The velocity-jump amplifier retains many of the advantages of the travelling-wave tube amplifier, such as simple construction and a large bandwidth. The absence of a continuous circuit in the velocity-jump tube overcomes the possibility of oscillation that is present in the travelling-wave tube. Further developments on this tube were reported by Tien and Field in 1952, and a similar experiment was performed by Agdur (1954) at Chalmers University.

TUBE DESIGN

The essential parts of a velocity-jump tube, as shown by Fig. 1, are the electron gun, short helices for coupling to the electron beam at the input and output stages, and the amplifying or jump section. A planar gun structure of the Pierce (1954) type was developed; the design was similar to that employed by Robinson and Kompfner (1951) in their noise studies on travelling-wave tubes. An auxiliary electrode, incorporating a short coaxial cylinder, was attached primarily to facilitate centering of the gun with respect to the tube. In order to maintain the physical properties of the electron beam it was necessary to provide a strong axial magnetic field along the entire length of the tube.

Information on current density and perveance obtained from a test gun was used to determine the physical dimensions of the drift tube in the ampli-

[1]Manuscript received February 7, 1957.
Contribution from the Eaton Electronics Research Laboratory, McGill University, Montreal, Canada.

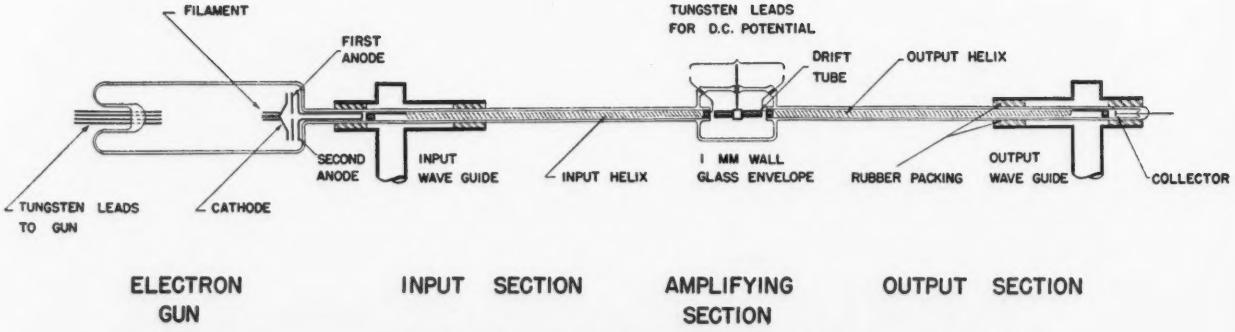

FIG. 1. A typical single-stage velocity-jump tube.

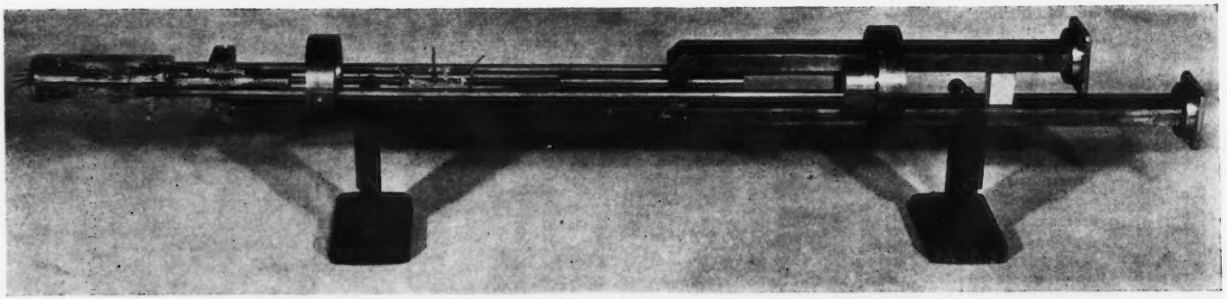

FIG. 2. The centering device with a tube in position.

fying section. A cylindrical tube 3.0 cm. long was used with beam currents of approximately 500 μa., and an estimated beam radius of 0.5 mm. For a range of drift tube potential from 0 to 1000 volts with respect to the cathode, there were at least three distinct potentials at which such a tube would provide optimum conditions for velocity-jump gain. The radius of the drift tube was 1.5 mm., which was the same as that of the gun cylinder and the coupling helices. The radius of the cylinder was chosen to be three times that of the beam in order to relax tolerances on mechanical alignment; this ratio of radii provided low but adequate coupling.

Short probes were attached to the ends of the helices to couple to the TE_{10} mode in the waveguide when positioned as shown in Fig. 1. Short cylindrical stubs, added to each end of the helix, were intended to provide the proper electric field configuration for the voltage jump, and for the transition from the gun to the helix. The physical length of the helices was determined from standing-wave measurements on the waveguide to helix coupling, and from a consideration of the amounts and kinds of modulation produced by a given length of helix. For a helix length greater than 5.0 cm. a voltage standing-wave ratio of 1.5 to 1 was readily obtainable, and the coupling action of the short helices used in this experiment was found to approximate that of a narrow-gap modulator.

EQUIPMENT

A signal generator, operated at a frequency of 9450 Mc./s., was modulated with a square wave generator at 1000 cycles per second. A 10 db. fixed attenuator was used to decouple the signal generator from the input circuit of the velocity-jump tube. The modulation on the output signal was detected with a silicon diode, and the output taken directly to a narrow-band audio-amplifier.

The jump gain as a function of drift-tube potential was recorded automatically by an Esterline Angus moving-paper milliammeter. The drift-tube potential could be varied from 0 to 1000 volts by a potentiometer which was directly coupled to the moving paper. In this fashion, rapid and accurate recordings were made of the variation of gain as a function of potential.

As shown in Fig. 2, a rigid structure was designed to hold the waveguides and to center the tube in a solenoid. Each waveguide was brought through a 90° bend to couple to the helices in the usual manner. In order to accommodate tubes of different lengths, and to achieve maximum coupling, the position of the waveguides could be varied and then locked; the correct position was determined by means of standing-wave measurements. Short studs on a brass ring at the gun end of the device pivoted on the inside of the solenoid when the collector end was moved. When the optimum position of the tube in relation to the magnetic field was determined, the centering device could be locked in position by means of three screws set in an annular ring on the end of the solenoid. Because of the enlarged section for the drift tube, it was necessary to have a removable section on the input waveguide coupler, in order to mount the velocity-jump tube in the centering device.

EXPERIMENTAL RESULTS

In order to explain the measurement of insertion loss, coupling level, and jump gain, a zero power level will be defined as the power transmitted when the signal generator was directly coupled to the detector, through the fixed attenuator. The amount by which this power level dropped when it was coupled through the "cold" tube was interpreted as insertion loss. The gain of the audio-amplifier was adjusted so that a zero output was obtained with this latter power level. When the beam was turned on and the jump section operated as a drift tube (drift tube potential equal to helix potential), the increase in the output power level was referred to as the amount of coupling between the beam and the helices. When the drift tube potential was varied, any change in power with respect to the coupling level was interpreted as being due to the velocity-jump action.

Most measurements were taken with a signal generator output of 1 mw.; when this power level was reduced by 10 or 20 db., the response of the tube was linearly decreased. Voltage standing-wave measurements on the input and output microwave circuits were made at several frequencies in the vicinity

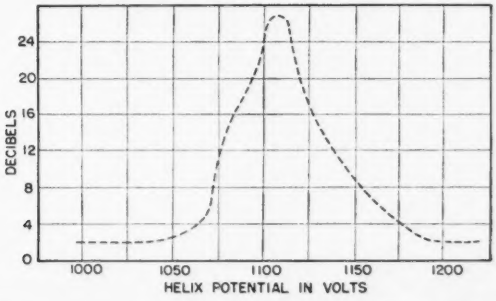

FIG. 3. The variation of coupling with d-c. helix potential. The data were obtained from a recording with a beam current of 0.100 ma. and a magnetic field of 1300 gauss.

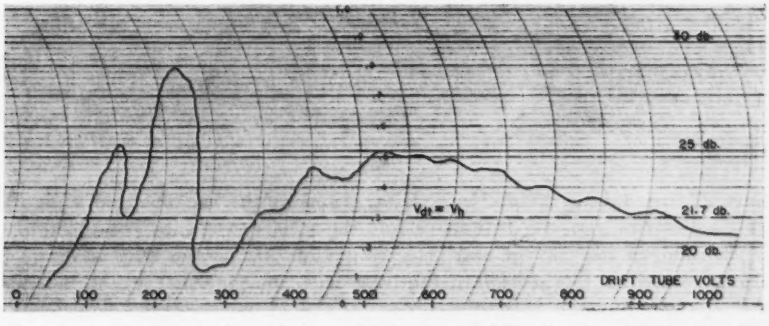

FIG. 4. A recording of the variation of jump gain with drift tube potential. The recording was made at a signal frequency of 9450 Mc./s. with a beam current of 0.350 ma., a helix potential of 1100 volts, and a magnetic field of 1650 gauss.

of 10,000 Mc./s. No appreciable differences in these measurements were found with the beam on and with the beam off. At 9450 Mc./s. the input s.w.r. was 3 to 1 and the output s.w.r. 2.7 to 1, which represents a combined power loss of 2.25 db. due to waveguide–helix coupling.

Aquadag was applied to the outside of the tube in an attempt to terminate the coupling helices. Before this application the insertion loss was −30 db., and after it was applied this level dropped to −48 db. By adjusting the d-c. helix potential for a given beam current, the average amount of coupling was 23 db. Fig. 3 indicates the variation of coupling with d-c. helix potential, and the variation of jump gain with drift tube potential is shown in Fig. 4.

THEORETICAL ANALYSIS

The experimental gain measurements were compared with those predicted by the application of Smullin's electronic equation (Smullin 1951) in the form used by Tien and Field (1952), together with approximations to the helix-coupling theory developed by Pierce (1950). As shown in Fig. 5 the amplifying

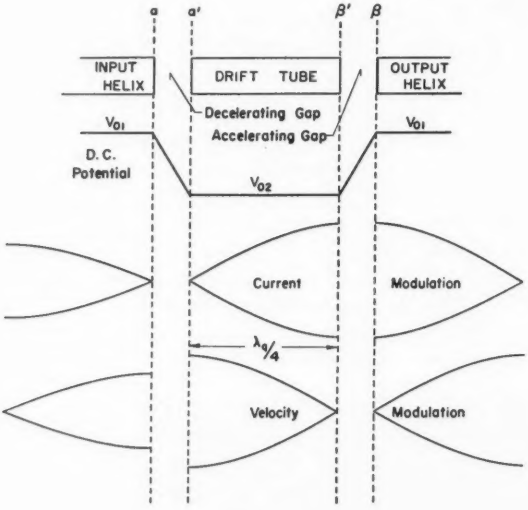

FIG. 5.

section of the tube is divided into three regions by the use of α and β planes: the decelerating gap, the drift space, and the accelerating gap. The theoretical relationship of the current and velocity modulation on the electron beam is also sketched for this section of the tube, with the potential V_{02} adjusted so that the length of the drift tube corresponds to a quarter plasma wavelength. The effective plasma wavelength of an electron beam of velocity v_0 is

$$\lambda_q = 2\pi v_0/\omega_q, \tag{1}$$

where ω_q is the angular plasma frequency of an electron beam of finite cross-section. The familiar form of the plasma angular velocity,

$$\omega_p = \sqrt{\eta\rho_0/\epsilon_0}\,, \tag{2}$$

applies to a beam of infinite cross-section and d-c. charge density ρ_0; here $\eta = e/m$ and ϵ_0 is the permittivity of space.

In order to determine the modulation at the β plane in terms of the modulation at the α plane, the electronic equation was applied to each of the three regions. Assuming a linear potential distribution across the narrow gaps, as shown in Fig. 5, the solution for the accelerating gap can be written in matrix notation as follows:

$$\begin{pmatrix} J_\beta \\ v_\beta \end{pmatrix} = \begin{pmatrix} E & F \\ G & H \end{pmatrix} \begin{pmatrix} J_{\beta'} \\ v_{\beta'} \end{pmatrix} e^{-\theta_1}, \tag{3}$$

where

$$E = \frac{s}{x}\left[\frac{J_1(y)N_2(s) - N_1(y)J_2(s)}{J_1(s)N_2(s) - J_2(s)N_1(s)}\right], \tag{4}$$

$$F = \frac{j2K}{x}\left[\frac{J_1(y)N_1(s) - J_1(s)N_1(y)}{J_1(s)N_2(s) - J_2(s)N_1(s)}\right], \tag{5}$$

$$G = \frac{js}{2K}\left[\frac{J_2(y)N_2(s) - J_2(s)N_2(y)}{J_1(s)N_2(s) - J_2(s)N_1(s)}\right], \tag{6}$$

$$H = \left[\frac{J_1(s)N_2(y) - J_2(y)N_1(s)}{J_1(s)N_2(s) - J_2(s)N_1(s)}\right], \tag{7}$$

$$x = \left[\frac{16\eta J_0}{\epsilon_0 k^3}\right]^{1/2} z^{1/4}, \qquad \theta_1 = j\omega\int\frac{dz}{v_0}, \qquad \text{and} \qquad K = \frac{m\omega J_0}{eE}.$$

In these equations the electric field E is equal to V_0/z, $k = v_0/z^{\frac{1}{2}}$, and s and y are the x co-ordinates corresponding to the β' and β planes respectively.

The decelerating gap can be analyzed by considering an electron beam traversing an accelerating gap in the reverse direction. The solution is written:

$$\begin{pmatrix} J_{\alpha'} \\ v_{\alpha'} \end{pmatrix} = \begin{pmatrix} A & B \\ C & D \end{pmatrix} \begin{pmatrix} J_\alpha \\ v_\alpha \end{pmatrix} e^{-\theta_2}. \tag{8}$$

Since the s and y planes of the accelerating gap have been interchanged, the matrix elements can be evaluated from equations (4)–(7) by interchanging s and y.

For the drift space the solution to the electronic equation can be written:

$$\begin{pmatrix} J_{\beta'} \\ v_{\beta'} \end{pmatrix} = \begin{pmatrix} Q & R \\ S & T \end{pmatrix} \begin{pmatrix} J_{\alpha'} \\ v_{\alpha'} \end{pmatrix} e^{-\theta_2}, \tag{9}$$

where

$$Q = T = \cos(\omega_q l/v_0), \tag{10}$$

$$R = jg\sin(\omega_q l/v_0), \tag{11}$$

$$S = (j/g)\sin(\omega_q l/v_0); \tag{12}$$

l is the length of the drift tube and $g = \omega J_0/\omega_q v_0$.

Combining the three matrices, it is possible to write the output modulation in terms of the input modulation in the form

$$(13)\quad \begin{pmatrix} J_\beta \\ v_\beta \end{pmatrix} = \begin{pmatrix} A(EQ+FS)+C(ER+FT) & B(EQ+FS)+D(ER+FT) \\ A(GQ+HS)+C(GR+HT) & B(GQ+HS)+D(GR+HT) \end{pmatrix} \begin{pmatrix} J_\alpha \\ v_\alpha \end{pmatrix} e^{-\theta_t},$$

where $\theta_t = \theta_1+\theta_2+\theta_3$. The elements of the matrices for each region were evaluated for a variation in drift tube potential from 0 to 1000 volts, for a d-c. beam current density $J_0 = 4.45\times10^2$ amp./meter^2, for a d-c. helix potential $V_{01} = 1100$ volts, for a gap width $\Delta z = 2.0$ mm., and for a drift tube length $l = 3.0$ cm.

Using relations developed by Pierce (1950) in connection with travelling-wave tubes, the modulation at the α plane in terms of the input power can be written:

$$(14)\quad J_\alpha = J_{\alpha_1}+J_{\alpha_2}+J_{\alpha_3},$$

$$(15)\quad v_\alpha = v_{\alpha_1}+v_{\alpha_2}+v_{\alpha_3},$$

where

$$(16)\quad J_{\alpha_1} = \frac{-I_0 V_{\alpha_1}}{2V_0 C^2\delta_1^2} = \frac{-V_{\alpha_1}}{\gamma\delta_1^2},$$

$$(17)\quad v_{\alpha_1} = \frac{-j\eta V_{\alpha_1}}{v_0 C\delta_1} = \frac{-jV_{\alpha_1}}{\mu\delta_1},$$

and similarly for the other components. The three components in equations (14) and (15) correspond to the three forward waves in the combined circuit and electron beam; δ is related to a small perturbation of the propagation constant of the circuit due to the presence of the electron beam. V is a voltage parameter used by Pierce, which is related to power through the formula

$$(18)\quad P = |V^2|/K,$$

K being the characteristic impedance of the circuit. The gain parameter

$$(19)\quad C = [KI_0/4V_0]^{1/3}$$

here has a value of 3.65×10^{-3} for a beam current of $I_0 = 350$ μa. Dividing equation (17) by equation (16) and evaluating the result from the experiment,

$$(20)\quad |v_{\alpha_1}/J_{\alpha_1}| \doteq 2\times10^8\,|\delta_1|.$$

Similar analysis applies to the other components. Since there is a predominant wave for even a short helix, and since the values of δ are the roots of a cubic equation, it is unlikely that the resultant J_α will approach a significant value. That is, v_α will be small for a short length of helix with this value of C, and since J_α is very small in comparison, it is reasonable to conclude that to a close approximation only velocity modulation is present at the α plane.

At the end of the output helix of length s, one component of V_s can be expressed in terms of the modulation at the β plane:

$$(21)\quad V_{s_1} = \frac{-j\delta_1^2(\delta_2+\delta_3)\mu v_\beta - \delta_1^2\delta_2\delta_3\gamma J_\beta}{(\delta_1-\delta_2)(\delta_1-\delta_3)} \exp(-j\beta_e s+\beta_e C\delta_1 s).$$

Equation (21) can be rearranged to give

$$(22) \qquad V_{s_1}' = \frac{-\delta_1^2\delta_2\delta_3\gamma J_\beta}{(\delta_1-\delta_2)(\delta_1-\delta_3)}\left[\frac{(\delta_2+\delta_3)j\mu v_\beta}{\delta_2\delta_3\gamma J_\beta}+1\right]\exp(-j\beta_e s+\beta_e C\delta_1 s) .$$

Examining the magnitude of the first term in the brackets, it appears that

$$(23) \qquad \frac{\mu}{\gamma}\left|\frac{\delta_2+\delta_3}{\delta_2\delta_3}\right| \cdot \left|\frac{v_\beta}{J_\beta}\right| \doteqdot 5\times10^{-9}\left|\frac{\delta_2+\delta_3}{\delta_2\delta_3}\right| \cdot \left|\frac{v_\beta}{J_\beta}\right| .$$

In equation (23) the product of the δ's is not equal to zero, $|\delta_2\delta_3| \neq 0$, since they are both roots of a cubic equation. The sum of the δ's, $|\delta_2+\delta_3|$, could be zero depending on relative phases and magnitudes. The range of values of $|v_\beta/J_\beta|$ was obtained from equation (13) by putting $J_\alpha = 0$. For the complete range of drift tube potential it was found that the contribution of the v_β term to each component of V_s can be ignored in comparison with J_β. This approximation may be invalid for those values of drift tube potential (87.5 volts and 212.5 volts) for which the drift tube length corresponds to some multiple of a half plasma wavelength.

Assuming linear coupling between the output helix and the crystal detector, a measure of power gain due to velocity-jump action can be written:

$$(24) \qquad \text{power gain} = 10\log_{10}(|V_j^2|/|V_d^2|) \text{ db.}$$

In this equation V_d is the voltage parameter (equation 18) evaluated at the end of the output helix for the case where the helix and drift tube are both at the same potential; in consequence, V_d is related to what has been defined as the coupling. V_j is the same parameter evaluated for the case where a velocity jump exists. Since the output helix responds only to current modulation, it is convenient to write the gain equation (24) in terms of current modulation at the input to this helix :

$$(25) \qquad \text{power gain} = 10\log_{10}(|J_j^2|/|J_d^2|)_{\beta \text{ plane}} \text{ db.}$$

where

$$(26) \qquad J_j|_\beta = [B(EQ+FS)+D(ER+FT)]\, v_\alpha\, e^{-\theta_t}$$

and

$$(27) \qquad J_d|_\beta = R'\, v_\alpha\, e^{-\theta_4}.$$

In equation (27), $R' = jg\sin(\omega_q l'/v_0)$ from equation (11) and $\theta_4 = (j\omega l'/v_0)$, where l' is the distance from the α plane to the β plane.

Using the values of the matrix elements previously calculated, equation (25) was evaluated for the complete range of drift tube potential (Fig. 6). For purposes of comparison, an experimental curve from manually-recorded data is reproduced on the same graph. In order to determine the effect of the finite width, Δz, of the accelerating and decelerating gaps, a simplified calculation of gain was made, assuming instantaneous voltage jumps, in addition to the previous approximations for J_α and v_β. The results of this calculation were found to be identical to the corresponding values obtained from equation (25) for the full variation of drift tube potential.

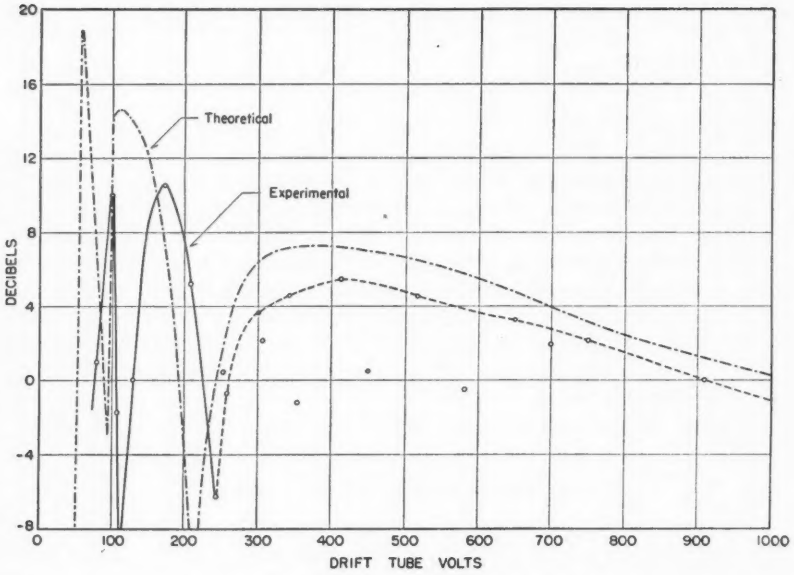

FIG. 6. A comparison of the experimental and theoretical variation of jump gain with drift tube potential. The experimental data were manually recorded, using a beam current of 0.350 ma. and a magnetic field of 1500 gauss.

DISCUSSION

The deterioration of experimentally measured gain at low drift tube potentials is to be expected from the defocusing of the beam which is produced by the jump region. The discrepancy in the gain levels at high potentials in Fig. 6 may be partly due to the value of gap width, Δz, used in the theoretical calculation. Although theoretical considerations indicate that a gap width of 2.0 mm. does not affect the gain, the effective gap width is probably more than the physical spacing of 2.0 mm. A calculation of the gain to be expected with a gap width three times this value was made for the maxima (65, 115, and 350 volts), and the results obtained were of the order of 10% less than those obtained with the smaller gap. Apparently Tien and Field (1952) used gridded gaps to obtain a sharper transition at the voltage jumps, but this technique increases the alignment difficulties. In addition to the effect of the gap width, there is also the possibility of slight misalignment of the cylinders in the jump region, which would detract from the maximum effect of the voltage jump.

It will be noted that the experimental gain curve in Fig. 6 from manually-recorded data indicates higher gain levels at low drift tube potentials than the automatically recorded data in Fig. 4. However, in the former case there are numerous discontinuities in the gain measured at higher drift tube potentials. A broken curve has been drawn through the peak values obtained in this

region. This instability is due mainly to variations in the strength of the magnetic field, which in turn are related to poor regulation of the solenoid power supply under heavy load. When the magnetic field strength was deliberately varied, a quasi-periodic variation in velocity-jump gain was obtained. At a drift tube potential of 750 volts, variations in gain of 2 or more decibels were obtained for changes of approximately 100 gauss in field strength. When recordings were made in much shorter periods of time, these discontinuities disappeared, but it was not possible to adjust the magnetic field for optimum gain over the complete range of drift tube potential.

The variation of coupling with d-c. helix potential (Fig. 3) was taken with a second tube, as the two helices in this tube were more nearly identical than in the first tube. When the two helices differ physically, the curve has two distinct maxima corresponding to the voltages at which they would couple independently. It is interesting to note that from the pitch angle for the helices, after annealing, they should have coupled most effectively at 1450 volts. The experimental value of 1100 volts is approximately 75% of this value, which is much greater than any possible discrepancy in determining pitch angle. This phenomenon is not unusual in tubes using helical structures, and is due to the effect upon the helix of the supporting structure. In this case the glass decreases the velocity of the circuit wave to less than the theoretical value.

As has been mentioned previously, there was an increase of 18 db. in the insertion loss after aquadag had been applied to the tube. Ideally, the insertion loss should be infinite for a velocity-jump tube, as there should be no coupling between the input and output stages in the absence of the beam. It is impossible for the drift tube to operate as a cylindrical waveguide, as its physical dimensions are far below the cutoff values for the signal frequency employed. The transmission of power in the "cold" tube may be due to leakage between the input and output microwave circuits, although the effect of the aquadag is significant. It should be noted that the addition of the aquadag also improved the frequency response of the tube; the bandwidth was increased and the number of subsidiary coupling maxima was decreased. Thus it appears that the aquadag improved the termination of the helices, and so decreased the amounts of power reflected and transmitted from the ends.

CONCLUSIONS

(i) General space-charge wave theory, in conjunction with the modified helix-coupling theory, appears to be adequate to explain the operation of a velocity-jump tube operating at 3 cm. wavelengths.

(ii) It is possible to achieve the maximum theoretical gain in such a tube if particular attention is paid to the over-all alignment of the structure, and to its position in a stable magnetic field.

(iii) The over-all efficiency of the tube would be improved if the coupling helices were properly terminated by means of some lossy material.

(iv) The theoretical effect of narrow gaps in the accelerating and decelerating regions of such a tube is negligible.

(v) Short coupling helices behave like narrow-gap modulators, although this approximation is qualified to a large extent by the value of the gain parameter C.

ACKNOWLEDGMENTS

The author expresses his appreciation to Professor G. A. Woonton for valuable advice and for his encouragement during the course of this research. This project formed part of the work on the physics of electron beams and of high frequency tubes which is financed at the Eaton Electronics Research Laboratory of McGill University by the Defence Research Board, Ottawa, under Consolidated Grant DRB 9512-20. The author also acknowledges certain direct financial assistance from this Grant during the period of this work.

REFERENCES

AGDUR, N. B. 1954. Transactions of Chalmers University of Technology, No. 140.
FIELD, L. M., TIEN, P. K., and WATKINS, D. A. 1951. Proc. Inst. Radio Engrs. **39**, 194.
PIERCE, J. R. 1950. Travelling wave tubes (D. Van Nostrand Company, Inc., New York).
——— 1954. Theory and design of electron beams (D. Van Nostrand Company, Inc., New York).
ROBINSON, F. N. H. and KOMPFNER, R. 1951. Proc. Inst. Radio Engrs. **39**, 918.
SMULLIN, L. D. 1951. J. Appl. Phys. **22**, 1496.
TIEN, P. K. and FIELD, L. M. 1952. Proc. Inst. Radio Engrs. **40**, 688.

ON A REPORTED ISOMERIC STATE IN Mn^{54} [1]

K. G. McNeill,[2] J. D. Prentice,[2] L. Katz,[3] and W. Link[3, 4]

ABSTRACT

An attempt was made to detect the 2 minute isomeric state in Mn^{54} reported by Caldwell and Stoddart. Irradiation of pure Mn^{55} with various energy bremsstrahlung of 12 to 24 Mev. failed to disclose any (γ, n) reactions leading to this state. Iron targets irradiated by 13.5 Mev. neutrons failed to disclose any positron activity of 2 minute half-life resulting from an (n, p) reaction to this state. In view of these experiments we conclude that the existence of the reported isomeric state in Mn^{54} should not be accepted without reservation.

A negatron radioactivity of 2 minute half-life ascribed to an isomeric state in Mn^{54} has been reported by Caldwell and Stoddart (1951). By absorption measurements they estimated the negatron end point energy to be about 2 Mev. (Caldwell, private communication). The activity was assigned to an isomeric state in Mn^{54} because of the ratio of activities produced in natural iron and iron enriched in Fe^{54} after bombardment by 10 Mev. deuterons or 14 Mev. neutrons. Some attempts to produce this activity by $Cr^{54}(p, n)$ at U.C.L.A., and by $Mn^{55}(\gamma, n)$ at U.C.L.A. and other centers, were unsuccessful (Caldwell, private communication). It was therefore decided to make a thorough investigation of the possibility of producing this activity by a photoneutron reaction on manganese, the results of which are reported below.

SEARCH FOR NEGATRON ACTIVITY

Manganese of 99.9% purity was irradiated with 25 Mev. bremsstrahlung. With a Geiger counter a weak activity was detected which had a half-life of 3.4 ± 0.3 minutes. In an attempt to assign this activity to a particular element a chemical separation was carried out. Irradiated $MnCl_2$ was first treated with $K_2S_2O_5$ to reduce any MnO_2 present. Then NH_4Cl with $CrCl_3$ carrier was added and $Cr(OH)_3$ precipitated out by adding NH_4OH drop by drop. The short-lived activity was found preferentially in the chromium fraction; any vanadium present would also be carried down with the chromium. The half-life and chemical properties suggested that the activity was due to 3.7 minute V^{52} formed by $Mn^{55}(n, \alpha)V^{52}$; there are always fast neutrons present in the X-ray beam. Confirmation for this assignment was obtained by irradiating manganese with such a thickness of lead between the betatron and the sample that almost all the X-rays were absorbed while the fast neutron flux was comparatively unaffected: the short-lived activity was still formed.

From these experiments an upper limit can be placed on the yield of any short-lived negatron activity induced by photoreaction. If one assumes a reasonable form of giant resonance shape for the cross-section curve, the

[1]Manuscript received January 21, 1957.
Contribution from the Departments of Physics of the University of Glasgow, Glasgow, Scotland, and the University of Saskatchewan, Saskatoon, Sask.
[2]University of Glasgow.
[3]University of Saskatchewan.
[4]Present address: Department of Physics, McGill University, Montreal, Que.

maximum permissible cross-section is 10^{-28} cm.^{2}—for comparison the peak cross-section of the $Mn^{55}(\gamma, n)Mn^{54}$ ground state reaction is 10^{-25} cm.^{2}

SEARCH FOR GAMMA RAYS

As it is energetically possible for an excited state of Mn^{54} to decay by β^-, β^+, or γ ray emission, a search was made for γ rays or annihilation quanta associated with this level. This permitted the efficient use of a thicker target than was possible for β^- counting.

A solid sample of spectrographically pure manganese was irradiated in a beam of 23 Mev. peak energy bremsstrahlung, and then quickly removed to a scintillation spectrometer consisting of a 2 in. in diameter by 2 in. NaI(Tl) crystal and conventional circuitry. The pulse height spectrum was displayed on a Hutchison and Scarrott 100-channel pulse height analyzer. A very weak activity was observed, with a peak in the spectrum corresponding to a γ ray of 0.51 Mev. No other short-lived gamma rays were seen: an upper limit on the intensity of any gamma ray of energy E in the range 100 kev. $< E <$ 3 Mev. could be set at 5% of the intensity of the 0.5 Mev. peak. That the observed peak was due to positron annihilation quanta was confirmed by coincidence measurements taken with counters arranged at 90° and 180° with respect to each other and the source. The half-life of the positrons was found to be 2.0 ± 0.1 minutes, and the approximate end point energy, measured with a plastic scintillator, 2.0 ± 0.3 Mev.

The energy and half-life measurements suggested that the activity might be due to O^{15}, which would be produced by a (γ, n) reaction on any oxygen contamination of the manganese. Using a single channel pulse height analyzer to select pulses corresponding to the positron annihilation quanta, counts were taken of samples of manganese irradiated by X-ray Bremsstrahlung spectra of peak energies between 12 and 24 Mev. The yields thus obtained fitted very well the shape of the known $O^{16}(\gamma, n)$ reaction excitation curve and gave the same threshold value. The 23 Mev. yield was compared to that from a similar sample of copper irradiated under the same conditions. If we assume that all the counts from the manganese sample were in fact due to a positron decay of Mn^{54*} (rather than, as is believed, of O^{15}) and that the cross-section curve for its production is of giant resonance shape, then the maximum cross-section for the production of the positron branch was found to be $\sim 10^{-29}$ cm.^{2} However 0.1% oxygen contamination could account for all the observed activity.

If the above activity were due to a branch of the decay of Mn^{54*} it should also be observed from samples of iron irradiated with high energy neutrons. No evidence for positron activity of 2 minute half-life could be found either in the γ ray spectrum of, or by coincidence measurements on, iron targets irradiated with 13.5 Mev. neutrons. With a Geiger counter a beta activity was observed which had a half-life of 1.75 ± 0.1 minutes. Using a plastic scintillator the end point was measured as 2.3 ± 0.3 Mev. Both these measurements suggest that this activity should be identified with the known negatron decay of Mn^{57} (half-life = 1.7 minutes, E_{max} = 2.6 Mev.) (Cohen *et al.* 1954).

Since separated isotopes were not available in sufficient quantity, it was not possible to confirm or deny the existence of a 2 minute decay produced by neutron irradiation of Fe^{54}.

DISCUSSION

The above results show no evidence for the production of Mn^{54*} by a Mn^{55} (γ, n) reaction, and therefore the question arises whether Mn^{54*} can be produced by the reaction $Fe^{54}(n, p)Mn^{54*}$ as proposed by Caldwell and Stoddard and yet cannot be formed by a photoneutron reaction.

Let it be considered, in the first place, that the isomeric state does exist, and that it decays by emission of a negatron with a 2 Mev. maximum energy (as will be seen later, the particular energy chosen is immaterial). In this case the isomeric level must be 1.46 Mev. above the Mn^{54} ground state (Nuclear Level Schemes 1955). In order that it can have a half-life against gamma de-excitation to the Mn^{54} ground state of greater than 2 minutes, the spin difference between it and the ground state must be at least $\Delta I = 4$ (Montalbetti 1952). As the Mn^{54} ground state is probably 3^+ (Nuclear Level Schemes 1955), this indicates that the assumed isomeric level has a spin of at least 7.

Centrifugal barriers prevent neutrons from carrying very high angular momenta into an iron nucleus. From the figures given by Feld *et al.* (1951) it may be calculated (Katz *et al.* 1952) that on the average 14 Mev. neutrons carry in $\Delta I = 3.5$, but values up to $\Delta I = 6$ are quite probable. Thus the highest spin state of the compound nucleus of Fe^{55} would be expected to be the spin of the ground state of Fe^{54}, 0, plus the highest ΔI value of the 14 Mev. neutrons, 6, plus the spin of the neutron, 1/2, giving a total of 13/2. Thus a spin state of 7 or even higher in Mn^{54} should be easily reachable by a $Fe^{54}(n, p)$ reaction using 14 Mev. neutrons.

In the case of photon absorption, a spin of 5/2 (for Mn^{55}) is the initial condition. Dipole or quadrupole absorption will give an excited state of Mn^{55} of 7/2 or 9/2 respectively.

To reach from a 9/2 state a spin state of 7 or higher requires emission of a $\Delta I = 2$ neutron. The likelihood of this reaction is supported by the results on the reaction $Pb^{208}(\gamma, n)Pb^{207*}$ (Reid and McNeill 1954; Prentice and McNeill 1956), where the isomeric state of Pb^{207} has a spin of 13/2 while the initial state of Pb^{208} has zero spin—a total change of 13/2 against 9/2 in the present case. Thus it should be possible to reach a spin state of 7 or more in Mn^{54} using a photoneutron reaction. Competitive de-excitation of the compound nucleus to states other than the isomeric one should be of the same order in both the (n, p) and (γ, n) cases.

A further point must now be discussed, however. A 2 minute half-life 2 Mev. β decay implies an allowed transition. In the previous discussion it has been assumed that the beta decay was to the zero spin Fe^{54} ground state. This is not allowed by the selection rules if the isomeric state has a high spin. If the 2 Mev. end point is correct, the only way out of the difficulty is to assume that the isomeric state energy is higher than the 1.46 Mev. previously taken, and that it decays to a high spin excited state of Fe^{54}. As the first excited state

of Fe^{54} is reported to be at 1.41 Mev. and to have a spin of 2, we need to assume that the Mn^{54*} level is higher than (1.46+1.41) Mev. At once the probability of gamma de-excitation to the ground state is greatly increased, and to forbid this a spin even higher than 7 must be assumed for this level, with corresponding difficulties of formation of the state by either the (n, p) or the (γ, n) reaction.

If it is assumed that the beta energy is in fact less than the 2 Mev. previously considered, the difficulties associated with spin change can be made to disappear, by, say, assuming an $I = 0$ level less than 0.1 Mev. above the ground state of Mn^{54}. In this case there is a spin change of 3 between the isomeric and ground states and this, with the small energy difference, makes gamma de-excitation unlikely. Such a zero spin low lying level should, however, be reachable equally easily by the $Fe^{54}(n, p)$ and the $Mn^{55}(\gamma, n)$ reactions.

If it is assumed that the beta energy is in fact more than 2 Mev., the difficulties previously treated are merely accentuated.

To summarize, whatever the maximum energy of the suggested beta ray, it would appear that the isomeric state could be reached by a (γ, n) reaction if it can be produced by the reaction $Fe^{54}(n, p)$. Moreover, no evidence has been found for the production of the reported isomeric state by the Mn^{55} (γ, n) reaction.

Since the original report of the Mn^{54} isomer two other isotopes in this region of the periodic table, V^{53} (Schardt and Dropesky 1956) and Mn^{57} (Cohen *et al.* 1954), have been found to have negatron decays of 2.0 minutes and 1.7 minutes, of negatron energies 2.5 Mev. and 2.6 Mev. respectively.

In view of these facts, the existence of the reported isomeric state of Mn^{54} should not be accepted without reservation.

REFERENCES

Caldwell, D. O. and Stoddart, H. F. 1951. Phys. Rev. **81**, 660A.

Cohen, B. L., Charpie, R. A., Handley, T. H., and Olson, E. L. 1954. Phys. Rev. **94**, 953.

Feld, B. T., Feshbach, H., Goldberger, M. L., Goldstein, H., and Weisskopf, V. F. 1951. Final Report of the Fast Neutron Data Project NYO-636.

Katz, L., Pease, L., and Moody, H. 1952. Can. J. Phys. **32**, 476.

Montalbetti, R. 1952. Can. J. Phys. **30**, 660.

Nuclear Level Schemes, $A = 40$ to $A = 92$. 1955. (U.S. Atomic Energy Commission).

Prentice, J. D. and McNeill, K. G. 1956. Phil. Mag. **1**, 373.

Reid, J. M. and McNeill, K. G. 1954. Phil. Mag. **45**, 957.

Schardt, A. W. and Dropesky, B. J. 1956. Bull. Am. Phys. Soc. **1**, No. 4, 162-B4.

A STUDY OF THE APPROXIMATE THEORY OF AN ELASTIC THICK BEAM[1]

SEIICHI HIGUCHI,[2] HIDEO SAITO,[3] AND CHIAKI HASHIMOTO[3]

ABSTRACT

The flexural vibration of a thick beam is analyzed two-dimensionally by using the general equation of flexural motion. The characteristic equations and the frequencies of thick beams for the various end conditions are obtained and comparisons are made between the frequencies obtained from the present calculations and those from the elementary theory of a thin beam.

1. INTRODUCTION

It seems to us that the vibration theory of an elastic thick beam has not yet been solved thoroughly, owing mainly to the mathematical difficulties encountered in the course of the deduction of the solution. Concerning this problem, previously we have dealt with the problem of the exact theory of the vibrating thick beam (Higuchi and Hashimoto 1955), intending mainly to know the quantitative relations between the dimension of the beam and its corresponding frequency. And, though we succeeded in obtaining the solution for the free–free thick beam and also its corresponding characteristic equation, yet, in spite of this, because the expression of the latter was given in the form of an infinite determinant, we were obliged to be satisfied with an approximate numerical root of it. However, we were able to ascertain numerically some noteworthy results, e.g., if the beam becomes thicker, the ratio of the frequency calculated as a thick beam to that calculated as a thin beam decreases.

Now, under the existing circumstances, if we wish to study the problem in question more thoroughly, our attention should be directed to raising as much as possible the degree of accuracy of an approximate calculation of the problem. On the other hand, as is generally known, a usual elementary theory of the vibration of a beam is constructed under the assumption that the thickness of the beam is small in comparison with the length, so the effect of the deformation due to shear and that of the rotary inertia is naturally not taken into account. Regarding this problem, however, Lamb (1917) discussed the vibration of a body bounded by two parallel planes; also Timoshenko (1921) published a paper introducing the several secondary effects mentioned above into the ordinary equation of motion of a thin beam; and, since then, similar investigations have been published showing almost good agreement with the theory and experiments (Kolsky 1953). However, the success mentioned here seems to be limited only to the case of the supported–supported beam, the simplest among all the cases of the beam classified by the end conditions, and does not apply for those having any other end conditions, so that it

[1]Manuscript received November 30, 1956.
Contribution from the Faculty of Engineering, Iwate University, Morioka, Japan, and the Department of Mechanical Engineering, Tohoku University, Sendai, Japan.
[2]Faculty of Engineering, Iwate University.
[3]Department of Mechanical Engineering, Tohoku University.

may be said that we have still no means of knowing theoretically the behavior of the general thick beam at the time of vibration.

In this paper, some approximations in regard to the end conditions are introduced, and the natural vibrations of the various thick beams are treated two-dimensionally. The solutions of the thick beams with various end conditions are first obtained and, secondarily, corresponding frequencies are deduced numerically. Comparisons are made between the frequencies obtained from the present calculations and those deduced from the elementary theory of a thin beam, and discussions about them are carried out in some detail.

2. EQUATION OF MOTION AND THE SOLUTION OF THE THICK BEAM

Taking the coordinate axes as shown in Fig. 1, we have the equation of flexural motion of a thick beam as

$$\frac{2}{1-\nu}\nabla^2\phi = \frac{\rho}{G}\frac{\partial^2\phi}{\partial t^2}, \tag{1a}$$

$$\nabla^2\psi = \frac{\rho}{G}\frac{\partial^2\psi}{\partial t^2}, \tag{1b}$$

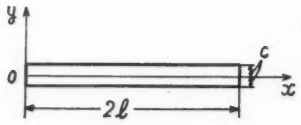

FIG. 1. Coordinates of beam.

and displacement and stress components are in the usual notation

$$u = \frac{\partial\phi}{\partial x}+\frac{\partial\psi}{\partial y}, \qquad v = \frac{\partial\phi}{\partial y}-\frac{\partial\psi}{\partial x}, \tag{2}$$

$$\sigma_x = \frac{2G}{1-\nu}\left(\frac{\partial u}{\partial x}+\nu\frac{\partial u}{\partial y}\right), \tag{3a}$$

$$\sigma_y = \frac{2G}{1-\nu}\left(\frac{\partial v}{\partial y}+\nu\frac{\partial u}{\partial x}\right), \tag{3b}$$

$$\tau_{xy} = G\left(\frac{\partial v}{\partial x}+\frac{\partial u}{\partial y}\right), \tag{3c}$$

where ρ, G, and ν denote the density, modulus of rigidity, and Poisson's ratio respectively and ∇^2 is

$$\nabla^2 = \frac{\partial^2}{\partial x^2}+\frac{\partial^2}{\partial y^2}.$$

If we put

$$\phi = \Phi e^{ipt}, \qquad \psi = \Psi e^{ipt}, \tag{4}$$

and using the notation

$$h^2 = \frac{(1-\nu)\rho}{2G}p^2, \qquad k^2 = \frac{\rho}{G}p^2, \tag{5}$$

we arrive at the following expressions instead of (1):

$$(\nabla^2+h^2)\Phi = 0, \tag{6a}$$

$$(\nabla^2+k^2)\Psi = 0. \tag{6b}$$

Φ and Ψ which satisfy (6) are

$$\Phi = A_1 \sinh \alpha y \cos \xi x + B_1 \sinh \alpha y \sin \xi x + C_1 \sin \gamma y \cosh \eta x + D_1 \sin \gamma y \sinh \eta x, \tag{7a}$$

$$\Psi = A_2 \cosh \beta y \sin \xi x + B_2 \cosh \beta y \cos \xi x + C_2 \cos \delta y \sinh \eta x + D_2 \cos \delta y \cosh \eta x, \tag{7b}$$

provided that

$$\alpha^2 = \xi^2 - h^2, \qquad \beta^2 = \xi^2 - k^2, \tag{8a}$$

$$\gamma^2 = \eta^2 + h^2, \qquad \delta^2 = \eta^2 + k^2. \tag{8b}$$

Then, from (2) and (3), displacements and stresses are given as

$$u = (-A_1\xi \sinh \alpha y + A_2\beta \sinh \beta y)\sin \xi x + (B_1\xi \sinh \alpha y + B_2\beta \sinh \beta y)\cos \xi x + (C_1\eta \sin \gamma y - C_2\delta \sin \delta y)\sinh \eta x + (D_1\eta \sin \gamma y - D_2\delta \sin \delta y)\cosh \eta x, \tag{9a}$$

$$v = (A_1\alpha \cosh \alpha y - A_2\xi \cosh \beta y)\cos \xi x + (B_1\alpha \cosh \alpha y + B_2\xi \cosh \beta y)\sin \xi x + (C_1\gamma \cos \gamma y - C_2\eta \cos \delta y)\cosh \eta x + (D_1\gamma \cos \gamma y - D_2\eta \cos \delta y)\sinh \eta x, \tag{9b}$$

and

$$\sigma_y/G = \{A_1(\beta^2+\xi^2)\sinh \alpha y - A_2\, 2\beta\xi \sinh \beta y\}\cos \xi x + \{B_1(\beta^2+\xi^2)\sinh \alpha y + B_2\, 2\beta\xi \sinh \beta y\}\sin \xi x + \{-C_1(\delta^2+\eta^2)\sin \gamma y + C_2\, 2\delta\eta \sin \delta y\}\cosh \eta x + \{-D_1(\delta^2+\eta^2)\sin \gamma y + D_2\, 2\delta\eta \sin \delta y\}\sinh \eta x, \tag{10a}$$

$$\tau_{xy}/G = \{-A_1\, 2\alpha\xi \cosh \alpha y + A_2(\xi^2+\beta^2)\cosh \gamma y\}\sin \xi x + \{B_1\, 2\alpha\xi \cosh \alpha y + B_2(\xi^2+\gamma^2)\cosh \beta y\}\cos \xi x + \{C_1\, 2\gamma\eta \cos \gamma y - C_2(\delta^2+\eta^2)\cos \delta y\}\sinh \eta x + \{D_1\, 2\gamma\eta \cos \gamma y - D_2(\delta^2+\eta^2)\cos \delta y\}\cosh \eta x, \tag{10b}$$

where A_1, B_1, C_1, etc. are arbitrary constants.

For the case of the natural vibration, regardless of any end conditions, the following boundary conditions should always be satisfied:

$$\text{on } y = \pm c, \qquad \sigma_y = \tau_{xy} = 0. \tag{11}$$

Substituting (11) into (10), we have

$$4\alpha\beta\xi^2 \cosh \alpha c \sinh \beta c - (\beta^2+\xi^2)^2 \cosh \beta c \sinh \alpha c = 0, \tag{12a}$$

$$4\gamma\delta\eta^2 \cos \gamma c \sin \delta c - (\delta^2+\eta^2)^2 \sin \gamma c \cos \delta c = 0, \tag{12b}$$

and

$$(13a)\qquad \frac{A_2}{A_1}=-\frac{B_2}{B_1}=\frac{2\alpha\xi\cosh\alpha c}{(\beta^2+\xi^2)\cosh\beta c}=\frac{(\beta^2+\xi^2)\sinh\alpha c}{2\beta\xi\sinh\beta c},$$

$$(13b)\qquad \frac{C_2}{C_1}=\frac{D_2}{D_1}=\frac{2\gamma\eta\cos\gamma c}{(\delta^2+\eta^2)\cos\delta c}=\frac{(\delta^2+\eta^2)\sin\beta c}{2\delta\eta\sin\delta c}.$$

Introducing (13) into (9) and (10) and arranging in regular order, we have

$$(14a)\quad u=\left\{-\xi\sinh\alpha y+\frac{(\beta^2+\xi^2)\sinh\alpha c}{2\xi\sinh\beta c}\sinh\beta y\right\}(A\sin\xi x-B\cos\xi x)$$
$$+\left\{\eta\sin\gamma y-\frac{(\delta^2+\eta^2)\sin\gamma c}{2\eta\sin\delta c}\sin\delta y\right\}(C\sinh\eta x+D\cosh\eta x),$$

$$(14b)\quad v=\left\{\alpha\cosh\alpha y-\frac{(\beta^2+\xi^2)\sinh\alpha c}{2\beta\sinh\beta c}\cosh\beta y\right\}(A\cos\xi x+B\sin\xi x)$$
$$+\left\{\gamma\cos\gamma y-\frac{(\delta^2+\eta^2)\sin\gamma c}{2\delta\sin\delta c}\cos\delta y\right\}(C\cosh\eta x+D\sinh\eta x),$$

$$\sigma_x/G=\left\{(2\alpha^2-\beta^2+\xi^2)\sinh\alpha y-\frac{(\beta^2+\xi^2)\sinh\alpha c}{\sinh\beta c}\sinh\beta y\right\}(-A\cos\xi x-B\sin\xi x)$$

$$(15a)\qquad +\left\{(2\gamma^2-\delta^2+\eta^2)\sin\gamma y-\frac{(\delta^2+\eta^2)\sin\gamma c}{\sin\delta c}\sin\delta y\right\}(C\cosh\eta x+D\sinh\eta x),$$

$$(15b)\quad \sigma_y/G=(\beta^2+\xi^2)\left(\sinh\alpha y-\frac{\sinh\alpha c}{\sinh\beta c}\sinh\beta y\right)(A\cos\xi x+B\sin\xi x)$$
$$+(\delta^2+\eta^2)\left(-\sin\gamma y+\frac{\sin\gamma c}{\sin\delta c}\sin\delta y\right)(C\cosh\eta x+D\sinh\eta x),$$

$$(15c)\quad \tau_{xy}/G=2\alpha\xi\left(-\cosh\alpha y+\frac{\cosh\alpha c}{\cosh\beta c}\cosh\beta y\right)(A\sin\xi x-B\cos\xi x)$$
$$+2\gamma\eta\left(\cos\gamma y-\frac{\cos\gamma c}{\cos\delta c}\cos\delta y\right)(C\sinh\eta x+D\cosh\eta x),$$

where A, B, C, and D are new arbitrary constants.

Here, rewriting (12), we have

$$(16)\qquad \frac{\tanh\beta c}{\tanh\alpha c}=\frac{(\beta^2+\xi^2)^2}{4\alpha\beta\xi^2},$$

$$(17)\qquad \frac{\tan\delta c}{\tan\gamma c}=\frac{(\delta^2+\eta^2)^2}{4\gamma\delta\eta^2}.$$

For the range where c/l is small, by the use of the relations (8), we can expand (16) and (17) as follows:

$$(18)\quad k^2=\frac{4}{3}\lambda\xi^4c^2\left\{1-\frac{7}{15}\xi^2c^2\left(1+\frac{20}{7}\lambda\right)+\frac{62}{315}\xi^4c^4\left(1+\frac{294}{31}\lambda+\frac{266}{31}\lambda^2\right)-\dots\right\},$$

$$(19)\quad k^2=\frac{4}{3}\lambda\eta^4c^2\left\{1+\frac{7}{15}\eta^2c^2\left(1+\frac{20}{7}\lambda\right)+\frac{62}{315}\eta^4c^4\left(1+\frac{294}{31}\lambda+\frac{266}{31}\lambda^2\right)+\dots\right\}.$$

Equating (18) to (19), we have the relation between ξ and η as

$$\eta = \xi\left[1-\frac{7}{30}(\xi c)^2\left(1+\frac{20}{7}\lambda\right)+\frac{49}{600}(\xi c)^4\left(1+\frac{20}{7}\lambda\right)^2+\cdots\right], \tag{20}$$

where $\lambda = \frac{1}{2}(1+\nu)$. Then the expression of the angular frequency is

$$p^2 = \frac{E}{\rho}\frac{\xi^4 c^2}{3}\left[1-\frac{7}{15}(\xi c)^2\left(1+\frac{20}{7}\lambda\right)+\frac{62}{315}(\xi c)^4\left(1+\frac{294}{31}\lambda+\frac{266}{31}\lambda^2\right)-\cdots\right]. \tag{21}$$

If we put $c\to 0$ into (21) and denote p by p_a in this case, it becomes

$$p_a{}^2 = \frac{E}{\rho}\frac{\xi^4 c^2}{3} \tag{22}$$

and this is the same as the angular frequency which is given in the usual elementary theory of a thin beam.

3. BEAMS HAVING VARIOUS END CONDITIONS

(i) *Free-Free Beam*

Though the free end of a vibrating beam must be satisfied by the condition of being free from the tractions, the difficulties in solving the present problem seem to lie mainly in the calculation of such a condition. Indeed, a so-called exact solution of the problem published recently by some of the present authors (Higuchi and Hashimoto 1955) still contains some approximated points in regard to the numerical calculations.

Here, setting aside the exact solution mentioned above, we will obtain the solution of the motion of a thick beam using some approximations which enter inevitably into the course of the calculation of the end conditions. Thus, instead of the true conditions of the present problem, let us take approximately

$$\text{at } x = 0, 2l, \qquad \int_{-c}^{c}\sigma_x y dy = 0, \qquad \int_{-c}^{c}\tau_{xy}dy = 0. \tag{23}$$

Substituting (15) into (23) and eliminating constants A, B, C, and D, we arrive at the following characteristic equation for the present problem:

$$1-\cosh 2\eta l\cos 2\xi l+\frac{g_2{}^2h_1{}^2-g_1{}^2h_2{}^2}{2g_1g_2h_1h_2}\sinh 2\eta l\sin 2\xi l = 0, \tag{24}$$

where

$$g_1 = 2\alpha\xi\left(\frac{2}{\alpha}\sinh\alpha c-\frac{2\cosh\alpha c}{\beta\cosh\beta c}\sinh\beta c\right) \tag{25a}$$

$$= \alpha\xi\left\{1-\frac{3}{10}(\xi c)^2+\frac{107}{840}(\xi c)^4\left(1+\frac{336}{107}\lambda+\frac{102}{107}\lambda^2\right)+\cdots\right\},$$

$$g_2 = 2\gamma\eta\left(\frac{2}{\gamma}\sin\gamma c-\frac{2\cos\gamma c}{\delta\cos\delta c}\sin\delta c\right) \tag{25b}$$

$$= \gamma\eta\left\{1+\frac{3}{10}(\xi c)^2-\frac{53}{4200}(\xi c)^4\left(1-\frac{560}{53}\lambda^2\right)+\cdots\right\},$$

$$(25c)\qquad h_1 = \frac{2(2\alpha^2-\beta^2+\xi^2)}{\alpha}\left(-c\cosh\alpha c+\frac{1}{\alpha}\sinh\alpha c\right)$$
$$+\frac{2(\beta^2+\xi^2)\sinh\alpha c}{\beta\sinh\beta c}\left(c\cosh\beta c-\frac{1}{\beta}\sinh\beta c\right)$$
$$=\alpha\left\{1+\frac{1}{30}(\xi c)^2+\frac{13}{2520}(\xi c)^4\left(1-\frac{224}{13}\lambda+\frac{366}{13}\lambda^2\right)+\ldots\right\},$$

$$(25d)\qquad h_2 = \frac{2(2\gamma^2-\delta^2+\eta^2)}{\gamma}\left(-c\cos\gamma c+\frac{1}{\gamma}\sin\gamma c\right)$$
$$+\frac{2(\delta^2+\eta^2)\sin\gamma c}{\delta\sin\delta c}\left(\cos\delta c-\frac{1}{\delta}\sin\delta c\right)$$
$$=\gamma\left\{1-\frac{1}{30}(\xi c)^2+\frac{29}{1406}(\xi c)^4\left(1-\frac{560}{261}\lambda+\frac{560}{87}\lambda^2\right)+\ldots\right\}.$$

If we assume that the thickness of the beam becomes thin in comparison with the length, we have from (20)

$$(26)\qquad \xi = \eta = \xi_a$$

and by substituting (26) into (24), the following well-known characteristic equation of the free–free thin beam may be obtained:

$$(27)\qquad 1-\cosh 2\xi_a l\cos 2\xi_a l = 0.$$

For the range where c/l is comparatively small, the relation between ξ_l and $\xi_a l$ may be assumed as

$$(28)\qquad \xi l = \xi_a l(1+\epsilon).$$

Taking $2\xi_a l = 4.73004$ (Timoshenko 1955) and substituting (28) into (24), we have

$$(29)\quad \epsilon = (-0.4808+0.8392\lambda)(c/l)^2+(1.1856-0.5564\lambda-1.4734\lambda^2)(c/l)^4+\ldots$$

Thus, by substituting (29) into (21), the ratio of frequencies of the first mode calculated from (24) and (27) is obtained as

$$(30)\quad p/p_a = 1-(2.267+2.050\lambda)(c/l)^2+(7.340+25.20\lambda+4.706\lambda^2)(c/l)^4+\ldots$$

(*ii*) *Clamped–Clamped Beam*

For the present case, if we take the following end conditions:

$$(31)\qquad \text{at } x = 0,\ y = 0 \text{ and } x = 2l,\ y = 0,\qquad v = \partial v/\partial x = 0,$$

we arrive at the corresponding characteristic equation

$$(32)\qquad 1-\cosh 2\eta l\cos 2\xi l+\frac{\eta^2-\xi^2}{2\xi\eta}\sinh 2\eta l\sin 2\xi l = 0.$$

The ratio of the frequency of the first mode which is obtained from the present investigation to that from the elementary solution of the thin beam is deduced as

$$(33)\quad p/p_a = 1-(0.718+2.050\lambda)(c/l)^2+(0.419+14.001\lambda+4.706\lambda^2)(c/l)^4-\ldots$$

(*iii*) *Clamped–Free Beam*

The end conditions of the cantilever are taken here as

$$\text{at } x = 0,\ y = 0, \qquad v = \partial v/\partial x = 0, \tag{34a}$$

$$\text{at } x = 2l, \qquad \int_{-c}^{c} \sigma_x y dy = 0, \qquad \int_{-c}^{c} \tau_{xy} dy = 0. \tag{34b}$$

The characteristic equation of the present case is

$$\xi f_1^2 g_2 h_2 + \eta f_1^2 g_1 h_1 - f_1 f_2 (\xi h_1 g_2 + \eta h_2 g_1) \cosh 2\eta l \cos 2\xi l - f_1 f_2 (\xi h_2 g_1 - \eta h_1 g_2) \sinh 2\eta l \sin 2\xi l = 0, \tag{35}$$

where g_1, g_2, h_1, and h_2 are given by (25) and

$$f_1 = \alpha - \frac{(\beta^2+\xi^2)\sinh \alpha c}{2\beta \sinh \beta c} = -\frac{\alpha}{\beta^2}\left\{1+\frac{\lambda}{3}(\xi c)^2 - \frac{\lambda(1+10\lambda)}{45}(\xi c)^4 + \dots\right\}, \tag{36a}$$

$$f_2 = \gamma - \frac{(\delta^2+\eta^2)\sin \gamma c}{2\delta \sin \delta c} = \frac{\gamma}{\delta^2}\left\{1-\frac{\lambda}{3}(\xi c)^2 + \frac{2\lambda(3+5\lambda)}{45}(\xi c)^4 - \dots\right\}. \tag{36b}$$

Thus, the frequency ratio of the first mode for the present case becomes

$$p/p_a = 1-(0.179-0.143\lambda)(c/l)^2+(0.041+0.091\lambda-0.725\lambda^2)(c/l)^4- \dots \tag{37}$$

(*iv*) *Supported–Supported Beam*

The end conditions of the supported–supported beam are assumed here as

$$\text{at } x = 0, 2l, \qquad v = 0, \qquad \int_{-c}^{c} \sigma_x y dy = 0. \tag{38}$$

In this case, if we put in (14) and (15)

$$\sin (2\xi l) = 0 \tag{39}$$

and take $B \neq 0$, $A = C = D = 0$, it is shown that the necessary boundary conditions mentioned above are satisfied naturally. Hence (39) is just the frequency equation of the present case. Rewriting the roots of equation (39) as

$$\xi c = \tfrac{1}{2} n\pi (c/l), \qquad n = 1, 2, 3, \dots, \tag{40}$$

and substituting this into (8*a*) and (16), we obtain the values of p.

The frequencies of the first mode corresponding to the various end conditions deduced above are arranged and shown in Fig. 2, in which the values of p/p_a are plotted against the ratio l/c, with a proviso that for the sake of simplicity, Poisson's ratio of the vibrating material is assumed as zero in the figure.

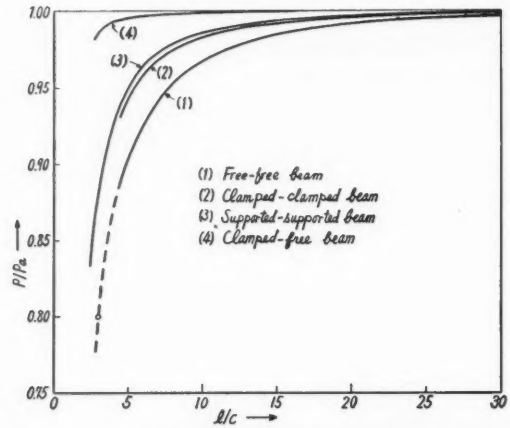

FIG. 2. Frequency-ratios corresponding to the various end conditions (the point O is the value obtained from the exact solution (Higuchi and Hashimoto 1955)).

4. CONCLUSION

The end conditions of the various beams, such as cantilever, built-in beam, used in the present investigation differ from one another in degree of approximation, so that, strictly speaking, the comparison of the frequencies of the various beams lays no claim to being always exact; this is very much regretted.

The most important results obtained in the present studies are summarized as follows:

(*i*) The larger the ratio of thickness to length becomes, the smaller will be the frequencies calculated as the thick beam compared with those from the elementary theory.

(*ii*) As a matter of fact, contrary to our expectations, the error due to misapplication of the theory of the thin beam for moderately thick beams, e.g., for the range about $10 > l/c > 5$, seems almost to be slight. For example, for the case of the free–free beam for which maximum error due to misapplication may be expected, the error is registered only as 10% even when $l/c = 5$.

(*iii*) Beams may be arranged in the following order on the basis of the decrease in the error which occurs when the elementary theory of the thin beam is misused: free–free, clamped–clamped, supported–supported, clamped–free. On the free–free beam, since there is no constrainment upon its motion, various effects, such as shear and rotary inertia, seem to be freely produced and result in the diminution of the flexural vibration. And it seems to us that this may be the reason why this beam shows the maximum error. As for the cantilever, a reason why it shows remarkable minimum errors due to misapplication of the theory of the thin beam may perhaps be attributed to its mode of vibration because it behaves like a beam twice the length of any of the other three.

REFERENCES

HIGUCHI, S. and HASHIMOTO, C. 1955. Tech. Repts. Iwate Univ. **9**, 1 (in Japanese with English summary).
KOLSKY, H. 1953. Stress waves in solids (Oxford At the Clarendon Press).
LAMB, H. 1917. Proc. Roy. Soc. (London), A, **93**, 114.
TIMOSHENKO, S. 1921. Phil. Mag. **41**, 747; **43**, 125.
——— 1955. The vibration problems in engineering (D. van Nostrand Company, Inc., New York).

THE WAVELENGTH DISPLACEMENTS OF SOME INFRARED LINES BETWEEN LIMB AND CENTER OF THE SUN[1]

LUISE HERZBERG

ABSTRACT

The wavelength displacements between the solar limb and the center of the disk, $(\lambda_L - \lambda_C)$, have been measured for six infrared solar lines, belonging to two multiplets of SiI. The displacements of the lines of one of the multiplets are the same, within the accuracy of the measurements; the displacements of the lines of the other multiplet, although varying somewhat amongst themselves, are systematically larger. This grouping of the results according to multiplet structure suggests that the wavelength displacement of solar lines across the disk is term-dependent. It is noted that the variation of the values $(\lambda_L - \lambda_C)$ is, in its essential features, similar to the term-dependent variation of the differences $(\lambda_\odot - \lambda_{lab})$ between the published solar and laboratory wavelengths of silicon. Solar and laboratory data, taken together, appear to provide observational evidence that the observed wavelength variations across the solar disk are, at least in part, due to collision or field effects.

A. INTRODUCTION

The characteristic wavelength variation of solar absorption lines with distance from the center of the disk was discovered early in this century by Halm (1907), who was then occupied with the spectroscopic determination of the solar velocity of rotation. Halm found that the wavelengths of solar lines, measured at different positions on the quiet sun, and corrected for the Doppler effect due to solar rotation, were not constant across the disk. There remained a systematic, although very small, residual variation: an increase in wavelength from the center outward along a solar radius, becoming steep in the immediate neighborhood of the limb ("limb-effect" of the older literature). This effect was independent of position angle, but somewhat different in magnitude for lines believed to originate at different heights in the photosphere. (The lines for which Halm found different effects were due to Fe and Fe^+, respectively.)

This systematic wavelength variation of solar lines across the disk should, by itself, have considerable importance as a source of information on conditions in the photosphere. The sustained interest in the phenomenon and its interpretation, however, is due to the fact that it is inseparable from the more general problem of the gravitational red shift of solar lines, demanded by General Relativity Theory.

The gravitational displacement of solar against terrestrial lines, given by Relativity Theory, is strictly proportional to the wavelength $(2.1 \times 10^{-6}\lambda)$ and independent of position on the disk. Because of the wavelength increase from the center of the disk to the limb, the observed displacements against laboratory standards vary along the solar radius. As first established by St. John (1928), for most lines the wavelength displacement measured at the limb approaches closely the predicted value for the gravitational red shift.

[1]Manuscript received March 18, 1957.
Contribution from the Dominion Observatory, Department of Mines and Technical Surveys, Ottawa, Canada. Issued as Contribution No. 23, Vol. 2.
A preliminary account of this work was presented to the American Astronomical Society Meeting, Columbus, Ohio, March, 1956.

Since wavelength displacements of the expected magnitude and direction are actually observed in the solar spectrum, if only in the light coming from the limb, most authors incline to the opinion that Einstein's gravitational red shift is indeed present, but that it is masked by an additional wavelength shift to the violet. This assumed violet shift varies from approximately one-half the (absolute) value of the gravitational shift, at the center of the disk, to zero at the limb.

Various processes taking place in the photosphere have been suggested as the possible cause of such a violet shift. St. John (1928), on the basis of his wavelength measurements at the limb and at the center of the disk, suggested that it represented a Doppler shift due to turbulent motions of the photospheric gases. However, later observations at points between center and limb showed that St. John's hypothesis, at least in its original form, is untenable: it cannot account for the characteristic form of the variation, along a solar radius, of either the intensities (Burns 1927) of solar lines, or their wavelengths (Hunter 1934).

In subsequent studies, therefore, special attention has been paid to the form of the wavelength variation across the disk. In recent years, several contributions have been made to the problem, based on a new set of precise absolute wavelengths in the λ6100 Å region measured by Adam (1948) at a series of points along a solar radius. Miss Adam's, now almost classical, curve of wavelengths as a function of position on the sun confirms the well-known slow wavelength increase from the center of the disk outward and the abrupt rise near the limb.

Spitzer (1950), in his analysis of the observations, discusses the possible effect on the solar wavelengths of the interaction between the absorbing atoms and the surrounding photospheric material. He finds that collisions with neutral hydrogen or helium atoms could cause violet shifts which would account for the difference between the observed and predicted solar wavelengths.

An entirely different interpretation of the observations has been proposed by Finlay-Freundlich (1954). This author considers the displacement between solar and terrestrial lines to be the sum of a "truncated" gravitational shift, much smaller than the relativistic effect, and an additional shift to the red, produced by a new, hypothetical process of interaction between light and radiation field. Interpreted in this way, the observational results would constitute evidence against the relativistic gravitational red shift of solar lines. This treatment of the problem has met with various serious objections. Much of the criticism has been directed against the fundamental assumption that an interaction between light and radiation field does take place; but, in addition, questions have been raised as to the choice of essential numerical constants, and other matters affecting the theoretical results (McCrea 1954; Burbidge and Burbidge 1954; and others).

Additional observations appear to be needed to clarify the situation. These would have to be either even more precise than the earlier ones, or more diversified. Adam's (1952, 1955) application of Treanor's (1949) new interferometric method to the study of solar wavelengths is a step in this

direction. The results obtained, so far, at the center of the disk indicate a correlation between magnitude of wavelength displacement and line intensity.

It is probable that at very long wavelengths, where the total displacements can be expected to be proportionately large, differences in the wavelength displacements of different lines would be easier to detect and easier to analyze. Since recent improvements of the photographic emulsions have considerably reduced the necessary exposure times, it is possible now to extend investigations to the photographic infrared region of the solar spectrum, that is to approximately λ11000 Å. To test whether worth-while results could be obtained in this way, exploratory measurements were made of the relative wavelength displacements between the center of the disk and the limb ("limb-center displacement") of a group of lines in the λ10700 Å region. The results are given below, together with a tentative interpretation.

B. OBSERVATIONS

The equipment available for the observations consisted of the 80 ft. horizontal solar telescope of the Dominion Observatory, a 20 ft. grating spectrograph, and a mirror-type image turner.

The telescope produces a solar image of 230 mm. diameter. The guiding arrangement makes it possible to place any part of the solar image over the slit of the spectroscope in any desired direction, and to hold it there with an accuracy of 1 or 2 mm., the accuracy depending, to some extent, on seeing conditions.

At the center of the disk the spectra were obtained with the slit in random direction, at the limb with the slit along a chord, bisecting the solar radius, at a distance of 4 mm. from the limb. Exposures were made at 16 points at the limb, spaced 22.5° apart, including North and South poles and East and West points on the equator. The diagram, Fig. 1, gives the different slit positions used, and the number of spectrograms evaluated for each case.

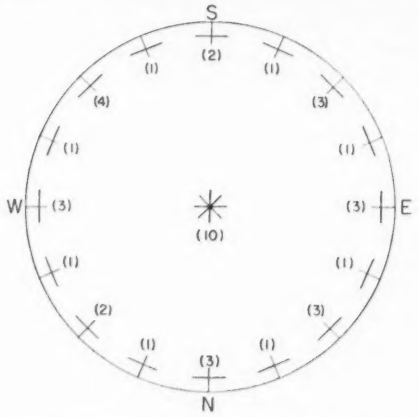

FIG. 1. Positions of the spectroscope slit relative to the solar image. The numbers in parentheses indicate the number of spectra evaluated for each position of the slit.

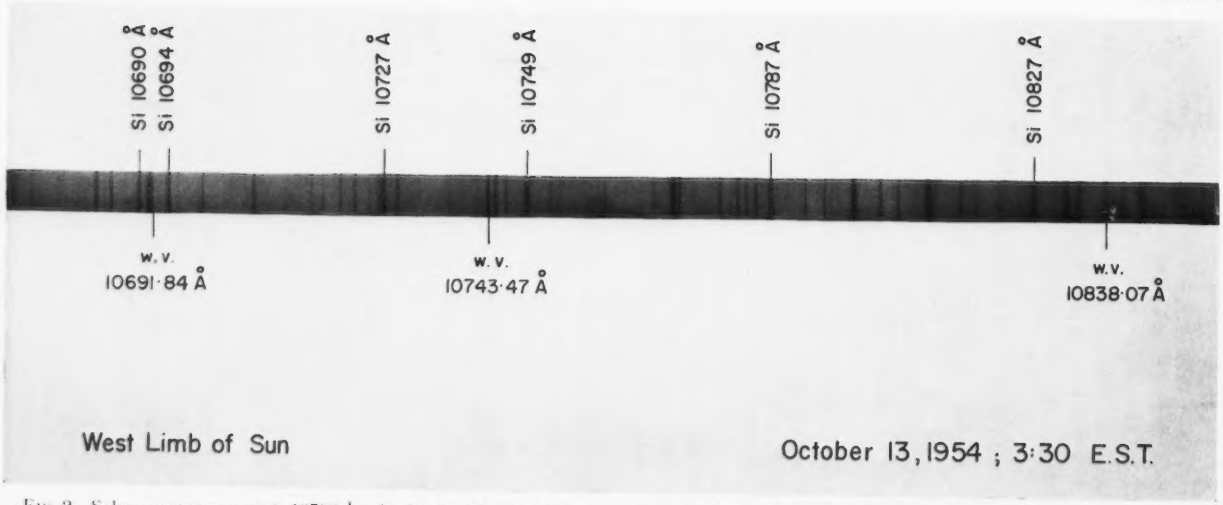

FIG. 2. Solar spectrum near λ 10700 Å, obtained with the 20 ft. spectrograph of the Dominion Observatory. Exposure time: 10 minutes. Reciprocal dispersion of original spectrogram: 1.2 Å/mm.

All spectra were taken in the second order of the 14400 lines/in. grating; the reciprocal dispersion on the plates is 1.2 Å/mm. With a slit width of 80 μ, 10-minute exposures at the limb and 3-minute exposures at the center of the disk were sufficient. The spectra were obtained on Kodak IZ spectroscopic plates which had been hypersensitized with ammonia in the usual way.

The 31-limb spectra which were evaluated, and six of the 10 center spectra, were obtained in October 1954, the remaining four center spectra in July 1955.

C. SELECTION OF LINES—METHOD OF PLATE REDUCTION

Since the present investigation was intended to be only exploratory, the lines to be studied could be freely selected amongst the many clear, well defined lines in the infrared region of the solar spectrum. For convenience's sake, lines were chosen the wavelength of which could be measured against a fixed framework of terrestrial absorption lines.

The spectral region of longest wavelength which contains solar and terrestrial lines of the type required for this purpose is the short wavelength edge of the $\lambda 1.14$ μ terrestrial water vapor band (Fig. 2). In this region the six solar lines of wavelengths $\lambda\lambda$ 10689.71 Å, 10694.25 Å, 10727.42 Å, 10749.39 Å, 10786.85 Å, and 10827.14 Å (indicated at the margin in Fig. 2) were selected for measurement. The lines are sharp and of medium intensity. Judging by their appearance, and by the data given in Babcock and Moore's (1947) table of the infrared solar spectrum, they could be expected to be relatively free from disturbing blends.

When choosing the lines for the present investigation, no attention was paid to their origin. As it turned out, the lines selected are all due to silicon (SiI). Of the other lines in the region, the stronger, but more diffuse ones are mostly due to carbon, the weak ones to iron.

The three terrestrial water vapor lines $\lambda\lambda$ 10691.84 Å, 10743.47 Å, and 10838.07 Å (cf. Fig. 2) were selected to serve as fixed wavelength standards. They are weak and narrow lines, and could therefore be expected to fulfill the rather stringent requirements as to their reproducibility, especially since all exposures were made at high sun, under very favorable and homogeneous atmospheric conditions. Their wavelengths (Babcock and Moore 1947) are not known with the precision usually required for wavelength standards. They are, however, acceptable for the present problem of determining very small wavelength displacements, where the dispersion need not be known to more than a first approximation.

The spectrograms were measured on a screw-type comparator, four times in each direction. The mean values of these eight measurements were used to obtain, for the six solar lines, a basic set of distances from a fixed reference point,

$$s_i = x_i - x_0,$$

where the x_i ($i = 1, 2, \ldots, 6$) stand for the x-coordinates of the solar lines, and

$$x_0 = \tfrac{1}{3}(x_A + x_B + x_C)$$

gives the reference point, defined by the coordinates x_A, x_B, x_C of the three terrestrial water vapor lines.

Given constant dispersion, the differences between corresponding distances s_i, measured on different spectrograms, would yield directly the wavelength shifts of the lines concerned. Actually, as indicated by discrepancies in the distances between the water vapor lines on different spectrograms, there are measurable variations in the dispersion, introduced by temperature effects and by the unavoidable inaccuracy in lining up the plates on the comparator stage. Therefore, to become comparable, all distances s_i had to be reduced to a standard dispersion, which was arbitrarily defined as the mean dispersion of the first 12 satisfactory spectrograms obtained in the course of the work.

For standard dispersion, the wavelengths are given by the formula

$$\lambda = 10757.95 + 1.1699(x - x_0) - 0.60 \times 10^{-4}(x - x_0)^2$$

where λ 10757.95 Å is the wavelength of the reference point x_0, defined above, and x is measured in millimeters. For the present purpose, only the first order term in this expression ("plate factor") is of interest.

In addition, the measured distances s_i had to be adjusted for the Doppler effects, due to the rotational and orbital motions of the earth. The necessary corrections were derived from the values for the velocity of the earth relative to points on the solar disk, computed for Ottawa by DeLury (1931). The effect of solar rotation was eliminated simply by using, in the final computations, the mean values of pairs of measurements, made at opposite points (East and West), at the solar limb.

D. RESULTS

(*a*) *Limb-center Displacement*

In Fig. 3 are presented the results for the limb-center displacements of the

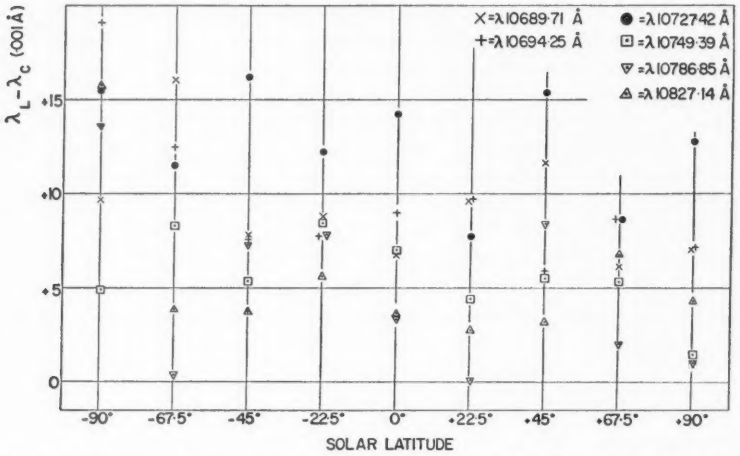

FIG. 3. Limb-center displacement of the individual lines for different solar latitudes.

six solar lines investigated, determined separately for different solar latitudes. As can be seen, there is, line for line, no variation of the wavelength displacements with solar latitude. This result agrees with that of observations made at shorter wavelengths, especially those of Freundlich, v. Brunn, and Brück (1930) at λ 4400 Å.

Final values for the limb-center displacements of the six solar lines, based on the complete observational material, are given in column 2 of Table I.

TABLE I

WAVELENGTH DISPLACEMENTS OF SOLAR ABSORPTION LINES

$\lambda_\odot$ (Å)*		$(\lambda_L-\lambda_C)$ (Å)	λ_{lab}(Å)†		$(\lambda_\odot-\lambda_{lab})$(Å)		
10784.57	(3)		10784.33	(5w)	+0.24	$4p\,^3D-4d\,^3F^0$ 5.95−7.09ev.	(53)‡
882.84	(3)		882.66	(5w)	+0.18		
689.71	(8)	$+0.008_6\pm0.001_6$	689.52	(20w)	+0.19		
694.25	(8)	$+0.008_9\pm0.001_6$	694.14	(50w)	+0.11		
727.42	(9)	$+0.013_7\pm0.001_5$	727.21	(75w)	+0.21		
749.39	(12)	$+0.005_3\pm0.001_9$	749.40	(60)	−0.01		
786.85	(7)	$+0.004_6\pm0.001_4$	786.86	(50)	−0.01	$4s\,^3P^0-4p\,^3P$ 4.92−6.06ev.	(5)‡
827.14	(12)	$+0.003_0\pm0.002_1$	827.09	(100)	+0.05		
603.426	(10)		603.38	(60)	+0.05		
660.99	(10)		660.98	(50)	+0.01		
979.34	(4)		979.27	(35)	+0.07		

*H. D. Babcock and C. E. Moore (1947).
†C. E. Moore (1945).
‡Multiplet number assigned by C. E. Moore.

(b) Velocity of Solar Rotation

While the value for the rotational velocity of the sun, determined from recurrent sun spot groups, has been remarkably constant over many years, the various values derived from the Doppler shift of solar absorption lines differ from each other by as much as 10% (Goldberg 1952). The reason for this scatter of the spectroscopic results does not seem to be entirely clear. In part, the discrepancies can be accounted for by the fact that different spectroscopic values refer to different effective depths in the photosphere, depending on wavelength and other properties of the lines used in the investigation. Since, so far, all measurements were made in the visible region of the spectrum, it appeared to be of interest to determine a value for the solar rotational velocity from measurements in the infrared.

The results obtained in the λ 10700 Å region (average for six lines) are as follows:

Angular velocity of rotation ω_ϕ, as a function of solar latitude ϕ, "law of solar rotation"

$$\omega_\phi = (13.^\circ10-2.^\circ23\sin^2\phi)\pm0.^\circ19;$$

linear velocity of rotation v_0 at the solar equator

$$v_0 = (1.85\pm0.03)\text{ km./sec.}$$

These results might be compared with the "law of solar rotation", derived

by Newton and Nunn (1951) from recurrent sun spot groups, over a period of six cycles (1878–1944),

$$\omega_\phi = (14.^\circ377 \pm 0.006) - (2.^\circ77 \pm 0.^\circ08)\sin^2\phi,$$

and with the most recent spectroscopic value, determined by Hart (1954) from the Doppler shift of lines in the λ 6000 Å region,

$$v_0 = (1.956 \pm 0.001) \text{ km./sec.}$$

The 5% difference between this value and the result obtained at λ 10700 Å does not seem unreasonable since it is of the same order as the scatter of the various spectroscopic values for the solar velocity of rotation, given in the literature.

E. DISCUSSION

The values for the limb-center displacements of the six infrared solar lines of the present investigation (cf. Table I) are presented graphically in Fig. 4, together with Adam's (1948) results for the λ 6100 Å region. The latter data

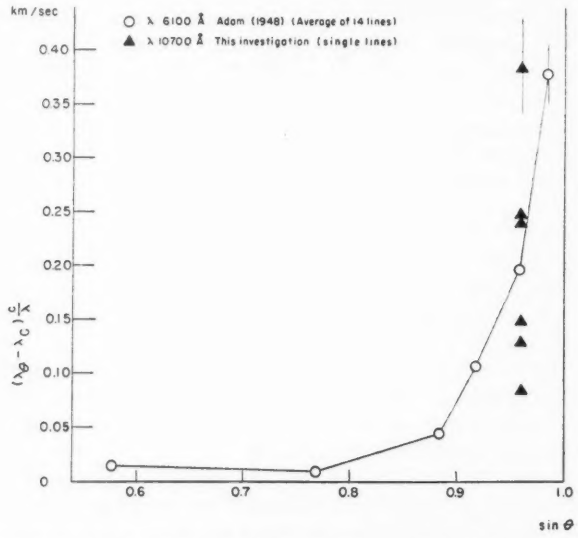

FIG. 4. Wavelength displacements of solar lines with respect to the center of the disk.

have been added to provide a scale of reference for the discussion. They represent results obtained for a group of 14 unselected metal lines; only the average values are given, because, in this case, the results obtained for individual lines agree with each other within the accuracy of measurement.

In the figure the distances from the center of the solar disk are given in terms of sin θ, where θ is the angle between the line of sight and the vertical to the solar surface at the point of observation. To facilitate comparison of the two

sets of data from different regions of the spectrum, the equivalent Doppler shifts $(\lambda_\theta - \lambda_C)\ c/\lambda$ have been plotted, instead of the wavelength displacements $(\lambda_\theta - \lambda_C)$ themselves.

The graphical presentation shows up clearly the characteristic dispersion of the wavelength displacements of the infrared lines, obtained for a given distance from the center of the disk. It should be noted that the infrared "limb" spectra were actually taken slightly inside the solar limb, at $\sin\theta = 0.96$, and not at $\sin\theta = 1.00$. In the λ 6100 Å region of the spectrum (cf. Fig. 4), this last 4% of the distance from the center means a difference of approximately 100% in the measured wavelength displacements. It does not seem unreasonable to assume that a similar steep rise in the immediate neighborhood of the limb occurs also in the infrared. Possibly therefore, with closer approach to the actual limb, the results would draw even further apart.

Discrepancies in the wavelength displacements measured for different lines might, conceivably, have some trivial cause, like overlapping with other Fraunhofer lines. This, however, is rather unlikely in the present case. As a matter of fact, the lines examined appear to be exceptionally free from disturbing "blends", as witnessed by the high internal consistency of the atomic energy levels, derived from the solar wavelengths (Moore 1953, 1956). One has therefore the impression that the variations in the present results are real, notwithstanding the relative inaccuracy of the individual data.

The dispersion of the wavelength displacements measured for the infrared solar lines is the more remarkable, because these lines, in contrast to the lines examined in the λ 6100 Å region, are very homogenous as to origin. The six infrared lines investigated belong to the arc spectrum of the same element, silicon, with three lines each being components of the same multiplet. These multiplets are, in Moore's (1945) notation, No. 5 and No. 53, corresponding to the $(4s\,^3P^0 - 4p\,^3P)$ and the $(4p\,^3D - 4d\,^3F^0)$ transitions.

From the very start of the present investigation, that is, when only a fraction of the observational material had been evaluated, the lines of one of the multiplets, No. 53, showed systematically larger wavelength shifts between center and limb than the lines of the other one, No. 5. This difference in the sensitivity of the two multiplets to change in position on the solar disk is clearly seen in the final results (Table I): the limb-center displacements measured for the lines of multiplet No. 53 are two to three times as large as those obtained for No. 5. The three relatively small values (No. 5) scatter only within the limits of accuracy; of the three larger values (No. 53) two coincide, while the third and largest one stands by itself.

If a definite relation between limb-center displacement and multiplet structure were found to exist, or, in other words, if the wavelength displacements of solar lines across the disk were term-dependent, it would be very important for their interpretation. Although the results obtained in the present investigation do show such a correlation, more observations are needed to establish its existence beyond doubt.

For the present, however, laboratory observations appear to provide some additional, indirect, evidence to show that the apparent relation between

limb-center displacement and multiplet structure is real, and not merely the result of chance coincidences. Comparing Babcock and Moore's (1947) wavelengths for the center of the solar disk with Kiess's (1938) laboratory measurements (silicon arc in nitrogen at reduced pressure), one finds, for some multiplets, complete agreement between the two sets of wavelengths, for others deviations in one or the other direction. (The gravitational shift of 0.02 Å, predicted by Relativity Theory, is within the limits of accuracy of the published absolute wavelengths.) The displacements between the measured solar and terrestrial wavelengths of silicon, therefore, are definitively term-dependent.

This fact is clearly shown by the two multiplets here under consideration. The relevant data have been included in Table I. It is seen that for multiplet No. 53 the solar wavelengths are consistently larger than those measured in the laboratory, while for multiplet No. 5 solar and laboratory wavelengths agree with each other within the accuracy of measurement.

Commenting on the differences between the published solar and laboratory wavelengths of silicon, Moore (1956) has pointed out that the values for the atomic energy levels, derived from the published laboratory data, are not as consistent as those computed from the solar wavelengths. This indicates that the spectrum obtained in the laboratory is affected by disturbing conditions in the light source employed. On the other hand, the quality of the silicon lines in the solar spectrum suggests that they are relatively free from such influences, and that, within the accuracy, they represent a satisfactory approximation to the spectrum of an ideal vacuum light source. The differences $(\lambda_{lab}-\lambda_{\odot})$ between laboratory and solar wavelengths, therefore, give essentially the displacements of the laboratory wavelengths against those of a standard light source. Significantly, the lines which show large values for $(\lambda_{lab}-\lambda_{\odot})$ are also, as a rule, perceptibly broadened in the laboratory spectrum.

The wavelength displacements in the laboratory spectrum are caused by collision or field effects, probably both. Strictly speaking, the values $(\lambda_{lab}-\lambda_{\odot})$, computed from the published data, refer only to one particular combination of disturbing factors. However, in their variation from multiplet to multiplet, they ought to present a picture of the relative sensitivity of the various lines to collision and field effects which should be valid for a fairly wide range of conditions.

The possibility that collision or field effects play a role in causing the observed wavelength variations of solar lines across the disk has variously been suggested in theoretical discussions of the subject (Spitzer 1950; Unsöld 1943; Wu 1955). This possibility, it should be stressed, is not precluded by the observation (cf. above) that the published absolute solar wavelengths appear to be free from such influences, since the values of the observed limb-center displacements are smaller than the error of measurement (approximately 0.02 Å) of the absolute wavelengths.

Since, in the photosphere, pressure and temperature increase with depth, the influence of pressure and field effects on the wavelengths of solar absorption lines will be greater at the center of the disk than at the limb. For the

different lines of silicon the resulting wavelength displacements between center and limb can be expected to follow the same pattern, as to relative magnitude and direction, as the displacements of the published laboratory wavelengths with respect to the solar wavelengths. As shown by the data given in Table I, this is indeed the case for the six silicon lines studied in the present investigation. For the lines of multiplet No. 53 the wavelength displacements between solar center and limb as well as the wavelength displacements between laboratory and solar spectrum are relatively large; for the lines of multiplet No. 5, on the other hand, the wavelength displacements between center and limb of the sun are relatively small, and solar and laboratory wavelengths are the same within the accuracy of the measurements. Furthermore, the wavelength displacements between solar center and limb are in the same direction as the wavelength displacements between laboratory and solar spectrum.

It seems possible, therefore, that the present results constitute observational evidence for the influence of collision or field effects on the solar spectrum. It is not surprising that the influence of effects of this type is recognized more easily in the infrared than in the visible region of the spectrum, because the wavelength displacement corresponding to a given disturbance by collision or field effects increases with the square of the wavelength.

The two silicon multiplets differ from each other in excitation potential by 1 ev. This means that one of the multiplets, No. 53, originates in a deeper effective layer of the photosphere than the other one, No. 5. For this reason alone, on the proposed interpretation, the limb-center displacements of the lines of multiplet No. 53 might be expected to be slightly larger than those of the lines of multiplet No. 5. The effect of the difference in excitation potential would, therefore, in this case, enhance the effect of the difference in sensitivity to disturbances by the environment.

In view of the positive results obtained so far, it is planned to extend the work to other infrared solar lines. It should be important to obtain measurements on additional lines with different excitation potentials, as well as on lines which show, in the laboratory, displacements of different magnitude, and in different directions. Multiplet No. 54 of SiI ($4p\,^3D-6s\,^3P^0$) at λ 8800 Å should be of special interest. This multiplet has the same lower energy level as multiplet No. 53, but the displacement ($\lambda_\odot-\lambda_{lab}$) is in the opposite direction.

ACKNOWLEDGMENTS

The author is greatly indebted to Dr. J. L. Locke for making his spectroscope and other equipment available for the investigation, and for his very generous assistance in its use. She also wishes to thank Dr. Ta-You Wu for discussion of the theoretical problems connected with the work, and Dr. C. E. Moore-Sitterly for valuable information on the absolute wavelengths of silicon from various sources. The continued interest and helpful advice of Dr. C. S. Beals, Dr. K. W. Meissner, and Dr. G. Herzberg is greatly appreciated. Computational help received from Mr. H. Bernstein is gratefully acknowledged.

REFERENCES

ADAM, M. G. 1948. Monthly Notices Roy. Astron. Soc. **108**, 446.
ADAM, M. G. 1952. Monthly Notices Roy. Astron. Soc. **112**, 546.
ADAM, M. G. 1955. Monthly Notices Roy. Astron. Soc. **115**, 405.
BABCOCK, H. D. and MOORE, C. E. 1947. The solar spectrum, λ 6600 to λ 13495. Carnegie Institution of Washington Publication 579, Washington, D.C.
BURBIDGE, E. M. and BURBIDGE, G. R. 1954. Phil. Mag. **45**, 1019.
BURNS, K. 1927. Publs. Allegheny Observatory, **6**, No. 9, 148.
DELURY, R. E. 1931. Publs. Dominion Observatory, **6**, 57.
FINLAY-FREUNDLICH, E. 1954. Phil. Mag. **45**, 303.
FREUNDLICH, E. F., BRUNN, A. v., and BRÜCK, H. 1930. Z. Astrophys. **1**, 43.
GOLDBERG, L. 1952. The sun, *edited by* Kuiper (The University of Chicago Press, Chicago), p. 21.
HALM, J. 1907. Astron. Nachr. **173**, 274.
HART, A. B. 1954. Monthly Notices Roy. Astron. Soc. **114**, 17.
HUNTER, A. 1934. Monthly Notices Roy. Astron. Soc. **94**, 594.
KIESS, C. C. 1938. J. Research NBS, **21**, 185.
MCCREA, W. H. 1954. Phil. Mag. **45**, 1010.
MOORE, C. E. 1945. A multiplet table of astronomical interest, Princeton, N.J.
——— 1953. J. Opt. Soc. Amer. **43**, 1014.
——— 1956. Discussion, Am. Astron. Soc. Meeting, Columbus, Ohio.
NEWTON, H. W. and NUNN, M. L. 1951. Monthly Notices Roy. Astron. Soc. **111**, 413.
ST. JOHN, C. E. 1928. Astrophys. J. **67**, 196.
SPITZER, L. 1950. Monthly Notices Roy Astron. Soc. **110**, 216.
TREANOR, P. J. 1949. Monthly Notices Roy. Astron. Soc. **109**, 389.
UNSÖLD, A. 1943. Vierteljahresschr. Astr. Gesellsch. **78**, 201 (*Quoted by* M. Minnaert, The sun, *edited by* Kuiper, Chicago, 1952, p. 168).
WU, TA-YOU. 1955. Private communication.

NOTES

CALCULATED INTENSITY AND PHASE DISTRIBUTION IN THE IMAGE SPACE OF A MICROWAVE LENS*

G. W. FARNELL

INTRODUCTION

In order to understand the image-forming properties of either optical or microwave lenses, it is necessary to study not only the intensity distribution in the image space but also the phase distribution. In the past, little experimental work has been done on this phase distribution near the focus of a lens, primarily because of the difficulty of making point-by-point phase measurements at optical wavelengths. However, accurate and detailed phase measurements in the diffraction image can be made conveniently at microwave frequencies. As part of a theoretical and experimental investigation of the intensity and phase distributions near the focus of a microwave lens, the calculated results presented below were obtained. These calculations assume that the scalar diffraction theory of aberrations as used in optics (Nijboer 1943, 1947) is applicable to the microwave lens. As shown by recent experimental intensity studies, this assumption is justified provided the field very close to the lens is not considered (Bachynski and Bekefi 1956).

INTENSITY DISTRIBUTION

Scalar diffraction theory when applied to an error-free microwave lens of typical dimensions predicts the intensity distribution in the vicinity of the point-source image to be as shown in Fig. 1. Here the contours of constant intensity on a decibel scale are shown in a plane containing the principal ray of the system. The intensity distribution has rotational symmetry about this principal ray, which forms the axis of abscissa in the picture. The exit pupil of the lens has a radius of 25 cm. and lies to the left of the image point at a distance of 105 cm. (32.8 wavelengths at the assumed wavelength of 3.2 cm.). Experimental measurements of such contours show very close agreement with these theoretical calculations.

For such a lens it should be noted from Fig. 1 that the point of maximum intensity is appreciably displaced from the geometrical focus (at -7λ on axis), that the Airy ring pattern lies not in a plane but on the surface of a sphere centered at the middle of the exit pupil, and that the axial minima are not spaced at equal increments from the image point. The corresponding region in the optical case is physically so small that these characteristics are not usually significant.

*This research forms part of a project on microwave optics that is supported at McGill University by the United States Air Force through its Cambridge Research Center, Contract AF 19(122)-81.

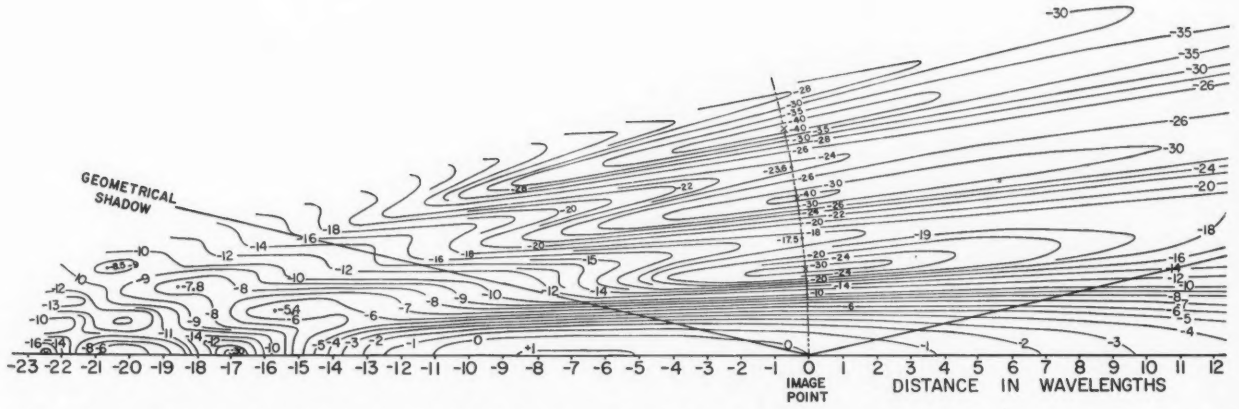

FIG. 1. Intensity contours in meridional plane for a microwave lens (in decibels relative to intensity at geometrical image point), wavelength $\lambda = 3.2$ cm., radius of exit pupil $a = 25$ cm., distance from exit pupil to geometrical image point $R = 105$ cm.

PHASE DISTRIBUTION

In Fig. 2(*a*) are shown the contours of constant phase for the same lens system and, for convenience, Fig. 2(*b*) shows similar contours for an optical lens of about the same *f*-number. The latter contours are similar to those given by Linfoot and Wolf (1956), but extend over a larger region of the image space. The zero rings of the Airy pattern are phase singularities and a phase jump of π radians is encountered along any path which intersects one of these rings (Matthews and Cullen 1956). If a path is traversed which loops one of the zero rings, then on return to the starting point the phase has advanced or retarded 2π radians depending on the direction of travel. With the microwave lens, the phase pattern is not symmetrical about the "image plane" nor are the phase fronts close to the geometrical image as nearly plane as in the optical lens.

The contours of Fig. 2 were obtained with the aid of an electronic analogue computer by calculating the departure of the actual scalar phase fronts from those of a spherical wave emanating from the center of the exit pupil. The contours of equal phase departure* for the microwave lens are shown in Fig. 3, and from this plot the detailed phase behavior in any small region of the image space can be examined more closely.

Initial phase measurements made on microwave lenses of such small *f*-number give phase contours which are in general agreement with the calculated contours but they do not show the 180°-phase jumps at the axial intensity minima which are predicted by the approximate scalar theory (see Figs. 2 and 3). A more critical study of the effect of the approximations involved in such computations is being made and more refined measurements with an automatic phase plotter are in progress.

ENERGY FLOW

It can be shown that in scalar fields, and in many electromagnetic fields, the direction of energy flow, i.e. the direction of Poynting's vector, is normal to the phase front at each point in the field (Nisbet and Wolf 1954). Fig. 4 is a sketch of the normals to the phase fronts given in Fig. 2(*a*). The density of lines crossing the focal arc has been made proportional to the intensity in decibels over that arc. It should be noted that the region of maximum trajectory density occurs about the point of maximum intensity. The wave crossing the "image plane" is essentially a wave diverging from a point at the center of the exit pupil. Thus the energy flow across the "image plane" is radially outwards from a phase center in the middle of the exit pupil whether the lens is focused at infinity or at a finite image distance. The energy flow bypasses the intensity nulls on the axis and the zero rings of the Airy pattern.

Thus the insight into the formation of the diffraction image of a lens system can be increased by considering simultaneously the intensity distribution, the phase distribution, and the energy flow pattern in the image space.

---

*Off the axis such phase departures are not the same as the phase anomaly defined by Linfoot and Wolf (1956).

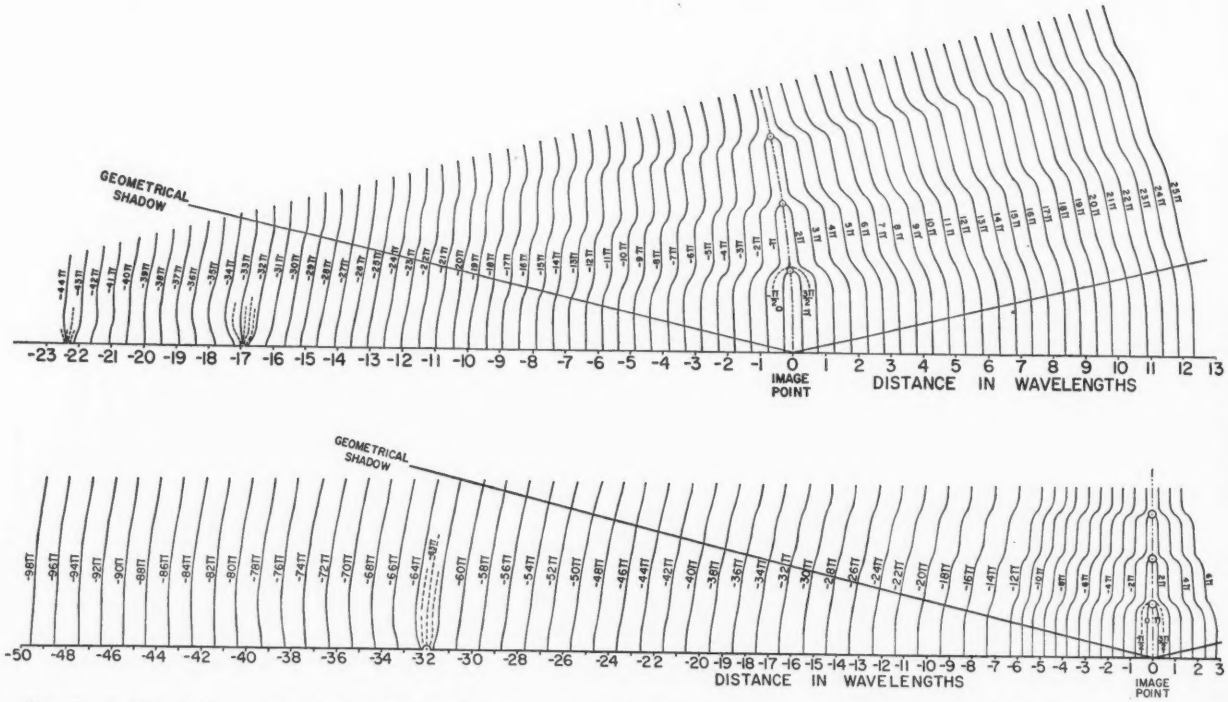

FIG. 2. Contours of constant phase; phase at geometrical image taken as $\pi/2$ radians. (*a*) (Upper) Microwave lens: dimensions as in Fig. 1. (*b*) (Lower) Optical lens: $\lambda = 5\times10^{-5}$ cm., $a = 2.5$ cm., $R = 10$ cm.

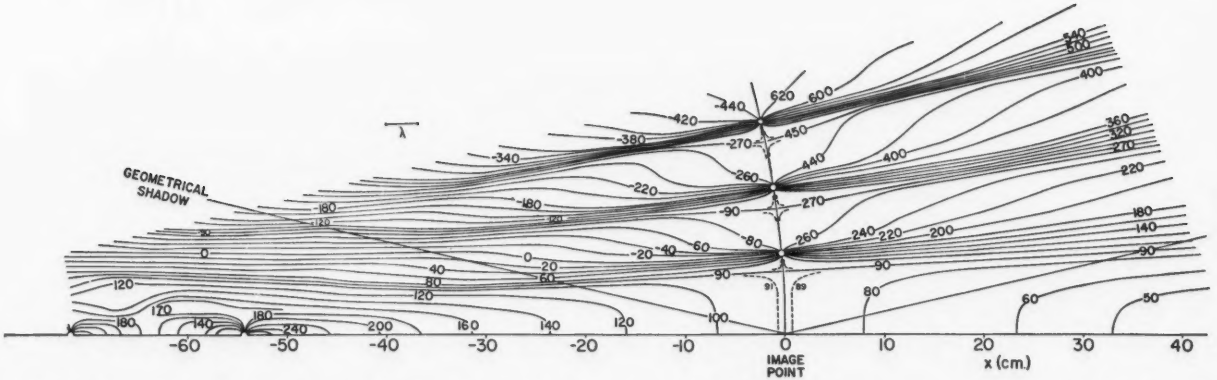

FIG. 3. Contours of constant phase departure; departure of phase from that of spherical wave emanating from center of exit pupil; dimensions as in Fig. 1.

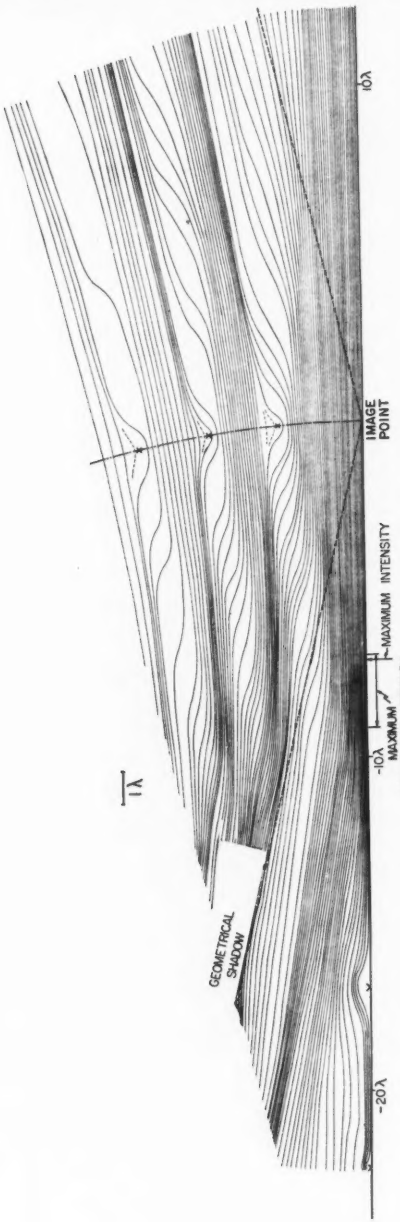

FIG. 4. Direction of energy flow; normals to the phase fronts of Fig. 2(*a*).

BACHYNSKI, M. P. and BEKEFI, G. 1956. I.R.E. Trans. on Antennas and Propagation AP-4, 412.
LINFOOT, E. H. and WOLF, E. 1956. Proc. Phys. Soc. B, **69**, 823.
MATTHEWS, P. A. and CULLEN, A. L. 1956. Proc. Inst. Elec. Engrs., Pt. C, **103**, 449.
NIJBOER, B. R. A. 1943. Physica, **10**, 679.
——— 1947. Physica, **13**, 605.
NISBET, A. and WOLF, E. 1954. Proc. Cambridge Phil. Soc. **50**, 614.

RECEIVED FEBRUARY 12, 1957.
THE EATON ELECTRONICS RESEARCH LABORATORY,
MCGILL UNIVERSITY,
MONTREAL, QUE.

SOME UPPER LIMITS OF ISOTOPIC ABUNDANCE—III: C, O, and Zn

LARKIN KERWIN, D. E. MCELCHERAN, AND MAURICE COTTIN

Continuing the search for possible rare isotopes of elements which do not appear to have been closely scrutinized (Kerwin 1956; Kerwin and McElcheran 1956), we have been able to establish some upper limits of abundance for isotopes of the elements carbon, oxygen, and zinc. The present status of the isotopic abundance of these elements is therefore as follows:

Isotope	Abundance, %	Reference
	Carbon	
C 10	<0.005	This note
C 11	<0.005	This note
C 12	98.892 variable	Nier (1950)
C 13	1.108 variable	Nier (1950)
C 14	<0.01	This note
C 15	<0.005	This note
	Oxygen	
O 14	<0.005	This note
O 15	<0.003	This note
O 16	99.759 air	Nier (1950)
O 17	0.0374 air	Nier (1950)
O 18	0.2039 air	Nier (1950)
O 19	<0.005	This note
O 20	<0.005	This note
	Zinc	
Zn 61	<0.02	This note
Zn 62	<0.04	This note
Zn 63	<0.001	Nier (1936)
Zn 64	48.89	Leland and Nier (1948) Hess, Inghram, and Hayden (1947)
Zn 65	<0.002	Nier (1936)
Zn 66	27.81	*idem* Zn 64
Zn 67	4.11	*idem* Zn 64
Zn 68	18.56	*idem* Zn 64
Zn 69	<0.0015	Nier (1936)
Zn 70	0.62	*idem* Zn 64
Zn 71	<0.01	This note
Zn 72	<0.005	This note
Zn 73	<0.005	This note

ADDENDUM

To the data given for chlorine in a previous report (Kerwin and McElcheran 1956) should be added that recently published by Boyd, Brown, and Lounsbury (1955).

It is a pleasure to acknowledge the support of the Defense Research Board (Grant No. DRB-9510-13) and the National Research Council (Grant No. T-45) during the progress of this work.

BOYD, A. W., BROWN, F., and LOUNSBURY, M. 1955. Can. J. Phys. **33**, 35.
HESS, D. C., Jr., INGHRAM, M. G., and HAYDEN, R. J. 1947. Plutonium Project Report ANL-4082, p. 5.
KERWIN, L. 1956. Can. J. Phys. **34**, 1080.
KERWIN, L. and MCELCHERAN, D. E. 1956. Can. J. Phys. **34**, 1497.
LELAND, W. T. and NIER, A. O. 1948. Phys. Rev. **73**, 1206.
NIER, A. O. 1936. Phys. Rev. **50**, 1041.
——— 1950. Phys. Rev. **77**, 789.

RECEIVED MARCH 11, 1957.
DÉPARTEMENT DE PHYSIQUE,
UNIVERSITÉ LAVAL,
QUÉBEC.

THE PHYSICAL SOCIETY

MEMBERSHIP of the Society is open to all who are interested in Physics.

FELLOWS pay an Entrance fee of £1 1*s*. ($3.00) and an Annual Subscription of £2 2*s*. ($6.00).

STUDENTS: A candidate for Studentship must be between the ages of 18 and 26, and pays an Annual Subscription of 5*s*. ($0.75).

MEETINGS: Fellows and Students may attend all Meetings of the Society including the annual Exhibition of Scientific Instruments and Apparatus.

PUBLICATIONS include the *Proceedings of the Physical Society*, published monthly in two sections, and *Reports on Progress in Physics*, published annually. Volume XIX, 1956, is now available (price 50*s*. ($7.15)). Members are entitled to receive any of the Publications at a reduced rate.

Further information can be obtained from:

THE PHYSICAL SOCIETY

1, LOWTHER GARDENS, PRINCE CONSORT ROAD

LONDON, S.W.7, ENGLAND

CANADIAN JOURNAL OF PHYSICS

Notes to Contributors

Manuscripts

(i) General. Manuscripts, in English or French, should be typewritten, double spaced, on paper 8½×11 in. **The original and one copy are to be submitted.** Tables and captions for the figures should be placed at the end of the manuscript. Every sheet of the manuscript should be numbered.

Style, arrangement, spelling, and abbreviations should conform to the usage of this journal. Names of all simple compounds, rather than their formulas, should be used in the text. Greek letters or unusual signs should be written plainly or explained by marginal notes. Superscripts and subscripts must be legible and carefully placed.

Manuscripts and illustrations should be carefully checked before they are submitted. Authors will be charged for unnecessary deviations from the usual format and for changes made in the proof that are considered excessive or unnecessary.

(ii) Abstract. An abstract of not more than about 200 words, indicating the scope of the work and the principal findings, is required, except in Notes.

(iii) References. References should be listed **alphabetically by authors' names,** unnumbered, and typed after the text. The form of the citations should be that used in current issues of this journal; in references to papers in periodicals, titles should not be given and only initial page numbers are required. The names of periodicals should be abbreviated in the form given in the most recent *List of Periodicals Abstracted by Chemical Abstracts.* All citations should be checked with the original articles and each one referred to in the text by the authors' names and the year.

(iv) Tables. Tables should be numbered in roman numerals and each table referred to in the text. Titles should always be given but should be brief; column headings should be brief and descriptive matter in the tables confined to a minimum. Vertical rules should be used only when they are essential. Numerous small tables should be avoided.

Illustrations

(i) General. All figures (including each figure of the plates) should be numbered consecutively from 1 up, in arabic numerals, and each figure referred to in the text. The author's name, title of the paper, and figure number should be written in the lower left corner of the sheets on which the illustrations appear. Captions should not be written on the illustrations (see Manuscripts (i)).

(ii) Line Drawings. Drawings should be carefully made with India ink on white drawing paper, blue tracing linen, or co-ordinate paper ruled in blue only; any co-ordinate lines that are to appear in the reproduction should be ruled in black ink. Paper ruled in green, yellow, or red should not be used unless it is desired to have all the co-ordinate lines show. All lines should be of sufficient thickness to reproduce well. Decimal points, periods, and stippled dots should be solid black circles large enough to be reduced if necessary. Letters and numerals should be neatly made, preferably with a stencil (**do NOT use typewriting**) and be of such size that the smallest lettering will be not less than 1 mm. high when reproduced in a cut 3 in. wide.

Many drawings are made too large; originals should not be more than 2 or 3 times the size of the desired reproduction. In large drawings or groups of drawings the ratio of height to width should conform to that of a journal page but the height should be adjusted to make allowance for the caption.

The original drawings and one set of clear copies (e.g. small photographs) are to be submitted.

(iii) Photographs. Prints should be made on glossy paper, with strong contrasts. They should be trimmed so that essential features only are shown and mounted carefully, with rubber cement, on white cardboard with no space or only a **very** small space (less than 1 mm.) between them. In mounting, full use of the space available should be made (to reduce the number of cuts required) and the ratio of height to width should correspond to that of a journal page (4¾×7½ in.); however, allowance must be made for the captions. Photographs or groups of photographs should not be more than 2 or 3 times the size of the desired reproduction.

Photographs are to be submitted in duplicate; if they are to be reproduced in groups one set should be mounted, the duplicate set unmounted.

Reprints

A total of 50 reprints of each paper, without covers, are supplied free. Additional reprints with or without covers, may be purchased.

Charges for reprints are based on the number of printed pages, which may be calculated approximately by multiplying by 0.6 the number of manuscript pages (double-spaced typewritten sheets, 8½×11 in.) and including the space occupied by illustrations. An additional charge is made for illustrations that appear as coated inserts. The cost per page is given on the reprint requisition which accompanies the galley.

Any reprints required in addition to those requested on the author's reprint requisition form must be ordered officially as soon as the paper has been accepted for publication.

Contents

Page

Neutron Spectrum of an Actinium–Beryllium Source—*W. R. Dixon, Alice Bielesch, and K. W. Geiger* - - - - - - - 699

Variations in the Intrinsic Strength of the 1956 Quadrantid Meteor Shower—*C. O. Hines and E. L. Vogan* - - - - - - 703

Structure of the Fundamental Infrared Band of Hydrogen in Pressure Induced Absorption—*H. P. Gush, A. Nanassy, and H. L. Welsh* - - - - - - - - - - - - - - - - 712

The Effect of Pressure on the Electrical Resistance of Rubidium—*J. S. Dugdale and J. A. Hulbert* - - - - - - - - - - 720

High Resolution Raman Spectroscopy of Gases. IX. Spectra of H_2, HD, and D_2—*B. P. Stoicheff* - - - - - - - - - - 730

Velocity-jump Amplification at 10,000 Mc./s.—*B. V. Dore* - - 742

On a Reported Isomeric State in Mn^{54}—*K. G. McNeill, J. D. Prentice, L. Katz, and W. Link* - - - - - - - - - - 753

A Study of the Approximate Theory of an Elastic Thick Beam—*Seiichi Higuchi, Hideo Saito, and Chiaki Hashimoto* - - - 757

The Wavelength Displacements of Some Infrared Lines between Limb and Center of the Sun—*Luise Herzberg* - - - - - - 766

Notes:

Calculated Intensity and Phase Distribution in the Image Space of a Microwave Lens—*G. W. Farnell* - - - - - - 777

Some Upper Limits of Isotopic Abundance—III: C, O, and Zn—*Larkin Kerwin, D. E. McElcheran, and Maurice Cottin* - - 783

Printed in Canada *by* University of Toronto Press